Instituto de Pesquisas Jardim Botânico do Rio de Janeiro
Escola Nacional de Botânica Tropical
Programa de Pós-Graduação em Botânica

Programa de Doctorado en Ciencias de la Tierra
Universidad de Granada

Tese de Doutorado / Tesis Doctoral

Caracterização de recifes mesofóticos em áreas chave da Plataforma Continental Brasileira: Margem Equatorial e Bacia Sergipe-Alagoas

Caracterización de arrecifes mesofóticos en áreas clave de la plataforma continental brasileña: Margen Ecuatorial y Cuenca Sergipe-Alagoas

Nicholas Farias Lopes do Vale

Granada
2022

Instituto de Pesquisas Jardim Botânico do Rio de Janeiro
Escola Nacional de Botânica Tropical
Programa de Pós-Graduação em Botânica
Programa de Doctorado en Ciencias de la Tierra
Universidad de Granada

Caracterização de recifes mesofóticos em áreas chave da Plataforma Continental Brasileira: Margem Equatorial e Bacia Sergipe-Alagoas

Caracterización de arrecifes mesofóticos en áreas clave de la plataforma continental brasileña: Margen Ecuatorial y Cuenca Sergipe-Alagoas

Nicholas Farias Lopes do Vale

Tese apresentada em regime de cotutela ao Programa de Pós- Graduação em Botânica, Escola Nacional de Botânica Tropical, do Instituto de Pesquisas Jardim Botânico do Rio de Janeiro, como parte dos requisitos necessários para a obtenção do título de Doutor em Botânica e ao Programa de Doctorado en Ciencias de la Tierra, da Universidad de Granada, como parte dos requisitos necessários para a obtenção do título de Doutor em Ciencias de la Tierra.

Orientadores: Dr. Leonardo Tavares Salgado (JBRJ), Dr. Juan Carlos Braga (UGR, Espanha) e Dr. Alex Cardoso Bastos (Univ. Federal do Espírito Santo)

Tutor: Dr. Julio Aguirre (UGR)

Granada
2022

Editor: Universidad de Granada. Tesis Doctorales
Autor: Nicholas Farias Lopes do Vale
ISBN: 978-84-1117-399-5
URI: http://hdl.handle.net/10481/75618

The doctoral candidate **Nicholas Farias Lopes do Vale**
and the thesis supervisors, Prof. **Juan Carlos Braga Alarcón** y Prof. **Leonardo Tavares Salgado**.

Guarantee, by signing this doctoral thesis, that the work has been done by the doctoral candidate under the direction of the thesis supervisor and, as far as we know, during the development of the research, the rights of the authors to be cited (when their results or publications have been used) have been respected.

Granada, May 2022.

Thesis supervisors:

Prof. **Juan Carlos Braga Alarcón** Prof. **Leonardo Tavares Salgado**

Doctoral candidate:

Nicholas Farias Lopes do Vale

Vale, Nicholas Farias Lopes do.

V149c

Caracterização de recifes mesofóticos em áreas chave da Plataforma Continental Brasileira: Margem Equatorial e Bacia Sergipe-Alagoas = Caracterización de arrecifes mesofóticos en áreas clave de la plataforma continental brasileña: Margen Ecuatorial y Cuenca Sergipe-Alagoas / Nicholas Farias Lopes do Vale. – [Rio de Janeiro], Granada, ES, 2022.

xv, 134f.: il.; 28 cm.

Tese (doutorado) – Instituto de Pesquisas Jardim Botânico do Rio de Janeiro / Escola Nacional de Botânica Tropical, Universidad de Granada / Programa de Doctorado em Ciencias de la Tierra, 2022.

Orientadores: Leonardo Tavares Salgado; Juan Carlos Braga Alarcón; Alex Cardoso Bastos.

Tutor: Julio Aguirre.

Tese defendida em cotutela com a Universidad de Granada, Espanha.

Bibliografia.

1. Banco de rodolitos. 2. Algas coralináceas. 3. Recife carbonático. 4. Holoceno. 5. Plataforma continental brasileira. I. Título. II. Escola Nacional de Botânica Tropical. III. Universidad de Granada.

CDD 589.30981

Agradecimentos

Agradeço inicialmente ao nosso querido líder, Prof. Dr. Gilberto M. Amado-Filho, que me supervisou, ajudou na concepção deste trabalho e forneceu condições para continuar com o seu legado. Igualmente agradeço aos Professores Dr. Juan Carlos Braga., Dr. Leonardo Tavares Salgado e Dr. Alex Cardoso Bastos pela orientação, motivação, apoio e colaboração incondicional na elaboração dos manuscritos que compõem esta tese. Foi um privilégio contar com a experiência e conhecimento de vocês. Também agradeço ao meu tutor Dr. Julio Aguirre, por sua ajuda e seus pareceres ao longo desses anos.

À Coordenação de Aperfeiçoamento de Pessoal de Nível Superior (CAPES) e ao Conselho Nacional de Desenvolvimento Científico e Tecnológico (CNPq) pelo apoio financeiro e financiamento do período sanduíche na Espanha através do Programa de Mobilidade Internacional, sem os quais este trabalho não seria possível.

Ao Programa Internacional de Descobrimento do Oceano (IODP)/CAPES Brasil, Agência Nacional do Petróleo, Gás Natural e Biocombustíveis (ANP/PetroRio) e Dalio *Philanthropies*/OceanX *Initiative* por subsidiar as expedições na Margem Equatorial Brasileira. À Marinha do Brasil e Instituto Chico Mendes de Conservação da Biodiversidade (ICMBio) pelas licenças de pesquisa concedidas.

À Petrobras por fornecer dados utilizados em um dos artigos que compõe esta tese, bem como à Maria Eulália R. Carneiro (Petrobras) e equipe do Laboratório de Bentos da Universidade Federal de Sergipe pela coleta e fornecimento das amostras, e pela colaboração com o IPJBRJ.

A todos os membros participantes das expedições oceanográficas que ajudaram no campo. Aos colegas do Laboratório de Algas do IPJBRJ e do Departamento de Estratigrafía y Paleontología da UGR pelas palavras de incentivo e auxílios quando foram necessários.

Agradeço também aos editores e revisores das revistas por seus comentários e sugestões, que ajudaram a melhorar consideravelmente os capítulos desta tese. Aos coautores das publicações por suas contribuições e disposição em revisar os manuscritos. Aos colegas de trabalho que dedicaram tempo para ajudar com a identificação dos organismos. À Dra. Cláudia S. Karez, por suas revisões e conselhos linguísticos e científicos. Ao Pedro S. Menandro pela sua ajuda na elaboração dos mapas. Por último, mas não menos importante, sou grato aos amigos e familiares que sempre me apoiaram.

Resumo

A Margem Continental Amazônica (MCA) e Bacia Sergipe-Alagoas (SEAL) se destacam pelo desenvolvimento de formações carbonáticas/siliciclásticas, desde períodos geológicos passados até o presente. O foco deste estudo foi avaliar a evolução das estruturas recifais da MCA e rodolitos da Bacia SEAL após o Último Máximo Glacial (LGM). Com os resultados obtidos, foi possível definir a estrutura das formações recifais; as fácies dominantes nas amostras estudadas, caracterizando-as nas distintas idades de sua formação. Três principais formações foram reconhecidas em diferentes faixas de profundidade: bancos de rodolitos, concreções carbonáticas e 'recifes'. Um total de 22 morfo-taxons de algas vermelhas (rodofíceas) foram identificadas nos locais de estudo. A transição entre a plataforma externa e a quebra da plataforma no Setor Norte da MCA traz consigo uma série de estruturas proeminentes de alto relevo. Os topos destas feições estão entre 110-165 m de profundidade e parecem ter se originado durante o baixo nível do mar (NM), através da erosão dos arenitos Pleistocênicos. Os depósitos carbonáticos e siliciclásticos acumulados no topo dessas feições durante o LGM e deglaciação precoce foram gradualmente submersos pela elevação do NM e pela subsidência. Uma fina camada de organismos incrustantes (algas coralináceas, esponjas, briozoários e serpulídeos) coloniza atualmente a maioria dessas superfícies e contribui para a agregação de uma camada carbonática fina com siliciclásticos de grão fino. O Setor Central, em frente à foz do rio, está associado ao acúmulo de sedimentos a longo prazo e carece de uma ruptura na plataforma. No entanto, comunidades bentônicas vivas ocorrem em afloramentos rochosos. O Setor Sul é menos influenciado pela pluma do rio e inclui uma plataforma mais rasa e um cânion proeminente. Os afloramentos rochosos do Pleistoceno a 180 m carregam coberturas finas de uma comunidade bentônica dominada por esponjas e algas coralináceas, que são responsáveis pelo acúmulo de um depósito fino de bioclastos, areia de quartzo e lama sobre o substrato rochoso. Assim, os 'recifes' da plataforma externa e a margem mesofótica da Amazônia são tipicamente rochas antigas erodidas, colonizadas por organismos incrustantes durante o LGM e deglaciação formando uma camada carbonática, que agora suporta uma comunidade mesofótica. Operações com Veículo Operado Remotamente e a amostragens com rede de arrasto de fundo na Bacia SEAL revelaram a ocorrência de bancos de rodolitos entre 25-54 m de profundidade. Nas profundidades mais rasas, rodolitos ramificados (maërl) aparecem nos leitos de ondulações (*ripples*) e outros rodolitos não ramificados ocorrem associados a corais e esponjas circundadas por areia bioclástica. Rodolitos também ocorrem em manchas e alguns são fundidos entre 30-39 m de profundidade. Em profundidades maiores (40-54 m) a abundância de rodolitos aumenta e ocorre associada a macroalgas carnosas, localmente alguns são maërl e outros são parcialmente enterrados por sedimentos de granulação fina. Duas fases de crescimento podem ser distinguidas em alguns rodolitos. Os núcleos apresentaram idades entre 1.600-1.850 anos, enquanto as camadas externas eram muito mais jovens (180-50 anos). As camadas de crescimento pareciam ter sido separadas por um longo período de enterramento no sedimento do fundo do mar.

Palavras-chave: Bancos de rodolitos; algas coralináceas; depósitos carbonáticos e siliciclásticos; mudanças no nível do mar; Holoceno; Plataforma Continental Brasileira.

Resumen Amplio

El Margen Continental Amazónico (MCA), que se extiende en la parte noroeste del Margen Ecuatorial Brasileño e incluye la desembocadura del río Amazonas, representa una de las mayores plataformas mixtas (carbonatadas-siliciclásticas) del mundo, desarrollada durante el Neógeno en un período de transición de ambientes dominados por carbonatos a siliciclásticos en la región.

El objetivo de este estudio fue evaluar la evolución de las estructuras arrecifales de la MCA y de los rodolitos de la cuenca SEAL después del Último Máximo Glacial (LGM). Con los resultados obtenidos, se ha determinado la estructura interna de las formaciones arrecifales, caracterizando las facies dominantes en las distintas edades de su formación. En la transición entre la plataforma y el talud en el sector Norte de la MCA existen una serie de estructuras prominentes de alto relieve (hasta 15 m sobre el fondo) que están influenciadas por los procesos fluviales. La parte superior de estas estructuras tienen una profundidad de entre 110 y 165 m y parecen haberse originado durante bajos niveles de mar por la erosión de las areniscas del Pleistoceno. Los depósitos carbonáticos (consistentes en boundstones y rudstones de serpúlidos, balánidos, sabelláridos, y algas corallinas) y siliciclásticos acumulados sobre estas estructuras durante el LGM y la deglaciación temprana fueron sumergidos gradualmente por el aumento del nivel del mar y la subsidencia. Una fina capa de organismos incrustantes (algas corallinas -AC, esponjas, briozoos y serpúlidos) coloniza actualmente la mayoría de estas superficies y contribuye a la agregación de finos depósitos siliciclásticos de grano fino. El sector Central, frente a la desembocadura del río, está asociado a la acumulación de sedimentos a largo plazo y carece de ruptura de la plataforma. Las comunidades bentónicas vivas se dan en los afloramientos rocosos. El sector Sur está menos influenciado por la pluma del río e incluye una plataforma menos profunda y un cañón prominente. Los afloramientos rocosos del Pleistoceno a 180 m presentan finas cubiertas de una comunidad bentónica dominada por esponjas y AC, que son responsables de la acumulación de un fino depósito de bioclastos, arena de cuarzo y lodo en el sustrato rocoso. Así, los “arrecifes” de la plataforma exterior y el margen mesofótico de la Amazonia son típicamente rocas antiguas erosionadas, colonizadas por organismos incrustantes durante el LGM y la deglaciación formando una capa de carbonato, que ahora sostiene una comunidad mesofótica. La acreción de sedimento favorecida por estas comunidades mesofóticas es negligible.

En la cuenca SEAL la distribución a gran escala de los bancos de rodolitos está controlada por la descarga de sedimentos de los principales sistemas fluviales de la región. Las

operaciones con Vehículos Operados Remotamente y el muestreo con redes de arrastre de fondo revelaron la presencia de bancos de rodolitos entre 25 y 54 m de profundidad. A menor profundidad, aparecen rodolitos ramificados (maërl) en los senos de las ondulaciones (*ripples*) y otros no ramificados asociados a parches de corales y esponjas rodeados de arena bioclástica. Los rodolitos también se presentan en parches y algunos están fusionados entre 30-39 m de profundidad. A mayores profundidades (40-54 m) la abundancia de rodolitos aumenta y se presenta asociada a macroalgas carnosas, localmente algunos rodolitos son ramificados (maërl) y otros están parcialmente enterrados por sedimentos de grano fino. En algunos rodolitos se pueden distinguir dos fases de crecimiento. Los núcleos mostraron edades entre 1.600-1.850 años, mientras que las capas más externas eran mucho más jóvenes (180-50 años). Las fases de crecimiento parecen estar separadas por un largo periodo de enterramiento en el sedimento del fondo marino.

Fueron identificadas un total de 6 morfotaxones de algas rojas (rodofíceas) en el Margen Continental Amazónico y 16 morfotaxones en la cuenca de Sergipe-Alagoas, pertenecientes a Corallinales, Hapalidiales y Sporolithales, dentro de las AC, y a Peyssonneliales, integrados en 4 familias y 10 géneros. Las imágenes y los vídeos obtenidos demuestran que los arrecifes mesofóticos y los bancos de rodolitos crecen activamente y pueden servir de hábitat a otros organismos marinos.

Sumário

Lista de figuras

Lista de tabelas

1. Introdução geral

O principal objetivo desta tese consiste em contribuir para o conhecimento dos sistemas mesofóticos da Plataforma Continental Brasileira, especialmente os sistemas produtores de carbonato de cálcio, nos quais as algas coralináceas (AC) desempenham um papel relevante. O estudo concentrou-se em duas áreas, a Margem Continental Amazônica (MCA) e a Bacia Sergipe-Alagoas (SEAL), nas quais havia material e dados disponíveis que poderiam permitir o avanço do conhecimento. Na MCA, já realizei trabalhos focados em nódulos de AC e nódulos de briozoários (Vale et al., 2018) e durante o desenvolvimento da tese meu trabalho concentrou-se nas estruturas identificadas como recifes mesofóticos na foz do rio Amazonas (Moura et al., 2016), tentando entender sua distribuição espacial, estrutura interna e o contexto no qual se desenvolveram a partir do Último Máximo Glacial (*Last Glacial Maximum* - LGM). No caso da Bacia SEAL, além das informações sobre a distribuição de sedimentos no fundo do mar, o material disponível era principalmente amostras de nódulos de AC (rodolitos), e por isso meu trabalho se concentrou na análise de sua composição e estrutura para entender sua história e o ambiente em que cresceram.

1.1. Recifes mesofóticos

Quanto se fala em recifes mesofóticos, em geral, se refere aos ecossistemas coralíneos mesofóticos (*Mesophotic Coral Ecosystems* - MCEs), que são comunidades bentônicas compostas por corais escleractíneos, AC, e espécies associadas, particularmente esponjas, que vivem entre 30-150 m de profundidade em regiões tropicais e subtropicais (Hinderstein et al., 2010). A distribuição e estrutura da comunidade dos MCEs são heterogêneas, e podem ser controladas por fatores como transparência da água, afloramento costeiro e fluxo de sedimentos (Bridge et al., 2019). Apesar de uma forte diminuição da riqueza de espécies abaixo de 60 m,

os MCEs em profundidades mesofóticas mais baixas são mais extensos e mais diversos do que se pensava anteriormente (Englebert et al., 2017).

Em geral, são sistemas pouco conhecidos porque os estudos eram limitados pela falta de tecnologia ou, quando existe disponibilidade da tecnologia apropriada (Veículos Operados Remotamente -ROV- e submersíveis tripulados), é bastante custoso. Apesar de que, pesquisas dos MCEs realizadas nas últimas duas décadas lançaram luz sobre sua distribuição e composição em diferentes regiões do mundo (por exemplo, Armstrong et al., 2006, 2019; Kahng & Kelley, 2007; Bridge & Guinotte, 2013; Sinniger et al., 2019; Weinstein et al., 2021). Entretanto, a compreensão do potencial de acreção vertical dos MCEs e os fatores que controlam seu início, crescimento e desaparecimento são bastante limitados.

Estes ecossistemas são considerados como extensões de ecossistemas coralíneos rasos, com os quais compartilham espécies em comum. Os MCEs servem como habitat para algumas espécies de peixes com importância econômica e ecológica, que utilizam essas áreas para desova, reprodução, alimentação e crescimento até a maturidade. Nos últimos anos, o potencial dos recifes mesofóticos como fontes para repovoamento ou restabelecimento de espécies degradadas em recifes de águas rasas, tem sido valorizado.

Na MCA, uma série de afloramentos rochosos são ocupados por comunidades bentônicas incrustantes, incluindo alguns corais hermatípicos, esponjas e algas coralináceas incrustantes (ACI), alguns dos quais são produtores de carbonato de cálcio (Moura et al., 2016; Francini-Filho et al., 2018; Araújo et al., 2021). Essas comunidades incrustantes podem ser consideradas mesofóticas, pois ocorrem a dezenas de metros de profundidade e incluem organismos que dependem da luminosidade, tais como algas e corais zooxantelados, e heterótrofos que não dependem da luminosidade, como as esponjas (Lesser et al, 2009).

1.2. Rodolitos e bancos de rodolitos

As AC pertencem ao filo Rhodophyta (Corallinales, Hapalidiales, Sporolithales) e podem se desenvolver desprendidas dos substratos, formando estruturas denominadas rodolitos (Fig. 1A), que são nódulos calcários de vida livre, formados na sua maior parte por uma ou mais espécies de ACI (>50% da cobertura) (Steneck, 1986; Foster, 2001; Le Gall et al., 2010). Apresentam ampla variedade de formas e tamanhos, e podem se fusionar formando concreções carbonáticas (Fig. 1B), como em alguns exemplos na Plataforma Continental Brasileira (Holz et al., 2020). Os rodolitos são encontrados agrupados, formando bancos de rodolitos, os quais modulam direta ou indiretamente a disponibilidade de recursos e, portanto, desempenham papel chave na ocorrência e abundância das espécies a eles associadas (Pereira-Filho et al., 2015). Durante seu lento processo de crescimento (cerca de 1,0 ± 0,5 mm yr^{-1} em espessura, Amado-Filho et al., 2012a), os bancos de rodolitos transformam fundos homogêneos de sedimentos inconsolidados em substratos duros e heterogêneos. Os bancos de rodolitos representam uma capa calcária viva sobre fundos, suportando comunidades diversificadas (Fig. 1C), e muitas vezes únicas, de espécies associadas (Foster et al., 2013), formadas por microrganismos, macroalgas, invertebrados e peixes (Pereira-Filho et al., 2011; Cavalcanti et al., 2013; Meirelles et al., 2015; Pinheiro et al., 2015; Brasileiro et al., 2015; Moura et al., 2016).

Os bancos de rodolitos são importantes locais de assentamento e viveiros de espécies, algumas das quais de importância econômica, raras e/ou endêmicas (Guimarães & Amado-Filho, 2008; Villas-Boas et al. 2009; Amado-Filho & Pereira-Filho, 2012c; Marins et al., 2012; Bahia et al., 2014a, 2014b, 2014c). Esse ecossistema suporta a ocorrência de espécies de grande porte como a macroalga '*kelp*' *Laminaria abyssalis* (Fig. 1B), endêmica da região norte do Rio de Janeiro e sul do Espírito Santo, grandes populações de lagostas (*Panulirus argus*) e peixes como o pargo (*Lutjanus purpureus*) e o dentão (*Lutjanus jocu*), além de espécies endêmicas de

peixes tipicamente recifais (Pinheiro et al., 2015), como o "tilefish" *Malacanthus plumieri*, que atua como um importante componente para aumento da área de extensão dos bancos de rodolitos e favorece a conectividade entre os bancos rasos e mesofóticos (Amado-Filho et al., 2017).

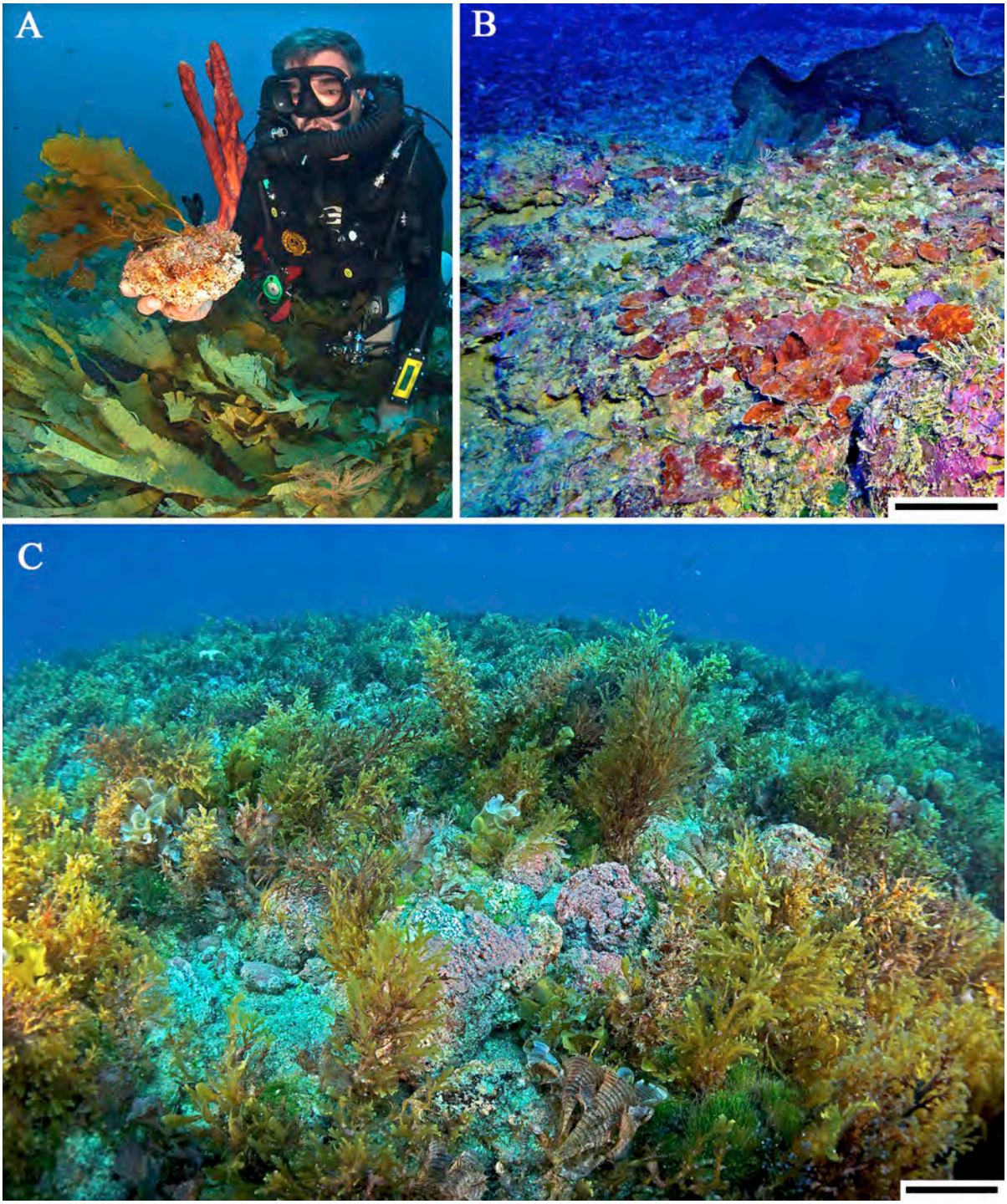

Figura 1. (**A**) Rodolito individual, com espécies de esponjas crescendo na superfície, encontrado a 28 m de profundidade, no banco de rodolitos em Abrolhos/BA. (**B**) Concreções carbonáticas cobertas por

ACI (coloração vináceas) e *Peyssonnelia* spp.(coloração avermelhada) com a alga *Laminaria abyssalis* (coloração escura, à direita e acima na imagem), a 70 m de profundidade no sul da plataforma do Rio Doce/ES. (**C**) Banco de rodolitos no Parque Nacional Banco dos Abrolhos/BA, a 8 m de profundidade. Note a presença AC vivas (coloração vináceas) e assembleia de macroalgas associadas aos rodolitos, que compõem o fundo (Fotos: Áthila Bertoncini, Nicholas Vale, Fernando Moraes/Rede Abrolhos). Barras de escala ≈ 10 cm.

Os bancos de rodolitos são amplamente distribuídos pelo mundo e, em termos de cobertura espacial, estão entre as maiores comunidades bentônicas marinhas do planeta dominadas por macroalgas (Foster, 2001). As ACI têm sido reconhecidas como um dos componentes mais abundantes do recobrimento do fundo dos ambientes costeiros e mesofóticos (entre 30 e 270 m de profundidade, Lesser et al. 2009) no Brasil (Pereira-Filho et al., 2011; Pereira-Filho et al., 2012; Amado-Filho et al., 2012a; Amado-Filho et al., 2012b; Amado Filho et al., 2017; Moura et al., 2013; Holz et al., 2020). Os primeiros estudos que localizaram fundos de algas calcárias no Brasil tinham apenas caráter geológico e focavam na caracterização dos sedimentos da plataforma continental e perspectivas de potencial exploração mineral deste recurso (Kempf, 1970; Mabessone et al., 1972; Milliman & Amaral, 1974; Milliman, 1977; Vicalvi & Milliman, 1977). Desse ponto de vista, depósitos de ACI, na forma de rodolitos, estão contidos em uma definição que abrange os sedimentos ricos em carbonato, chamados de “grânulos bioclásticos” (Cavalcanti, 2011). Como apresentado por Dias (2000), os depósitos naturais de granulados bioclásticos do Brasil são formados principalmente por ACI.

Amado Filho et al. (2017), em uma revisão de banco de rodolitos para o Atlântico Sul, ressaltam que a partir de meados dos anos 90 esses bancos começaram a ser estudados sob um ponto de vista biológico, e, em outros casos, do ponto de vista sedimentológico (Testa, 1997; Testa & Bosence, 1999), provendo informações sobre o mapeamento e estrutura do banco de rodolitos da costa Nordeste brasileira. Hoje, pode-se confirmar a proposição de Foster (2001) que aponta a costa brasileira como a região com a mais ampla faixa de distribuição latitudinal

de bancos de rodolitos no mundo (Amado Filho et al., 2017), apresentando uma variação da abundância e densidade seguindo o gradiente latitudinal entre ~3ºS e 27ºS, com valores mais altos em locais tropicais diminuindo em direção ao temperado quente (Carvalho et al., 2020). Os bancos de rodolitos ocupam extensas áreas da Plataforma Continental Brasileira, desde a Margem Equatorial na Foz do Amazonas (2ºN) até o Cabo Frio (23ºS) (Kempf, 1970; Milliman, 1977; Amado Filho et al 2007, 2010, 2012a; Moura et al., 2016; Vale et al., 2018), incluindo as plataformas insulares de Fernando de Noronha (Amado-Filho et al., 2012b; Pereira-Filho et al., 2015), do Atol das Rocas (Amado-Filho et al., 2016), os topos dos montes submarinos da Cadeia Vitória-Trindade (Pereira-Filho et al., 2012) e ocorrências isoladas nas ilhas de Queimada Grande (24ºS) (Pereira-Filho et al., 2019) e Arvoredo (27ºS) (Gherardi, 2004; Metri, 2006; Horta et al., 2016). Destaca-se a ocorrência do maior banco de rodolitos do mundo, descrito na plataforma continental de Abrolhos, com uma área de ca. 21.000 km^2 (Amado Filho et al., 2012a). Contudo, a principal lacuna geográfica de conhecimento sobre os aspectos biológicos e geológicos de bancos de rodolitos, incluindo suas espécies formadoras, é a região nordeste do Brasil, mais especificamente a região que compreende a plataforma continental entre Sergipe e Pernambuco, incluindo a região da foz do rio São Francisco (Amado-Filho et al., 2017).

1.3. Diversidade de algas coralináceas no Brasil

Muitos bancos de rodolitos em todo o mundo são compostos por duas ou três espécies de ACI (Konar et al., 2006) e cada rodolito é geralmente constituído por uma única espécie. Nos bancos de rodolitos do Brasil várias espécies podem ser encontradas formando rodolitos em uma área relativamente restrita (Amado-Filho et al., 2010, 2012a), e não é incomum encontrar até quatro espécies de ACI crescendo na superfície de um rodolito (Amado-Filho et al., 2017). Atualmente, estão registradas 35 espécies morfo-anatômicas de ACI formadoras de rodolitos da plataforma continental, montes submarinos e ilhas oceânicas do Brasil, a maioria

ocorrendo em águas tropicais correspondendo a uma riqueza maior do que a soma de todas as espécies descritas para outras regiões do planeta (Amado Filho et al., 2017; Richards et al., 2019; Leão et al., 2020). Entre os membros da ordem Hapalidiales, o gênero multiespecífico *Roseolithon* (anteriormente reconhecido como a espécie única *Lithothamnion crispatum* no Brasil) é uma das principais espécies de ACI formadoras de rodolitos da plataforma continental brasileira (Riul et al., 2009; Amado Filho et al., 2012b, 2017; Pascelli et al., 2013; Brasileiro et al., 2015; Coutinho et al. 2021). Entre as algas da ordem Sporolithales, atualmente, existem 29 espécies reconhecidas de *Sporolithon* no mundo, das quais 13 são registradas no Brasil, a saber, *S. amadoi*, *S. australasicum*, *S. durum*, *S. elevatum*, *S. episoredion*, *S. episporum*, *S. erythraeum*, *S. franciscanum, S. howei*, *S. molle*, *S. pacificum*, *S. tenue* e *S. yoneshigueae* (Bahia et al., 2014b, c, 2015; Jesioneck et al., 2016; Richards et al., 2019; Leão et al., 2020). Com exceção da *S. howei*, que foi registrada formando concreções calcárias, todas as espécies foram relatadas para ocorrer em bancos de rodolitos brasileiros (Bahia et al., 2014b, 2015; Jesioneck et al., 2016; Leão et al., 2020). A ordem Corallinales ocupa diferentes habitats nos recifes do sudoeste do Oceano Atlântico (Sissini et al., 2021), estruturando recifes biogênicos (por exemplo, *Porolithon* em Atol das Rocas, Gherardi & Bosence 2001), tanto em recifes rochosos (por exemplo, *Lithophyllum atlanticum* no Sudeste do Brasil, Sissini et al., 2021) quanto em bancos de rodolitos (Pascelli et al. 2013).

Sissini et al. (2021) revelaram 79 espécies filogenéticas de ACI delimitadas por métodos baseados em DNA nas diferentes ecoregiões da Plataforma Continental Brasileira (Fig. 2), com maior riqueza encontrada entre as latitudes 12° S e 22° S (Brasil Oriental), 5 registradas na ecoregião da Amazônia e 23 na costa Nordeste do Brasil (Sissini et al., 2021), onde ambas ecoregiões foram foco do presente estudo. Este resultado é congruente com o padrão de riqueza de gêneros de Rhodophyta em escala global observado por Keith et al. (2014). Ressalta-se que a diversidade taxonômica das comunidades de ACI varia de acordo

com a região geográfica em que se encontram e com os fatores ambientais, tais como as condições hidrodinâmicas, de luminosidade, profundidade, temperatura da água (Foster, 2001; Bassi et al., 2012), nutrientes e sedimentação (Sissini et al., 2021).

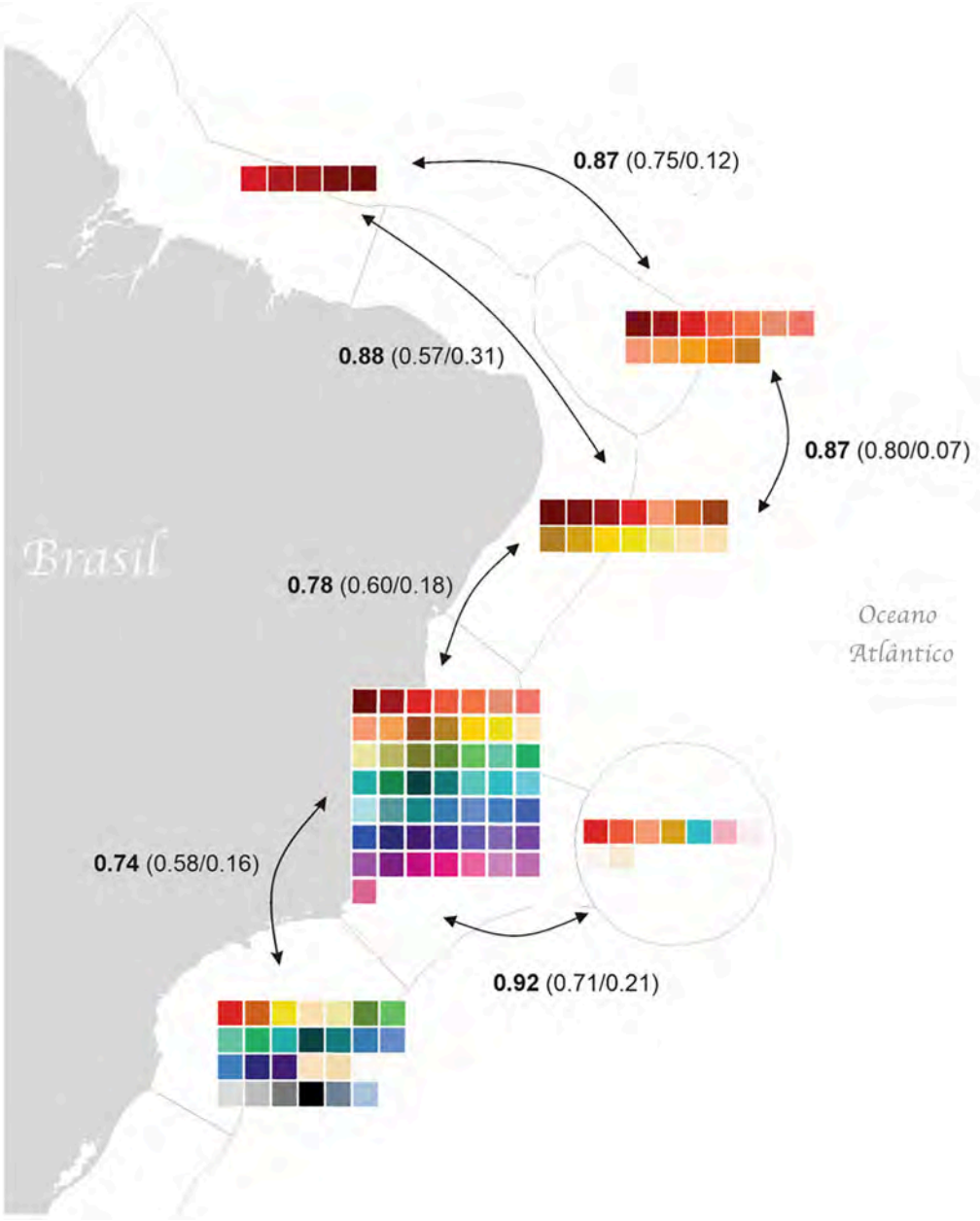

Figura 2. Riqueza de espécies de algas vermelhas coralináceas (79) e diversidade beta Jaccard ($ß_{JAC}$, números em negrito) ao longo e entre ecoregiões no sudoeste do Oceano Atlântico. Cada espécie filogenética está representada por um quadrado de uma cor específica [Adaptado de Sissini et al. (2021)].

1.4. Recifes e bancos de rodolitos e a variação do nível do mar

O Período Quaternário é marcado por mudanças climáticas globais que impuseram grandes variações do nível do mar, conduzindo alterações significativas no padrão ecológico e sedimentar das margens continentais. Os registros destas mudanças estão guardados nos sedimentos e rochas que hoje compõem a sequência estratigráfica destas plataformas. No LGM (cerca de 26 mil anos), o nível do mar chegou a uma cota de -120 m (por exemplo, Yokoyama et al., 2018). A posterior deglaciação, ou processo transgressivo, conduziu uma subida do nível do mar para a ordem de 120 m em pouco mais de 12 mil anos. Entretanto, mesmo no máximo glacial, evidências de colonização de recifes rasos nas bordas de plataformas continentais são descritos em todo o mundo, por exemplo, no Pacífico Sul (Flamand et al., 2008), Havaí (Webster et al., 2004), Caribe (Blanchon et al., 2002), Austrália (Woodroffe et al., 2010; Abbey et al., 2011b; Webster et al., 2018; Yokoyama et al., 2018), entre outros. Os pulsos de subida do nível do mar durante a última transgressão também estão registrados em recifes submersos ao longo das plataformas (Fairbanks, 1989; Abbey et al., 2011a, Camoin et al., 2012; Moura et al., 2013; Weil-Accardo et al., 2016), criando um registro geológico dos processos transgressivos.

Com a elevação do nível do mar, áreas recifais passam a ser afogadas, respondendo rapidamente a esta nova condição, seja por uma transição na comunidade formadora ou uma total parada de crescimento do recife (por exemplo, Webster et al., 2018). Logo, com o processo transgressivo, pode-se dizer que a plataforma carbonática e seus recifes associados registram a evolução paleoecológica e paleoceanográfica do sistema (Abbey et al., 2013). Contudo, uma plataforma carbonática não é representada apenas por recifes coralíneos. A sedimentação biogênica ou bioclástica (esqueletos, conchas, carapaças), incluindo os bancos de rodolitos, também formam extensos depósitos que refletem as variações relativas do nível do mar. Bastos et al. (2016) demonstraram como parte da plataforma carbonática de Abrolhos respondeu a

transgressão marinha ocorrida nos últimos 18 mil anos. Demonstrou-se, por exemplo, que a acreção média da plataforma carbonática a cada mil anos é de um metro de espessura de matriz carbonática derivada da mineralização em resposta a elevação do nível do mar (Bastos et al., 2016).

1.5. Áreas de estudo

O foco deste trabalho se deu em duas áreas chave da Plataforma Continental Brasileira, a Margem Continental Amazônica e a Bacia Sergipe-Alagoas (Fig. 3), ambas localizadas na região oceânica das duas maiores bacias hidrográficas do Brasil: Amazônica e São Francisco, respectivamente. Ressalta-se que a bacia Amazônica é a maior do mundo (Machado & Pacheco, 2010) e o rio Amazonas é responsável por aproximadamente 20% da descarga global fluvial no oceano (Coles et al., 2013) e produz uma descarga de sedimentos de aproximadamente 10×10^6 t ano^{-1} (Nittrouer & DeMaster, 1996). Sendo, portanto, uma área onde não se esperava que houvesse ambientes de recife e banco de rodolitos, devido à enorme entrada de sedimentos terrígenos na plataforma ao longo do tempo, o que impediria, em teoria, o crescimento de organismos fotossintetizantes.

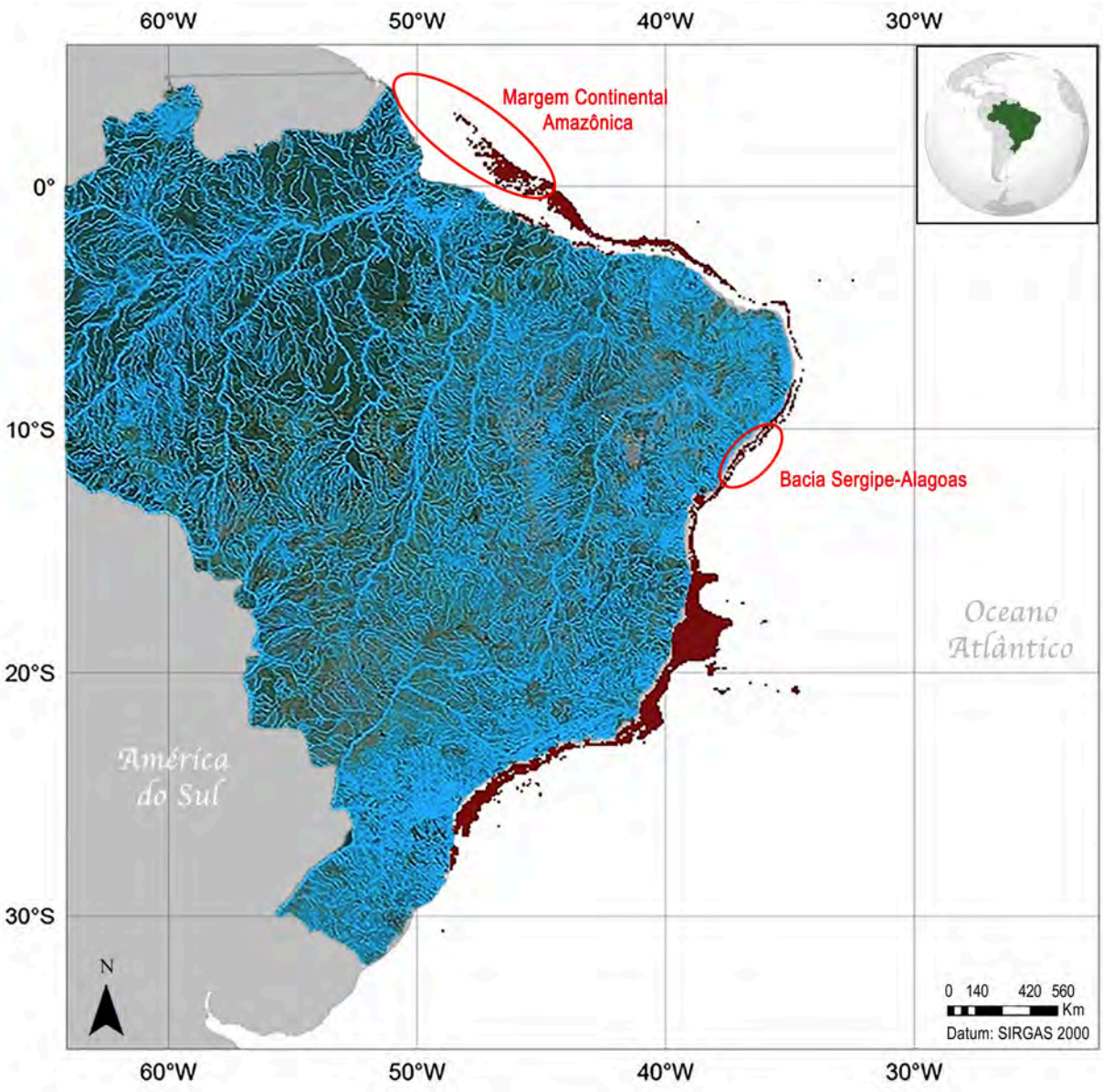

Figura 3. Mapa hidrográfico evidenciando a distribuição potencial dos bancos de rodolitos (coloração vermelho escuro) e as áreas de estudo (elipses em vermelho) ao longo da Plataforma Continental Brasileira [Adaptado de Carvalho et al. (2020) e *Google Earth tools* "Recurso Hídrico do Brasil"].

1.5.1. Margem Continental Amazônica (MCA)

A região da Margem Equatorial Brasileira, que está situada entre os estados do Amapá e Rio Grande do Norte, com aproximadamente 2.400 km de extensão é composta por cinco bacias sedimentares (Foz do Amazonas, Pará-Maranhão, Barreirinhas, Ceará e Potiguar) (Palma, 1979). A Margem Continental Amazônica (MCA) engloba as bacias Foz do Amazonas e Pará-Maranhão. Esta região representa uma das principais fronteiras de conhecimento no

contexto global. Até o final do século XX, o estado do Maranhão (MA) era considerado o limite norte para a ocorrência de recifes coralíneos no Brasil (Moura et al., 1999). Entretanto, a existência de um megasistema recifal na MCA, situada entre a fronteira Brasil-Guiana Francesa e o MA, já vinha sendo relatada desde a década de 1970 em estudos que sugeriram a presença de fundos carbonáticos na região, apesar da abordagem geológica com perspectivas de potencial exploração mineral e pesqueira (Kempf, 1970; Milliman & Amaral, 1974; Milliman, 1977; Colletti & Rützler, 1977). Em 2014, a coleta de material por dragagem e rede de arrasto, durante Expedição Oceanográfica ao longo da MCA, permitiu a caracterização básica dos 'recifes' e bancos de rodolitos e macróides (Moura et al., 2016; Vale et al., 2018). Moura e colaboradores (2016) evidenciaram a importância biológica dessas formações confirmando a ocorrência de um extenso sistema carbonático em um gradiente de condições singulares regidas pela pluma do Rio Amazonas ao longo do tempo e do espaço.

O mapeamento acústico e a obtenção de imagens em alta resolução recentemente obtidos durante expedição em 2017 a bordo do R/V *Alucia* (*Woods Hole Oceanographic Institution/ Ocean X*) permitiram o mapeamento de estruturas e fundos recifais (Fig. 4) entre 110 e 230 m de profundidade. O avanço das descrições permitiu Araújo et al. (2021) definir a área das formações carbonáticas ao longo da MCA, com cerca de 42,699 km^2. Essas formações sob influência do rio Amazonas representam um megahabitat marinho com biodiversidade, condições físico-químicas e geomorfologia acopladas à evolução e à dinâmica do rio. Portanto, além dos aspectos científicos e práticos já destacados, os resultados obtidos recentemente (Moura et al., 2016; Vale et al., 2018; Araújo et al., 2021) representam contribuição para alterar a percepção geral de que a Amazônia brasileira se restringe aos grandes rios, à floresta e sua fauna, uma vez que o ecossistema amazônico se estende pelo Atlântico, onde, além de proporcionar vultuoso sequestro de carbono, condiciona um sistema recifal ímpar.

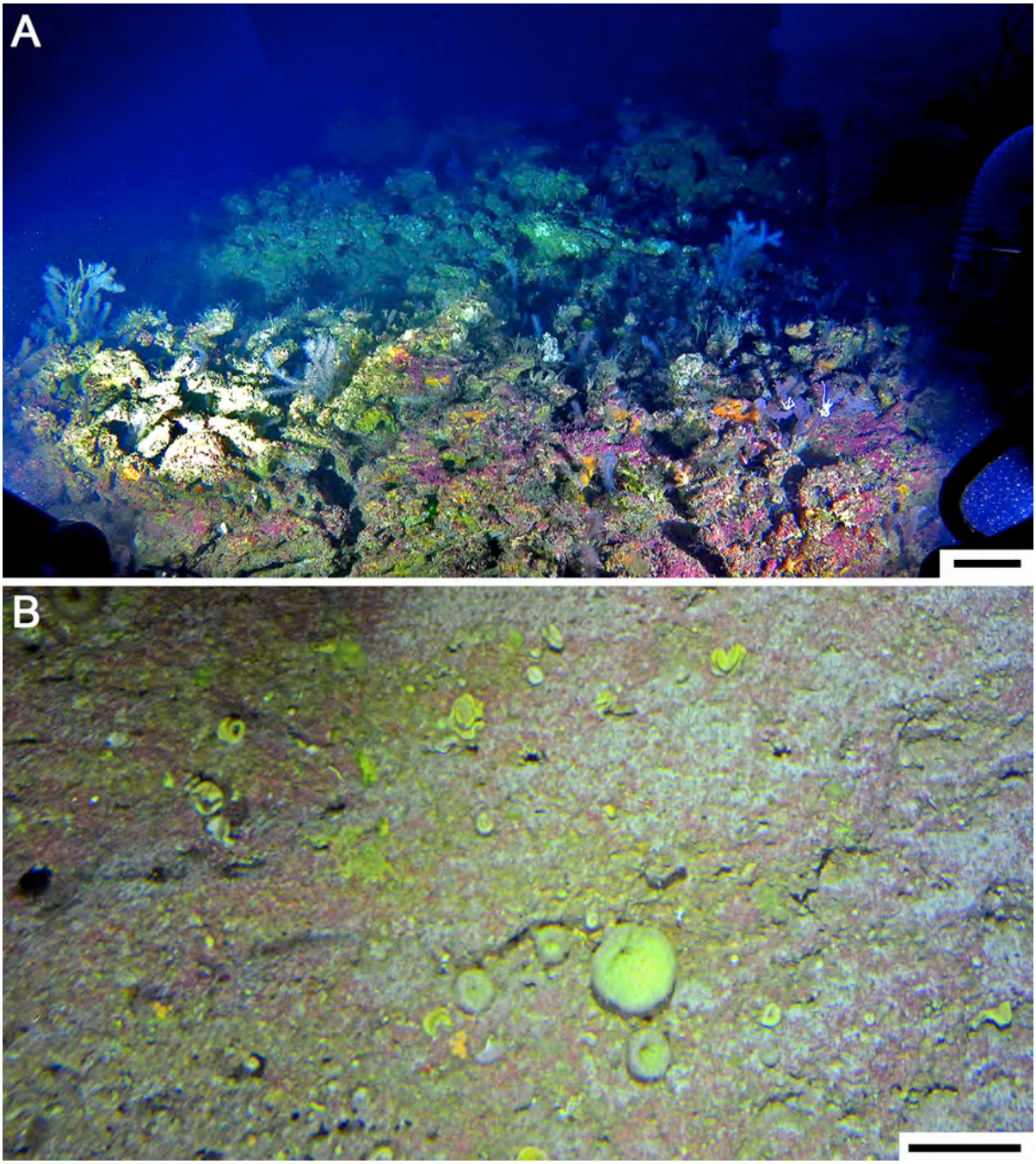

Figura 4. Imagens obtidas com submersível tripulado operado pelo *Alucia* (2017), mostrando algas coralináceas (representada pela coloração vináceas) e organismos bentônicos crescendo ativamente sobre estruturas recifais na Margem Continental Amazônica (MCA). (**A**) à 120 m de profundidade no setor Norte da MCA (no extremo norte Estado do Amapá). (**B**) à 230 m de profundidade no setor Sul da MCA (ao norte do Estado do Maranhão). (Fotos: Paulo Salomon, Rodrigo Moura /UFRJ). Barras de escala ≈ 10 cm.

1.5.2. Bacia Sergipe-Alagoas (SEAL)

A plataforma continental de Sergipe-Alagoas (SEAL), localizada na região Nordeste da plataforma brasileira, foi rapidamente inundada pela rápida elevação do nível do mar durante a última deglaciação. A inundação da plataforma começou por volta de 10.000 anos BP e chegou a seu ápice 3.000 anos depois (Bezerra et al., 2003; Caldas et al., 2006). A presença de sedimentos depositados na plataforma continental SEAL sobre uma história geológica representada pela última transgressão marinha, registra o estágio da atual regressão marinha (Fontes et al., 2017). Atualmente, a Bacia SEAL é caracterizada pela baixa entrada fluvial e maior influência das águas de superfície tropical da Corrente Equatorial Sul (SEC) (Santos, 2019; Medeiros et al., 2007). A região da foz do rio São Francisco apresenta uma área total de drenagem de 639.219 km² (7,5% do território nacional) e extensão de 2.863 km (Medeiros et al., 2007). Com a construção de várias barragens (Três Marias, Apolônio Sales, Sobradinho, Itaparica e Xingó), a maior parte dos sedimentos em suspensão que chegava na zona estuarina/costeira e contribuía para a pluma de turbidez, passou a ficar retida nestes reservatórios (Medeiros, 2003; Medeiros et al., 2007). A carga fluvial atual desses sedimentos suspensos é 94% menor do que aquela existente no período anterior à instalação das barragens das hidroelétricas, i.e., até 1973 (Medeiros et al., 2007). Essas condições ambientais promoveram uma predominância de feições carbonáticas entre 30 e 60 m de profundidade, dominadas por cascalho e componentes biogênicos (Coutinho, 2000; Guimarães, 2010; Fontes et al., 2017) com uma biota associada (Guimarães, 2010). Segundo Holz et al. (2020), o influxo de sedimentos depende da descarga de grandes rios e influencia diretamente a distribuição de sedimentos de fundo e bancos de rodolitos.

A sedimentação marinha da plataforma continental SEAL foi analisada em alguns estudos que caracterizaram a sedimentação holocênica, mapeando a distribuição espacial dos principais componentes carbonáticos e siliciclásticos do fundo marinho (Guimarães, 2010;

Nascimento, 2011; Fontes et al., 2017), e suas contribuições para a formação do sedimento superficial, comparando características bióticas e abióticas (Santos et al., 2019). Jesus et al., (2017) relatam um aumento da influência marinha na região a partir de 2.000 anos atrás, quando o nível do mar na costa brasileira ainda estava entre 1-2 m acima do nível atual. Devido à grande variedade de sedimentos biogênicos e siliclásticos associados, a identificação dos sedimentos biogênicos é de fundamental importância, pois indica a presença de organismos e sua relação com as condições ambientais (Mutti & Hallock, 2003). Segundo Fontes et al. (2017), a porção média e externa dos ca. 10.000 km^2 da plataforma SEAL são áreas que apresentaram fundos rugosos, topografias mais elevadas e teor mais elevado de carbonatos. Apesar da redução progressiva da entrada de sedimentos terrígenos nessa região da plataforma brasileira, com consequente aumento da sedimentação carbonática, esses ambientes dominados por banco de rodolitos, não apresentavam estudos sobre sua distribuição, estrutura e composição específica de espécies de AC até o momento.

1.6. Objetivos

O objetivo geral desta tese de Doutorado foi investigar a distribuição, composição e formação de estruturas recifais e fundos de rodolitos na Margem Continental Amazônica (MCA) e na Bacia Sergipe-Alagoas (SEAL); e relacionar as idades dessas estruturas recifais e bancos de rodolitos com as condições ambientais e mudanças no nível do mar, principalmente desde o último máximo glacial até o Holoceno, para inferir os possíveis eventos ambientais e geológicos regionais que influenciaram as variações nas comunidades de recifes e bancos de rodolitos.

Os objetivos específicos foram:

1. Determinar a distribuição, morfologia e composição de estruturas proeminentes mapeadas no Setor Norte da MCA e outras feições distintas na plataforma externa e

na borda da plataforma dos setores Centro e Sul, a fim de realizar interpretações paleoambientais da evolução dos recifes com base em novas datações do radiocarbono e características geomorfológicas, sedimentológicas e paleontológicas;

2. Determinar a estrutura e composição dos bancos de rodolitos da plataforma média e externa da Bacia Sergipe-Alagoas, e relacionar a datação radiométrica dos rodolitos obtidos em diferentes profundidades com mudanças ambientais ocorridas na plataforma.

2. Material e Métodos

2.1. Amostragem

O trabalho de campo na Margem Continental Amazônica (MCA) foi realizado durante a expedição oceanográfica a bordo do R/V *Alucia* (*Woods Hole Oceanographic Institution*/ *Ocean* X) em julho de 2017. Amostras de rochas (*n*= 9) foram coletados com ajuda de submersível tripulado em diferentes profundidades, ao longo dos três setores do MCA: Setor Norte, Central e Sul (Tabela 1). Posteriormente o material foi armazenado no Laboratório de Algas do Instituto de Pesquisas Jardim Botânico do Rio de Janeiro (IPJBRJ-Brasil).

O trabalho de campo na Bacia Sergipe-Alagoas (SEAL) foi realizado no âmbito do Projeto de Caracterização Regional da Bacia SEAL, pela Petrobras (Petróleo Brasileiro Inc., Rio de Janeiro, RJ, Brasil) e pela Universidade Federal de Sergipe (UFS). Amostras de rodolitos (*n*= 404) foram obtidas durante duas expedições oceanográficas: a bordo do R/V *Luke Thomas,* em fevereiro de 2011, e a bordo do R/V *Seward Johnson*, em junho de 2011, com auxílio de rede de arrasto em diferentes profundidades, ao longo dos três setores da Bacia SEAL: Setor Norte, Central e Sul (Tabela 1). As amostras foram inicialmente armazenadas no Laboratório de Bentos da UFS e posteriormente cedidas ao IPJBRJ para o presente estudo.

Tabela 1. Localização dos locais de estudo, faixas de profundidade da água, dispositivo de amostragem, número de amostras e data da coleta. Coordenadas em SIRGAS 2000 Datum. MCA = Margem Continental Amazônica; SEAL = Sergipe-Alagoas.

Área	Setor	Latitude	Longitude	Profundidade (m)	Dispositivos de amostragem	Amostras (*n*)	Data
MCA	Norte	4.372717	-49.922133	100-120	Submersível	7	07/2017
MCA	Central	1.521867	-46.742383	250-378	Submersível	1	07/2017
MCA	Sul	-0.453100	-43.983333	70-240	Submersível	1	07/2017
SEAL	Norte	-10.2789	-35.9792	30	Rede de arrasto	07	02/2011
SEAL	Norte	-10.4875	-36.1245	30	Rede de arrasto	173	02/2011
SEAL	Central	-10.8223	-36.6118	27	Rede de arrasto	04	06/2011
SEAL	Central	-10.8694	-36.5472	47	Rede de arrasto	141	06/2011

SEAL	Sul	-11.1642	-36.8839	47	Rede de arrasto	05	02/2011
SEAL	Sul	-11.3389	-37.0556	54	Rede de arrasto	18	02/2011
SEAL	Sul	-11.5989	-37.2384	50	Rede de arrasto	56	06/2011

2.2. Mapeamento do fundo oceânico

As imagens *in situ* incluíram vídeos de alta resolução (Material Suplementar dos Capítulos 3 e 4). Na plataforma externa da MCA os vídeos obtidos por operações submersíveis em julho/2017 mostraram três áreas que são tipicamente dominadas por estruturas de alto relevo (Setor Norte entre 100-120 m de profundidade) e afloramentos (Setor Central entre 250-378 m de profundidade e Setor Sul entre 180-230 m de profundidade) (Material Suplementar Video S1- Capítulo 3). Na Bacia SEAL as inspeções de vídeos foram realizadas pela Petrobras com um Veículo Operado Remotamente (ROV) obtidas de fevereiro a março de 2014 ao longo de quatro transectos com comprimento de 4 km cada transecto (53 vídeos de 33 horas no total), variando de 25 a 46 m de profundidade (Material Suplementar Tabela S1 e Video S1- Capítulo 4).

2.3. Dados batimétricos

A descrição geomorfológica de cada área de estudo foi baseada principalmente na batimetria, e três derivados batimétricos foram extraídos para melhorar a caracterização. Na ACM os dados acústicos foram obtidos com um *Reson Seabat* 7160 *Echo Sounder* operando a uma frequência nominal de 44 kHz. Posteriormente foram processados com o software CARIS HIPS e SIPS para remover o ruído e ajustar a velocidade do som na coluna de água. Os derivados batimétricos (Índice de Posição Batimétrica [BPI] escala fina, Declive e Robustez do terreno) foram calculados usando a caixa de ferramentas ArcGIS do Modelador de Terreno Bentônico. Todas as imagens foram feitas usando Fledermaus, Caris e ArcGIS (Figura 1 - Capítulo 3). Na Bacia SEAL as classes de biofacies e dados sedimentológicos (Fontes et al., 2017) foram sobrepostas ao conjunto de dados batimétricos (Santos et al., 2019) e incorporadas

em um ambiente de sistema de informações geográficas (GIS) na plataforma QGIS para produzir o mapa usado neste estudo (Figura 1 - Capítulo 4).

2.4. Petrografia

Pequenos blocos (3×3 cm) foram cortados de 22 amostras de rochas selecionadas da ACM e de 15 amostras da Bacia SEAL, posteriormente foram enviados ao *National Petrographic Service Inc.* (Rosenberg, TX, EUA) para confecção de 37 lâminas petrográficas (25×50 e 50×75 mm). Os dados de campo coletados incluíram litologia, litofacies, identificação das AC, componentes principais e secundários. As descrições litológicas/textura seguiram a classificação de Dunham (1962), modificada por Embry e Klovan (1972). As proporções médias (%) dos componentes principais de rochas e rodolitos, fósseis vestigiais, espaços vazios e sedimentos foram estimados a partir de imagens obtidas de cada lâmina fina usando o programa CoralNet (Beijbom et al., 2015) e estão detalhadas nos resultados dos Capítulos 3 e 4.

2.5. Taxonomia

Foram identificados macro invertebrados fósseis marinhos e bioerosores até o menor nível taxonômico possível. As formas não-geniculadas de crescimento das AC foram classificadas com base em sua morfologia como incrustadas, verrugas incrustadas, grumosas e ramificadas, de acordo com (Basso, 1998; Woelkerling et al. 1993). A identificação de AC nas superfícies externas das amostras foi baseada em seções histológicas de material fértil, seguindo Maneveldt e Van der Merwe (2012), Bahia (2014), Basso et al. (2018), Costa et al. (2019) e Leão et al. (2020). A lista dos espécimes identificados neste estudo com números de catálogo, nomes de localidade e números de estação foi inserida no Material Suplementar dos Capítulos 3 e 4.

2.6. Datação por Radiocarbono

Cinco subamostras de fósseis marinhos encontrados em amostras de rochas da ACM e 8 amostras da Bacia SEAL (10-20 mg de pó de carbonato de cálcio obtidos de cada amostra) foram analisados no *Center for Applied Isotope Studies* (*Georgia University*, Atenas, GA, EUA) utilizando a Espectrometria de Massa com Aceleradores (AMS, *nuPlasma II multi-collector*). Os dados convencionais de radiocarbono foram recalibrados usando o software CALIB 8.2 (Stuiver et al., 2020) e a curva de calibração Marine20 (Heaton et al., 2020) fatorizando um efeito de reservatório global. As datas foram relatadas como anos civis anteriores ao presente (ano calendário AP; "presente" = 1950 D.C.) usando um intervalo de confiança de 2-sigma.

3. Distribution, morphology and composition of mesophotic 'reefs' on the Amazon Continental Margin

Published in *Marine Geology* **2022**, v. 447, p. 106779. (Appendix 1)

AUTHORS: Nicholas F. Vale, Juan C. Braga, Rodrigo L. de Moura, Leonardo T. Salgado, Fernando C. de Moraes, Claudia S. Karez, Rodrigo T. de Carvalho, Paulo S. Salomon, Pedro S. Menandro, Gilberto, M. Amado-Filho, Alex C. Bastos

Abstract

The geomorphology of the Amazon Continental Margin (ACM) is highly heterogeneous and includes a variety of reef-like formations found in deep-water along the shelf-slope transition. The ACM has been divided into three Sectors (Northern, Central and Southern) according to the distribution of the carbonate producers and the 'reefs', influenced by the Amazon River plume. Here, we characterize these structures that were sampled with a manned submersible and multibeam surveys to depths of up to 230 m, exploring their relationship with the Amazon river plume and changing sea level following the Last Glacial Maximum (LGM). The shelf-slope transition and a deeper shelf break in the Northern Sector of the Brazilian portion of the ACM carry a series of prominent high-relief structures (HRS) that experience a strong fluvial influence. The tops of these features are between 110 and 165 m depths and seem to have originated during lowstands, through erosion of Pleistocene sandstones. Siliciclastic and carbonate deposits accumulated on the tops of these features in shallow waters during the LGM and early deglaciation and were gradually submerged by rising sea level and subsidence. A thin layer of encrusting organisms, coralline algae, sponges, bryozoans and serpulids presently colonizes most of these surfaces at the sites sampled and contributes to the aggregation of thin fine-grained siliciclastic deposits. The Central Sector, off the river mouth, is associated with long-term sediment accumulation and lacks a shelf break. Nevertheless, living benthic communities occur on rock outcrops. The Southern Sector is less influenced by the river plume and includes a shallower shelf-break and a prominent canyon. The surveyed outcrops of Pleistocene carbonate and siliciclastic rocks at 180 m carry thin covers of a benthic community dominated by sponges and coralline algae, which is responsible for the accumulation of a thin (up to a few centimeters) deposit of carbonate bioclasts, quartz sand and mud on the rocky substrate. Thus, the 'reefs' of the outer shelf and mesophotic Amazon margin are typically eroded older rocks, colonized by encrusting organisms during the LGM and deglaciation forming a carbonate veneer, which now support a mesophotic community.

Key words: Amazon reefs; Carbonate and siliciclastic deposits; Sea-level changes; Last Glacial Maximum; Reef morphology.

3.1. Introduction

The Amazon Continental Margin (ACM), extending in the north-western part of the Brazilian Equatorial Margin (BEM), resulted from the opening of the Equatorial Atlantic Ocean in the Early to Late Cretaceous (Doré, 1991; Tetteh, 2016; Pérez-Diaz and Eagles, 2017). It represents one of the world's largest mixed carbonate-siliciclastic platforms, developed during the Neogene in a period of transition from carbonate to siliciclastic-dominated environments in the region (Gorini et al., 2013; Cruz et al., 2019). During the late Miocene, between 8 and 5.5 Myr ago, carbonate sedimentation was dominant, but progressively increasing terrigenous sediment input from the Amazon buried the carbonates of the inner shelf and limited carbonate deposition to the outer north-western shelf until about 3.7 Myr ago (Cruz et al., 2019). The Amazon Cone, which results from the massive long-term terrigenous input from the river, is the dominant morphological feature of the region (Damuth and Kumar, 1975). Within this area, a series of rocky outcrops are encrusted by faunal assemblages with living carbonate producers, including barnacles and crustose coralline algae, which predominate on the outer shelves of the Northern and Southern sectors (up to 240 m depth) (Moura et al., 2016; Francini-Filho et al., 2018; Araujo et al., 2021). These encrusting communities can be considered mesophotic as they occur at tens of meters depth and include a combination of light-dependent organisms, such as algae and minor zooxanthellate corals, and heterotrophs independent of light such as sponges (Lesser et al., 2009). The shelf–slope transition is characterized by a steep shelf break at varying depths, that is generally shallower in the Southern Sector (100 m) than to the North (300 m) (Reis et al., 2016; Lavagnino et al., 2020). Rhodolith beds occur widely along the mid shelf of the Central and Southern sectors, from 23 to 55 m depth, accompanied by a high diversity of other calcifying organisms including bryozoans, barnacles, serpulids, foraminifera, and bivalves

(Vale et al., 2018; Araujo et al., 2021). Macroids, which are free-moving nodules built by encrusting invertebrates (Hottinger, 1983), are less common than rhodoliths and occur between 95 and 120 m depth in the Northern Sector (Vale et al., 2018). There is no clear shelf break in the Central Sector (Moura et al., 2016, Lavagnino et al., 2020), and the smooth shelf-slope transition adjacent to the Amazon Cone has only a few rocky outcrops.

The sedimentary mosaic that results from the dynamic interplay between the world's largest river and the high-energy western Equatorial Atlantic Ocean has been extensively studied in recent decades (e.g., Nittrouer et al., 2021), but the structures described as 'reefs' that occur along the shelf-slope transition (Moura et al., 2016; Lavagnino et al., 2020) remain poorly understood in terms of their distribution, morphology and compositions. They have recently been a subject of discussion in the scientific community and society for their significant biodiversity and the need for their protection and sustainable development (Mahiques et al., 2019; Omachi et al., 2019; Alencar, 2020; Araújo et al., 2021).

This study represents the first systematic description of these offshore rocky structures within the Brazilian portion of the ACM, and is based on multibeam data, rock sampling and video footage acquired during manned submersible dives operated from the R/V *Alucia* oceanographic cruise in 2017. Specifically, our objectives are: a) to analyze the distribution and morphology of the prominent structures mapped in the Northern Sector of the ACM and similar distinctive features on the outer shelf and shelf edge of the Central and Southern sectors, collectively included under the term 'Amazon reefs'; b) to investigate the internal composition of these structures, defining their main components, including bioeroders; c) to perform a paleoenvironmental interpretation of the evolution of the structures based on new radiocarbon dates, and geomorphological, sedimentological and paleontological features.

3.2. Study area

The main types of surficial deposits, from the shoreline to the shelf break of the ACM (Figure 1), include nearshore mud (~27,300 km^2), mud and sand patches (~40,000 km^2), laminated mud (~15,200 km^2), mottled mud (~14,700 km^2), sand (~120,600 km^2), 'reefs' and blocks (~21,400 km^2) and areas with macroids and rhodoliths (~21,300 km^2) (Araújo et al., 2021). The two latter habitats occur between 5°N (Brazil–French Guyana border) and 1°S (Maranhão State, Brazil), where they merge southward with the extensive carbonate domain along the outer shelf of the tropical Brazilian coast (Barreto et al., 1975; Vital, 2014). The area covered by the "reefs" (thousands of square kilometers) along the shelf and shelf break (Moura et al., 2016), may have been overestimated in the "Great Amazon Reef System" described by Francini-Filho et al. (2018). High-relief structures (HRS) or 'reefs' occur throughout the Northern sector outer shelf and comprise a mixture of eroded rigid substrate, forming the initial relief, and locally produced bioclastic debris, with relic components such as ooids (Milliman and Barreto, 1975; Moura et al., 2016). Cruz et al. (2019) suggests that outcrops or relief features in the outer shelf and shelf break are Pleistocene rocks eroded during sea-level lowstands. Unconsolidated Holocene terrigenous sediments dominate the inner shelf and most of the Central Sector, associated with the transition to the Amazon Cone (Damuth and Kumar, 1975).

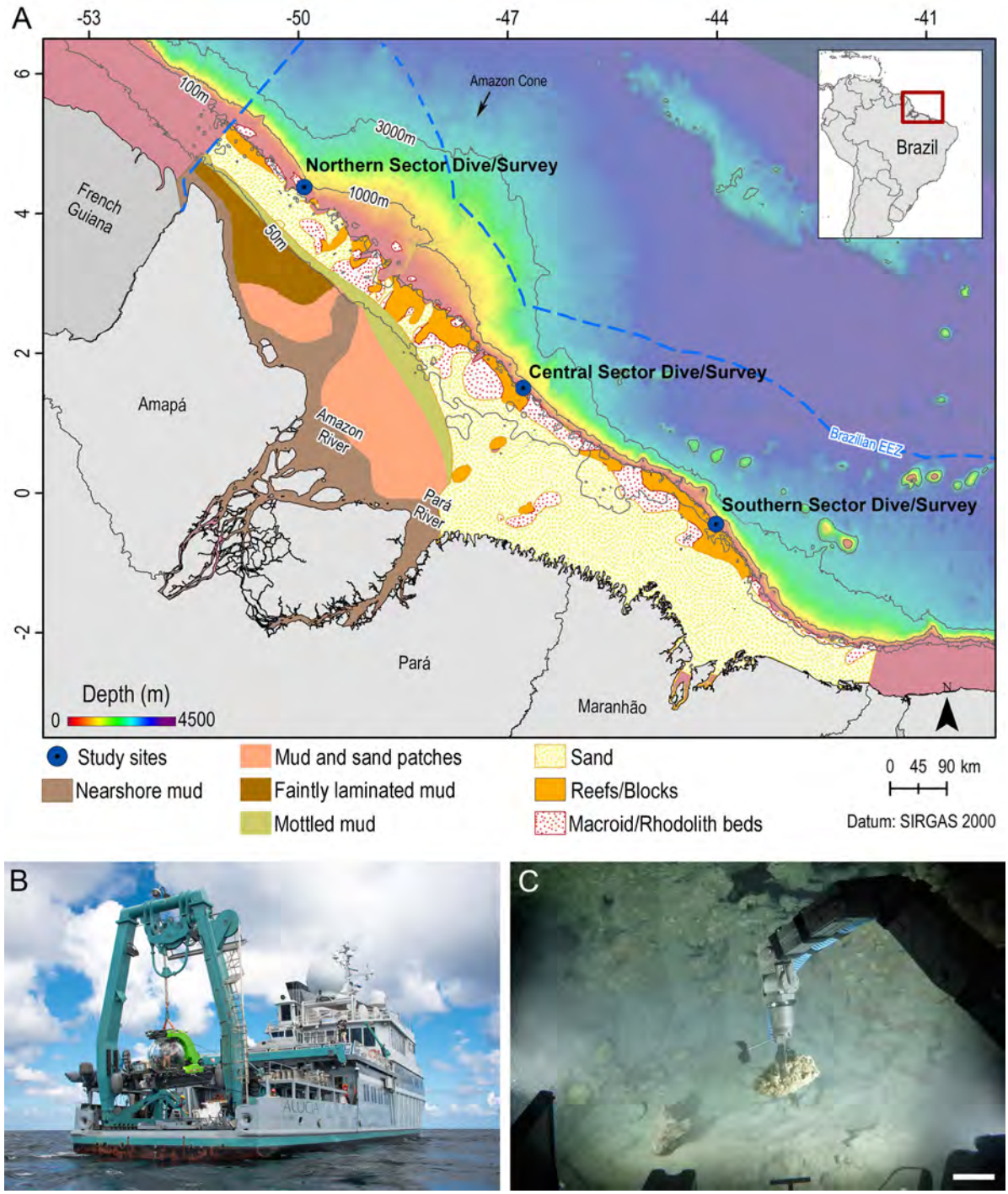

Figure 1. (**A**) Map of the Amazon Continental Margin (ACM) indicating the sites of the acoustic surveys and submersible dives carried out in 2017 (blue circles). EEZ: Exclusive Economic Zone. Bathymetry from GEBCO. (**B**) R/V *Alucia* deploying manned submersible *Deep Rover*. (**C**) Rock sampling at the Southern Sector (180 m depth) using a hydraulic arm. Scale bar = 20 cm.

The ACM is a complex environment subjected to seasonal fluctuations in water turbidity driven by oceanographic and meteorological conditions, fluvial cycles, macrotides and currents mixing sediments (Silva et al., 2005), a drainage basin 6.1 x 10^6 km^2; with a discharge

of 207.7 x 10^3 m^3 s^{-1}; and a sediment load of 1.154 Mt $year^1$ (Syvitski et al., 2005). The Amazon river alone is responsible for approximately 20% of the global discharge to the oceans (Coles et al., 2013), producing approximately 10 x 10^6 t $year^{-1}$ and resulting in a fine-grained submerged delta front (the Amazon Cone) with an area of ~3.3 × 10^5 km^2 (Meade et al., 1979; Nittrouer et al., 1986, 2021; Kuehl et al., 1996; Nittrouer and DeMaster, 1996). Much of the sediment deposited near the mouth of the Amazon and Pará rivers is re-suspended by tidal waves and currents and transported north-westward into the Caribbean by the North Brazil Current (Allersma, 1971). The mixed layer depth and isothermal layer depth in the presence of river discharge is 20−50 m shallower than in areas without continental flows (Varona et al., 2019). The plume is diverted eastward during September and October (Nittrouer and DeMaster, 1996) and its influence on the carbonate domain of the outer shelf is strongest and most significant in the Northern Sector (Moura et al., 2016), north-westward of the Amazon Cone. Southward, the influence of the plume on the shelf and slope lessens and becomes increasingly seasonal, with greater expression from February to April. Mixing and advection on the shelf are responsible for extensive mud deposits along the coasts of Northern Brazil, French Guyana, Suriname, and Guyana (Allison et al., 2000).

The Amazon shelf is up to 300 km wide, sloping gently offshore. The topography of the outer shelf, shelf edge and continental slope is highly heterogeneous because of long-term sediment accumulation, and the effects of ancient, incised river valleys and gravitational failure of slopes (Lavagnino et al., 2020). The sedimentary record of changes in water depth is equally heterogeneous, due to eustatic sea-level variations (Vital, 2014). Carbonate-rich sediments, consisting primarily of barnacles, bryozoans and coralline algal debris, dominate most of the outer shelf north of the Amazon Cone. Magnesian-calcite ooids (Milliman and Barreto, 1975; present study), are also locally abundant in this area together with the high-relief rocky outcrops that are the focus of this study. In the Central Sector, the shelf break is inconspicuous or absent

adjacent to the Amazon Cone due to long-term sediment accumulation. The Southern Sector of the shelf is characterized by an irregular topography, with a steep shelf break, and incised valleys leading to a series of submarine canyons (Lavagnino et al., 2020). Morphological features vary markedly between sectors (Lavagnino et al., 2020). Those in the Northern and Southern sectors are generally erosive, whereas those in the Central Sector reflect sediment deposition. However, slope failure was responsible for re-shaping both erosive and depositional slopes over time (Reis et al., 2016).

3.3. Material and methods

Sampling was carried out from the R/V *Alucia* (Woods Hole Oceanographic Institution/ Ocean X) in July 2017, using the *Deep Rover* submersible with a diving crew consisting of one scientist and a pilot (Fig. 1; Table 1). Acoustic data were obtained with a Reson Seabat 7160 Echo Sounder operating at a nominal frequency of 44 kHz. Data were processed with CARIS HIPS and SIPS software to remove noise and adjust for sound velocity in the water column. The geomorphological description of each study area was primarily based on bathymetry, and three bathymetric derivatives were extracted to improve the characterization. The bathymetric derivatives (Bathymetric Position Index [BPI] fine scale, Slope and terrain Ruggedness) were calculated using the Benthic Terrain Modeler ArcGIS toolbox. The BPI was calculated to assess the elevation differences between a reference point and the mean elevation of its surrounding cells. The terrain ruggedness measures capture variability in slope and aspect and range from 0 (no terrain variation) to 1. All images were made using Fledermaus, Caris and ArcGIS.

Table 1. Location of the study sites and water depth ranges (near the bottom) of the manned submersible dives in the Amazon Continental Margin, July 2017. Coordinates in SIRGAS 2000 Datum.

Dives	Latitude	Longitude	Water depth ranges (m)	Samples (n)
Northern Sector	4.372717	-49.922133	100-120	7

Central Sector	1.521867	-46.742383	250-378	1
Southern Sector	-0.453100	-43.983333	70-240	1

In the Northern Sector, rock samples were collected at depths of 114 (n=2), 117 (n=2) and 120 (n=3) m. In the Central Sector only one sample was collected, at 260 m depth (attached to the base of a Hexactinellida sponge). The Southern Sector dive also only recovered a single rock sample from 180 m depth. *In situ* imagery includes high-resolution videos (Supplementary Material Video S1) obtained with a GoPro Hero 4 camera, and high-resolution still photographs taken with a Nikon D7000 camera and Nikkor 18-105 mm lens. Fresh rock samples were photographed on board the R/V *Alucia*, using a Nikon D7100 camera and Nikkor Micro 60 mm lens. Petrographic thin sections of selected subsamples (n = 22) were produced by the National Petrographic Service (Texas, USA). Descriptions of the lithology and texture follow Dunham's (1962) classification, modified by Embry and Klovan (1972), with the classification of sandstones after Pettijohn et al. (1987). Fossil and living marine macroinvertebrates, foraminifera, and borings were identified for qualitative descriptions at the most precise taxonomic level possible. Identification of coralline algae on the external surfaces of samples was based on histological sections of fertile material, following Maneveldt and Van der Merwe (2012) and Bahia (2014). Sponge species were identified through the study of representative samples in the laboratory, mainly by using spicule characters, and comparison to specific literature (e.g., Rützler, 1971; Muricy et al., 2008; Moraes, 2011; Sandes et al., 2021; Moser et al.,2022). Voucher specimens of invertebrates and algae were deposited in the Museu Nacional - Universidade Federal do Rio de Janeiro and Herbarium of the Rio de Janeiro Botanical Garden (RB), respectively (Supplementary Material Table S1).

Representative rock samples from the Northern and Southern sector (27 cm^3 each) were sliced for mineralogical analyses using a petrographic saw. The samples were ground to powder and sieved through a 25 μm mesh. X-ray data were collected using a PANalytical

Empyrean diffractometer. An angular range of 5 to 80º 2θ was measured with a step size of 0.01º and 60 s per step. Phase identification was performed with PROFEX software (Döbelin and Kleeberg, 2015). Five subsamples of marine fossils found within rock samples were radiocarbon dated in the Center for Applied Isotope Studies (University of Georgia, Athens, Georgia, USA), using Accelerator Mass Spectrometry (AMS). Conventional radiocarbon dates were recalibrated using software CALIB 8.2 (Stuiver et al., 2020), and the Marine20 calibration curve (Heaton et al., 2020) factoring in a global reservoir effect. Dates are reported as calendar years before present (cal year BP; where "present" = 1950 CE) using a 2-sigma confidence interval. Additional radiocarbon ages were obtained from Milliman and Barreto (1975) and Vale et al. (2018). The curve proposed by Yokohama et al. (2018) was used to relate our data to global sea level changes.

3.4. Results

3.4.1. Northern Sector

3.4.1.1 High-Relief Structure Morphology

The area surveyed in the Northern Sector included the outer shelf, shelf-break, and continental slope, with canyons and ravines (Fig. 2A). The depth of the surveyed area, covered by the dive range of the submersible, varied between 110 and 175 m. The slope and ruggedness analysis of the outer shelf and shelf break revealed the presence of high-relief structures (HRS), (Fig. 2B) reaching up to 15 m above the adjacent seabed (Fig. 2C), at depths between 110 and 165 m. These show a patchy distribution with no clear orientation or clustering, but their tops are concentrated in two main water depth ranges: 115-121 m and 124-129 m (bathymetry histogram in Supplementary Material Fig. S1). The slope shows a gradient of values with higher slopes associated with the HRS tops in an area (mapped by BPI) of 0.69 km² (Fig. 2B). However, there is no clear relationship between depth and roughness, and some features appear

to coalesce (Fig. 2C). The elevation of the HRS above the seabed varies across the outer shelf. There are 51 high points in profile 1 (blue dotted line) and 29 high points in profile 2 (black dotted line) with heights up to 15 m and widths ranging from 20 – 330 m (Fig. 2A, C). It is important to note that these features occur on a relatively flat outer shelf–slope transition, observed on bathymetric, slope and ruggedness maps (Fig. 2B)

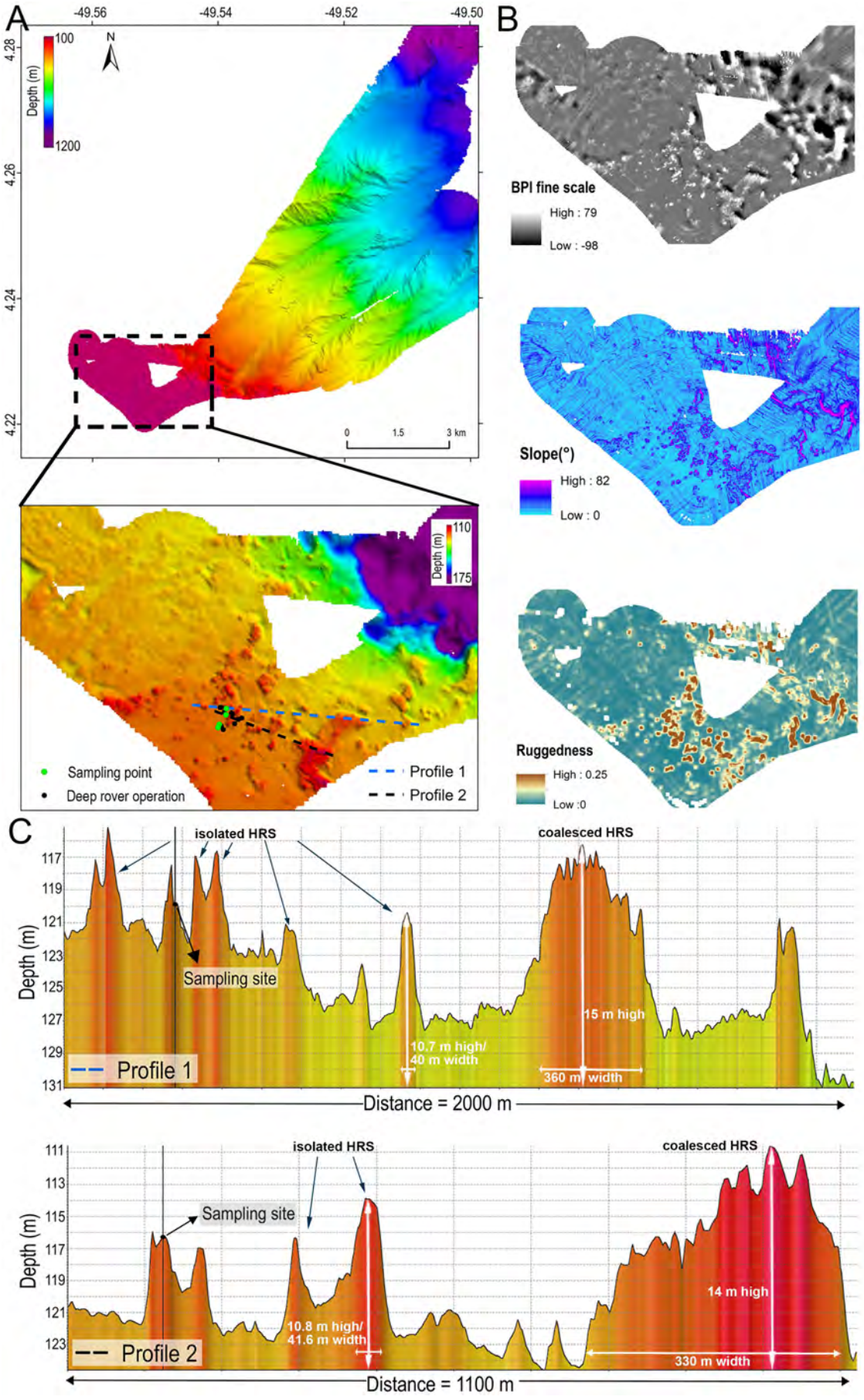
A
-49.56
-49.54
-49.52
-49.50
4.28
4.26
4.24
4.22
Depth (m)
100
1200
N
0
1.5
3 km
110
175
Sampling point
Deep rover operation
Profile 1
Profile 2
B
BPI fine scale
High : 79
Low : -98
Slope(°)
High : 82
Low : 0
Ruggedness
High : 0.25
Low :0
C
isolated HRS
coalesced HRS
Sampling site
15 m high
10.7 m high/
40 m width
360 m width
Profile 1
Distance = 2000 m
Depth (m)
117
119
121
123
125
127
129
131
isolated HRS
coalesced HRS
Sampling site
14 m high
10.8 m high/
41.6 m width
330 m width
Profile 2
Distance = 1100 m
111
113
115
117
119
121
123

Figure 2. Multi-beam profiles obtained around the Northern Sector dive/survey site. **(A)** General bathymetry illustrating the HRS. (**B**) Bathymetry derivatives: Bathymetric Position Index (BPI), fine-scale, Slope and Rugosity. (**C**) Bathymetric profiles oblique to the isobaths. Resolution in the plot at the operating point = 5 m.

3.4.1.2 HRS surface and internal composition

The rocky outcrops are surrounded by unconsolidated sediments and loose boulders covered by encrusting coralline algae (Figs. 3A, B, D). The structures are irregular but are bedded (Fig. 3C). The surfaces are colonized by red algae (Rhodophyta), with small green algae (Chlorophyta) and sponges (mainly thin encrusting species but some thickly encrusting, with massive cup-shaped lithistids). Associated cnidarians include hydroids, black corals and octocorals, together with encrusting bryozoans, large colonial ascidians, and benthic foraminifera (Fig. 3B-D). Among the red algae, the non-geniculate coralline genera *Harveylithon* sp., *Mesophyllum* sp., *Sporolithon* sp. and Peyssonneliales cover large areas of rock surfaces, especially close to the sandy bottom surrounding the outcrops. The hard rock forming the substrate shows evidence of erosion and corrosion, with intense bioerosion of the surface. Some are bedded, with strata enhanced by differential erosion (Fig. 3C), form a shelf-break parallel feature, but others are more massive (Fig. 3A-B). Surfaces are frequently vuggy, with sharp edges around the voids. Regular joint systems, locally widened by weathering are observed on the surface in many areas. Pebbles, cobbles, and boulder-sized blocks are common on top of some low-relief features and surrounding the bases of higher ones (Fig. 3A-B).

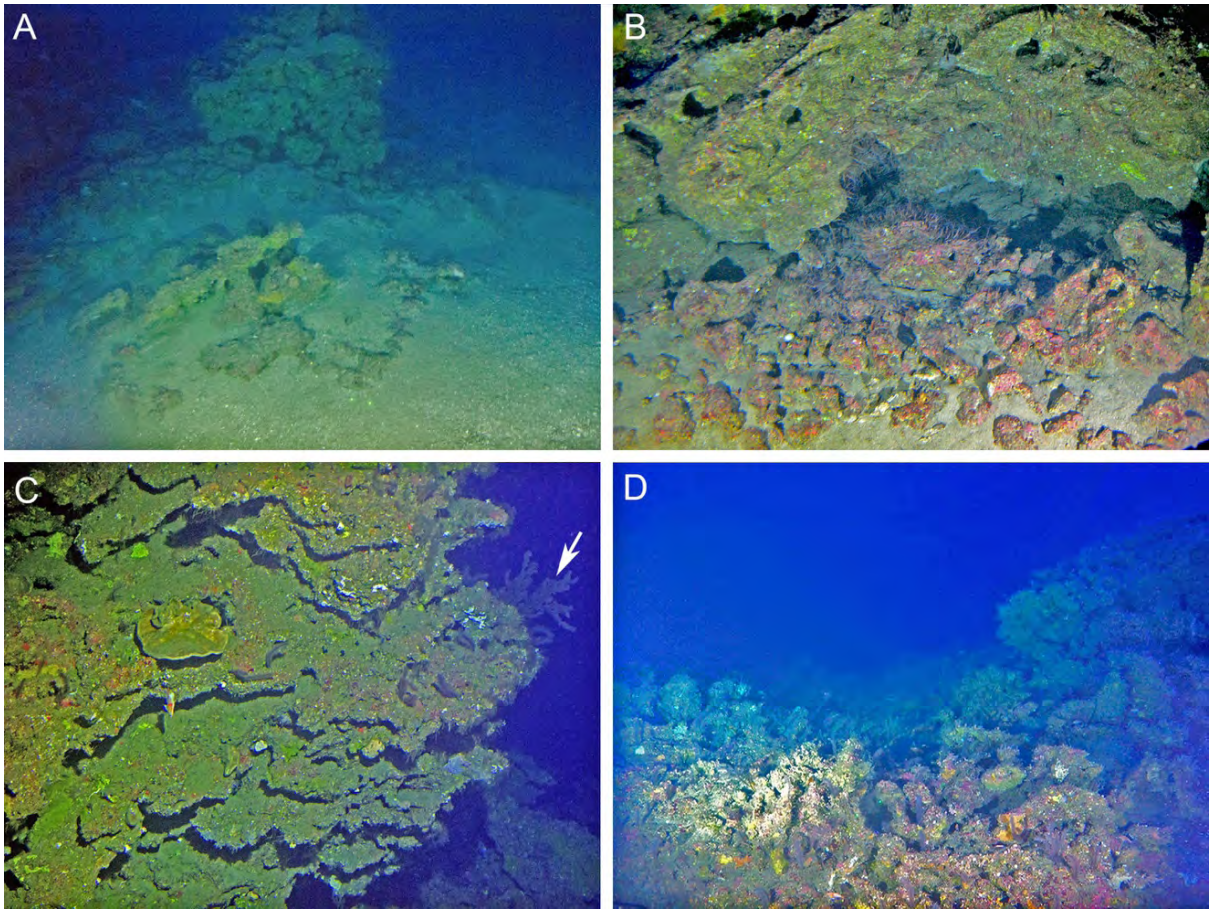

Figure 3. Images of the HRS in the Northern Sector of the ACM. (**A**) Unconsolidated sand surrounds the rocky HRS at 114 m depth. (**B**) Rocky bottom with loose boulders covered by living CCA at the sand-covered base of the HRS at 120 m depth. (**C**) General view of the bedded hard rock of the HRS at 117 m depth, with one dish-shaped sponge (in the center), living CCA (pink), and thin encrusting sponges (greenish-yellow patches at the bottom). The white arrow points to a black coral. (**D**) Bottomward view of an outcrop summit at 114 m depth.

Four samples from the Northern Sector are of angular blocks of sandstone, mostly covered by encrusting organisms. The encrusting species are mainly red calcareous algae and Peyssonnelians, accompanied by thin and some massive silica sponges, serpulids and benthic foraminifera (Fig. 4A-B). Images from the submersible and fresh samples reveal a colorful spectrum of sponge species, evident also in the petrographic sections as important elements of the rock surface community. Four encrusting sponges were identified: the thick and hypersilicified lithistid *Discodermia* sp., and very thin Demosponges (*Haliclona* sp., *Jaspis* sp., and *Clathria* sp.). In thin section, the sample from 120 m depth has a thin crust of the coralline

alga *Mesophyllum* sp. and fused spicules of *Discodermia* sp. (Fig. 4C-D). The rock beneath the surface crust in all samples is sandstone, with grains of quartz and feldspar ranging from 0.06 mm to 0.13 mm, between “coarse silt” to “very fine sand” and “fine sand” on the Wentworth scale. Grains are cemented by Mg calcite but this is partially dissolved near the surface (Fig. 4C-D). Thin patches (a few hundred microns) of micrite surrounding the silicate grains are present beneath sponges (Fig. 4D, F, G). Borings, including those of *Entobia*, are common in the rock surface (Fig. 4B-C), and are partially filled by wackestone to packstone consisting of minute calcareous (tunicate) and silica spicules of demosponges (Fig. 4C, E. G). The sandstone from 114 m depth consists of silicate grains (Table 2), mainly quartz, and feldspar minerals, with a calcite cement (Table 2). Close to the rock surface *Entobia* borings are partially filled by mudstone and micrite rich in organic matter, and with bryozoans and calcareous algae (Table 2).

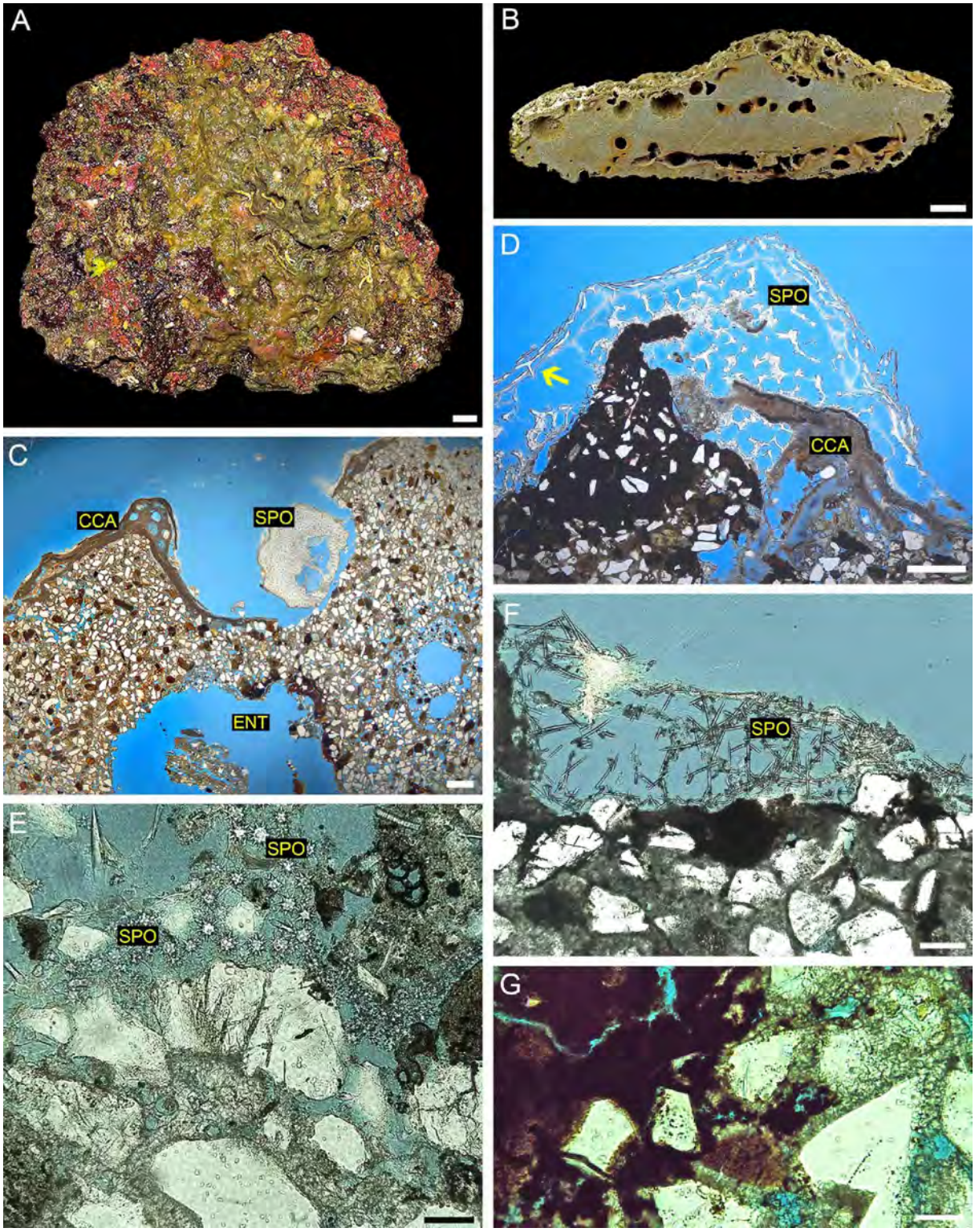

Figure 4. Sandstone sample and petrographic thin sections from the Northern Sector of the ACM at 120 m depth. (**A**) Fresh sample surface with living cover mainly composed of encrusting macroalgae (Rhodophyta), encrusting sponges (Demospongiae), polychaete tubes (Serpulidae) and benthic foraminifera. (**B**) Section of the sample with *Entobia* borings, bivalves and polychaetes. (**C**) Outermost portion of sandstone covered by *Mesophyllum* sp. (CCA). (**D**) Well-preserved spicule skeletal architecture of the lithistid sponge *Discodermia* sp. (SPO), depicting the diagnostic cortex of discotriane spicules

(arrow), intergrown with CCA. Note micrite patch engulfing quartz grains at the sandstone surface underneath sponge. (**E**) *Jaspis* sp. sponge microsclere spicules (oxyasters; SPO) and sand grains. (**F**) Well-preserved spicule skeletal architecture of the sponge *Haliclona* sp. Note thin micrite at the base of sponge. (**G**) Micrite rich in organic matter enclosing grains (left) and calcite cement (right) filling pores in the sandstone. Scale bars: A, B = 2 cm; C, D, E, G = 50 μm; F = 100 μm.

Two samples recovered from the surface of rocky outcrops at 117 m and 120 m depths are of boundstone, with crustose *Lithophyllum* sp. and *Mesophyllum* sp. growing on the surface. In the 117 m depth sample (Fig. 5A), intergrowing serpulids, barnacles, bryozoans and calcareous algae are the main components (Table 2). The surface of the boundstone has been bored by bivalves (*Gastrochaenolites*), sponges (*Entobia*) and polychaetes (*Trypanites*). Grazing marks of regular echinoids (*Gnathichnus*) occur on barnacles. In the 120 m depth sample, tubes of *Sabellaria alveolata* have aggregated very fine-grained quartz (Fig. 5B) and are the most common components, accompanied by barnacles, serpulids, calcareous algae, bryozoans (Table 2) and a few bivalves, some of which are articulated. Intra- and interskeletal pores include several distinct phases of borings by polychaetes (*Trypanites*) and sponges (*Entobia*) filled by mudstone to wackestone or peloidal micrite, which are locally rich in very fine to fine-grained angular quartz grains, but include bioclasts and ooids/coated grains (0.2 to 0.5 mm diameter) (Fig. 5C). The boundstone is itself coated with a thin layer of calcareous algae (Fig. 5A-D) and the hypersilicified spicule skeleton of a lithistid sponge (*Discodermia* sp.) (Fig. 5D), together with siliciclastic grains, mainly of quartz. Characteristic Didemnid ascidian spicules (spiked carbonate spheres) are common on the rock surface and embedded in micrite in the borings.

Barnacle bioclasts in the boundstones from both 117 and 120 m depths yielded ages of 14,920 and 16,395 cal yr BP, respectively. A foraminifer in rudstone from 120 m depth yielded an age of 12,160 cal yr BP (Table 3).

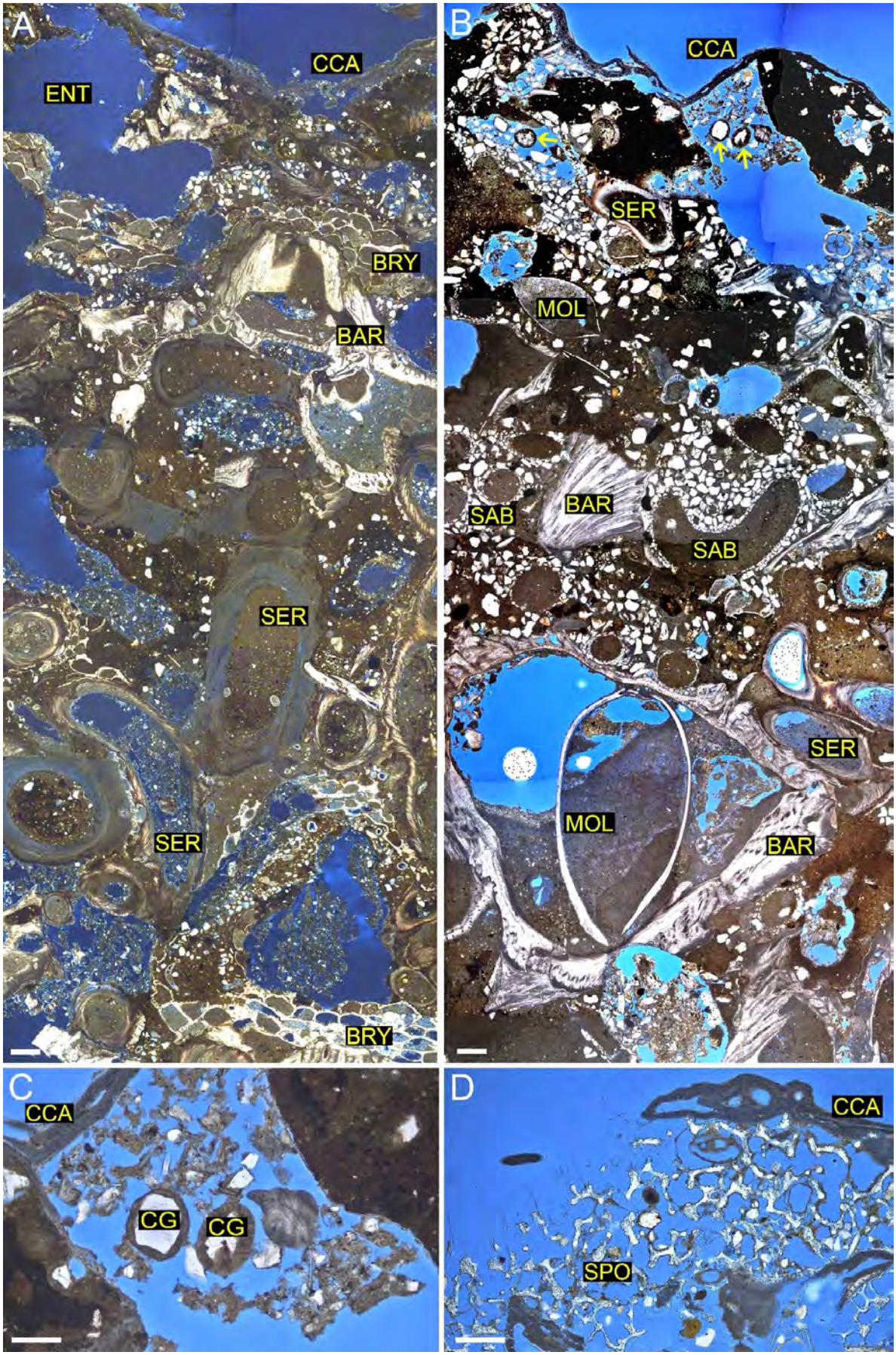

Figure 5. Micrographs of thin sections of boundstone collected from the Northern Sector of the ACM.

(**A**) Boundstone from 117 m depth formed by barnacles (BAR) and bryozoans (BRY), intergrown with serpulids (SER) and covered by a thin crust of *Lithophyllum* sp. (CCA). Sponges *(Entobia*) and polychaete worms (*Trypanites)* (a polychaete) formed the principal borings. Fillings of constructional voids and borings include several phases of wackestone and packstone with siliciclastic grains, mainly of quartz, and bioclasts. (**B**) Boundstone from 120 m depth consisting of barnacles (BAR), bryozoans (BRY), *Sabellaria* tubes (SAB), serpulids (SER) and thin shelled bivalves (MOL) covered by *Mesophyllum* sp. (CCA). Voids of *Trypanites* and *Entobia* filled by peloidal micrite, and several phases of wackestone-packstone with bioclasts, coated quartz grains (yellow arrows) (**C**) Detail of previous image showing coated quartz grains (CG). (**D**) Detail of rock surface with lithistid sponge silica spicule skeleton (SPO) encrusted by *Mesophyllum* sp. (CCA). Scale bars: A-B = 500 μm; C-D = 200 μm.

Table 2. Main components (%)[1] in five analyzed rock samples from the ACM structures.

Samples	Northern Sector - boundstone	Northern Sector - boundstone	Northern Sector - sandstone (outer)	Northern Sector - sandstone (inner)	Southern Sector - rudstone	Southern Sector - rudstone
Depth (m)	117	120	114	114	180	180
Barnacle	11.6	14.3	0.8	-	0.1	0.1
Bryozoan	3.7	4.3	9.3	-	2.0	0.5
Crustose coralline algae (CCA)	3.4	6.7	4.6	0.5	6.0	11.5
Foraminifera	-	-	-	-	3.4	3.6
Geniculate coralline algae	-	-	-	-	1.7	1
Serpulid	12.5	9.2	0.4	-	0.4	0.5
Sponge	-	-	6.3	0.2	0.1	1.2
Cement	2.5	0.1	3.	33.4	24.1	20.1
Micrite/ Sediment	35.6	37	30.	3.1	32.3	33.8
Voids	20.3	20.9	27.9	5.4	9	7.8
Siliciclastic grains	10	6.6	17.6	58.2	18.	18.5
Ooids	-	-	0.08	-	0.8	-

[1] Components in smaller proportions were also observed in the analysis, such as echinoderms (*Gnathichnus*), sabellarids (*Sabellaria alveolata*) and bioeroders like bivalves (*Gastrochaenolites*), sponges (*Entobia*) and polychaetes (*Trypanites*).

3.4.2. Central Sector

3.4.2.1 Outcrop morphology

Bottom imagery from multibeam data reveal the presence of numerous rock outcrops in the Central Sector (Fig. 6A), south of the Amazon Cone. These show elongated tensional joints, locally responsible for block detachment. Adjacent sediments vary from coarse sand to gravel. Acoustic surveys between 200 and 1100 m water depth reveal the presence of two canyons, but the submersible was only able to operate to a maximum depth of 380 m. The three maps (Fig. 6, BPI, Slope and Ruggedness) describe the morphometric attributes of the area surveyed and reveal a major pronounced step running a NW-SE strike orientation, that coincides with the main shelf break (Fig. 6B). Figure 6C shows a bathymetric profile depicting a 29 m high step positioned in a long and even stretch on the shelf slope, which follows the shelf break strike orientation.

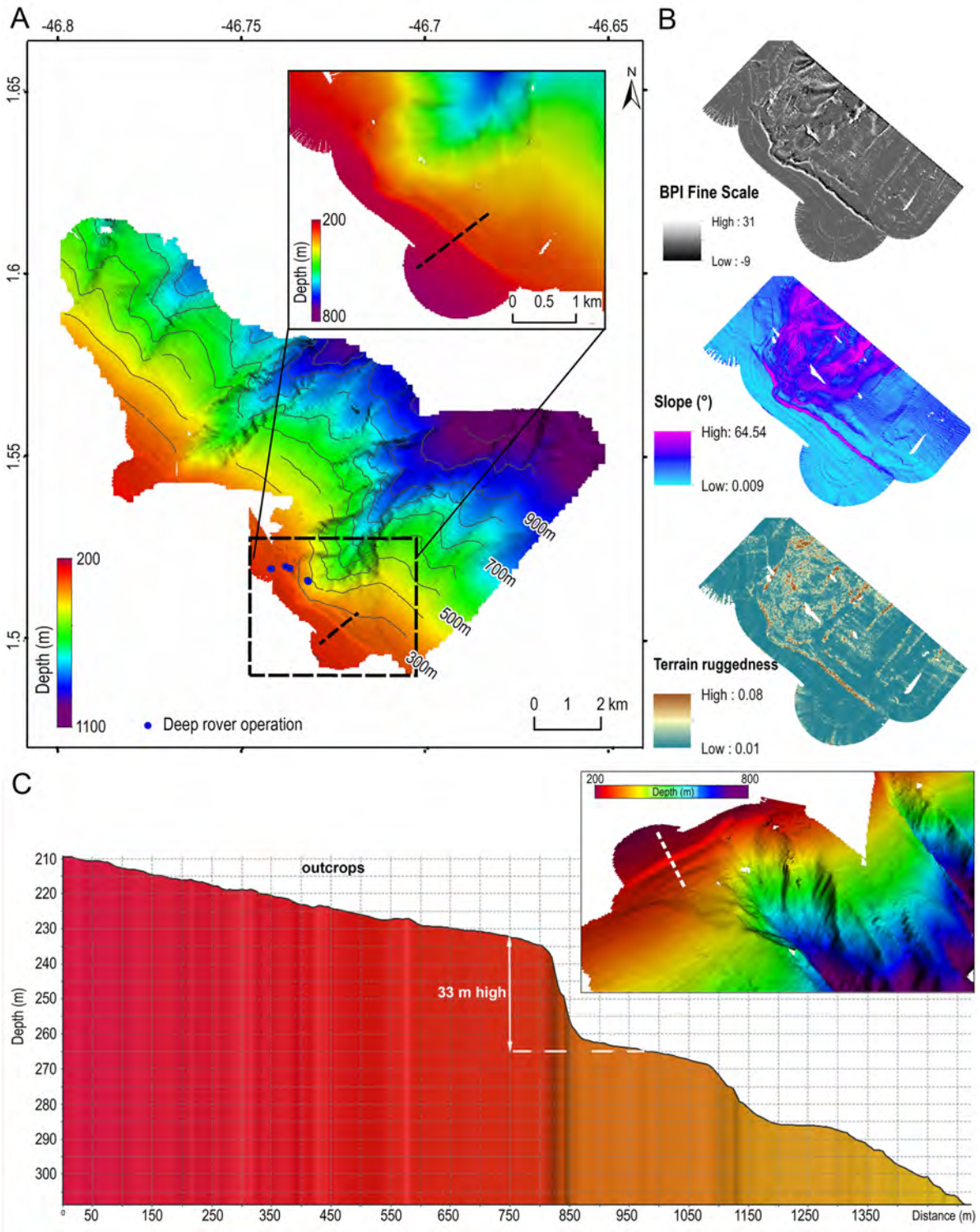

Figure 6. Multi-beam profiles from the Central Sector dive/survey site. (**A**) General bathymetry of the mapped area. (**B**) Three frames with bathymetry derivatives: BPI fine scale, Slope, and Rugosity. (**C**) Bathymetric profile normal to the isobaths along the white line shown in the bathymetric frame in 3D perspective. The profile starts close to the shelf break, around 210 m depth. The steps of more than 29 m, indicate the presence of rigid structures. Resolution in the image at the operating point in the central canyon = 10 m..

The outcrop surface in this area lacks calcareous algae but has a sparse cover of sponges, together with black corals and gorgonians, serpulids, sea stars, sea lilies, and brittle stars; Fig. 7A-B). A single small rock sample was recovered attached to the base of a sponge collected from the lower part of the surface, at 260 m depth. This is a poorly sorted coarse-grained lithic sandstone with a muddy matrix, with rock fragments as components in addition to quartz or feldspars. Grains are well-rounded, ranging from 0.5 to 1.0 mm (Fig. 7C-D).

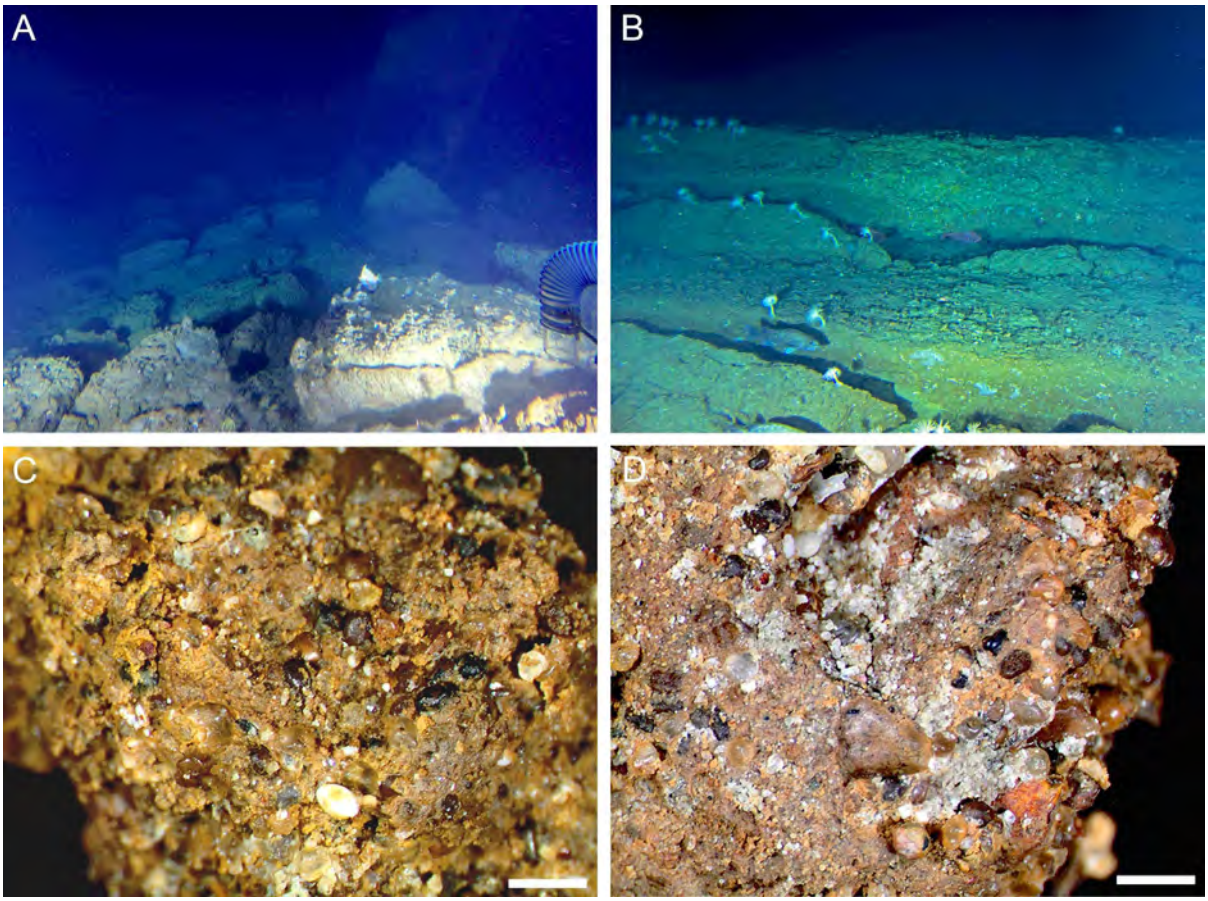

Figure 7. General view of rocky outcrop showing fractured surface (A-B) and details of rock lithology (C-D) from the Central Sector of the ACM. (**A**) View down from the outcrop summit at 250 m depth. (**B**) Outcrop summit with elongate parallel fractures at 250 m depth. (**C**, **D**) Rounded unsorted sand grains embedded in brown muddy matrix of the rock recovered from the base of a Hexactinellida sponge (*D. pumiceus*) from 260 m depth. Scale bars: C-D = 1 mm.

3.4.3. Southern Sector

3.4.3.1 Outcrop and canyon morphology

In the area surveyed in the Southern Sector, water depth ranges between 100 and 800 m including the shelf-break and a canyon head (Fig. 8A). The shelf break is well defined with a significant increase in slope at around 225 m depth. High slope and roughness values mark the canyon flanks, while the lowest values define the canyon floor (Fig. 8B). Closer to the canyon, multibeam data (Fig. 8A) and *in situ* bottom imagery (Fig. 9A-B) reveal the presence of rocky outcrops between 120 and 310 m depth on walls with heights between 20 and 120 m and widths ranging from 100 to 910 m (Fig. 8C).

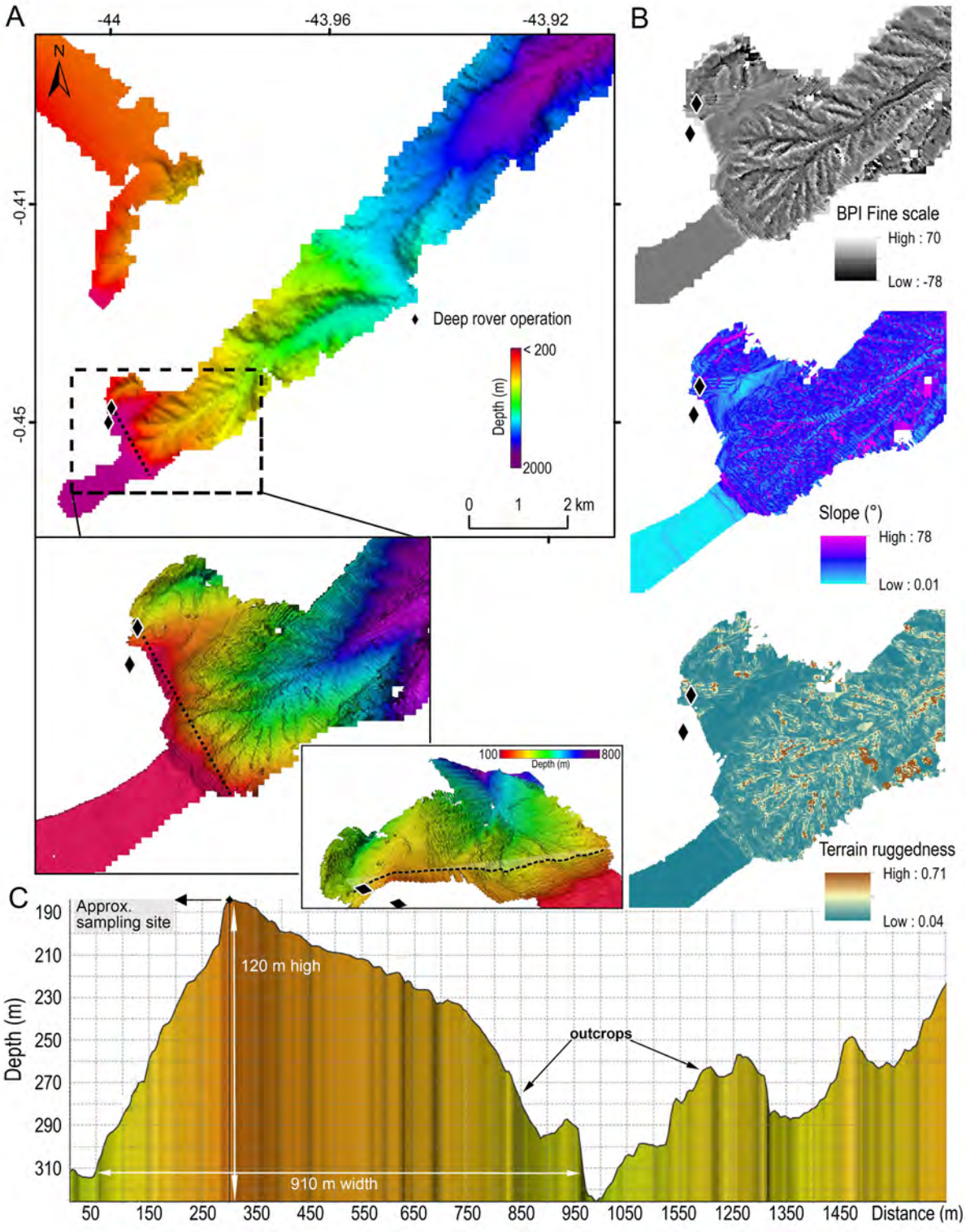

Figure 8. Multibeam profiles around the Southern Sector dive/survey site. (**A**) Shelf break and canyon bathymetry. (**B**) Frames with bathymetry derivatives in A: BPI Fine Scale, Slope and Rugosity. (**C**) Bathymetric profile along the dashed line depicted in A in three different scales and 3D perspectives. The sampling point is a few tens of meter away from the profile. Resolution in the zoom at the operating point = 10 m. Black diamonds indicate the manned submersible operations.

3.4.3.2 Outcrop surface and rock composition in the sampling site

The base of the outcrop at 230 m depth rises from a flat sediment covered ledge (Fig. 9A). The outcrop surface is irregular with exposed hard surfaces, thin accumulations of loose sediment, and scattered living organisms. The flanks of the outcrop are steep, locally vertical or overhanging, and forming shallow caves/ledges with fine-grained sediment on the floors. The steep surfaces are locally rugged around small cave entrances (Fig. 9B, C).

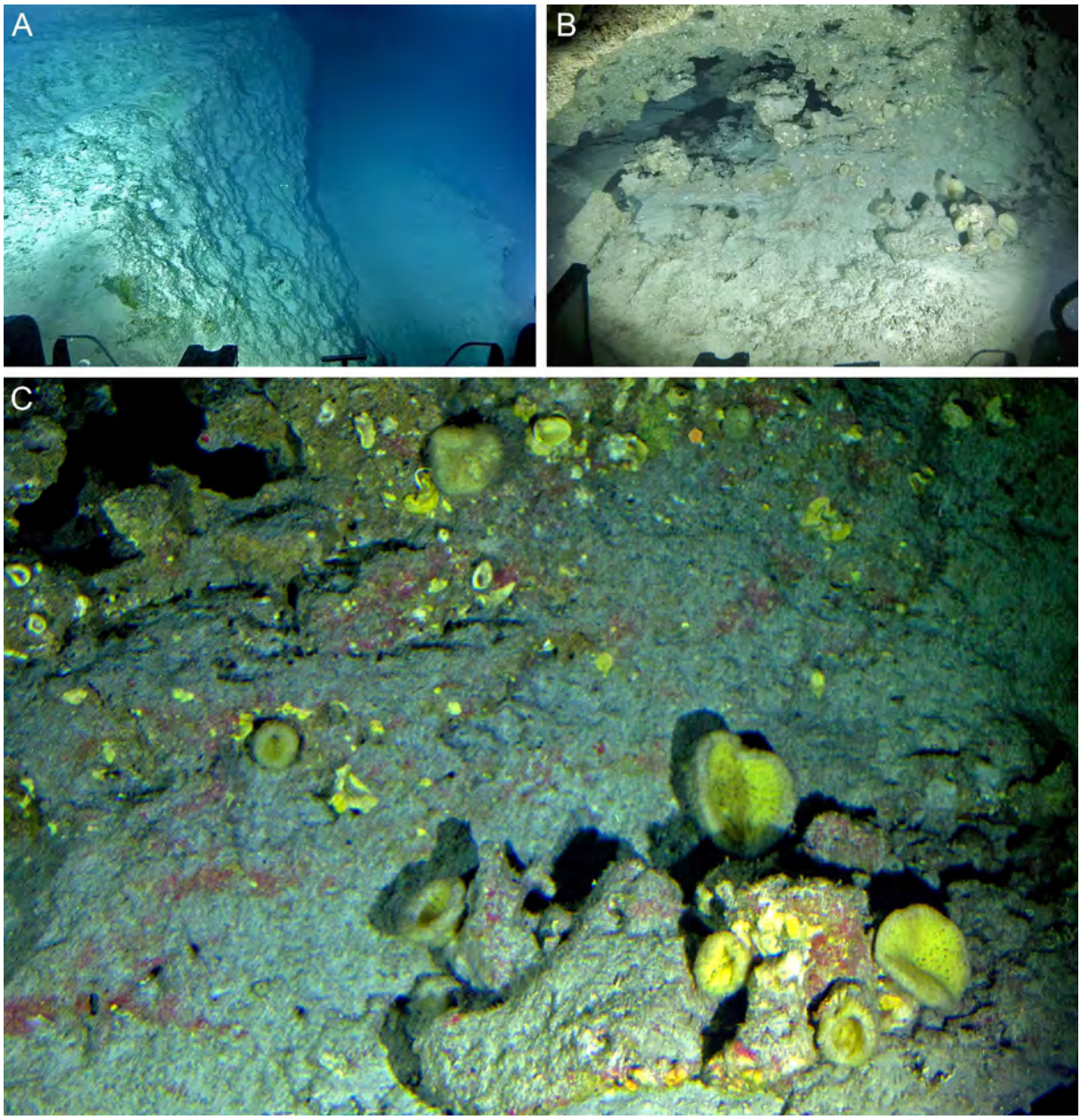

Figure 9. Views of sea floor in the Southern Sector of the ACM, 180-230 m depth. (**A**) Sea floor at 220 m depth showing steep vertical transitions into narrow plateaus. (**B**) Shallow cave with sandy sediment

on the floor at 180 m depth. (**C**) A shallow cave with living CCA (pink), hexactinellid (*Dactylocalyx pumiceus*) and lithistid (*Corallistes* sp.) sponges.

A loose rock sample was collected at the entrance to a shallow cave/ledge at 180 m depth. The rock surface is covered by sparse patches of living calcareous algae (*Sporolithon* sp. and *Harveylithon* sp.), lithistid sponges (*Corallistes* sp.) and encrusting to massive demosponges, with the skeletal structure of hexactinellid sponges (*D. pumiceus*) preserved as mold in carbonate cement (Fig. 10A-F). Sand grains (mainly fine-grained quartz) are common, included in and on the sponge network, forming cemented crusts up to 2 mm thick (Fig. 10G). Giant benthic foraminifera (Astrorhizids), and serpulid tubes attached to cemented sponge remains (Fig. 10H-I).

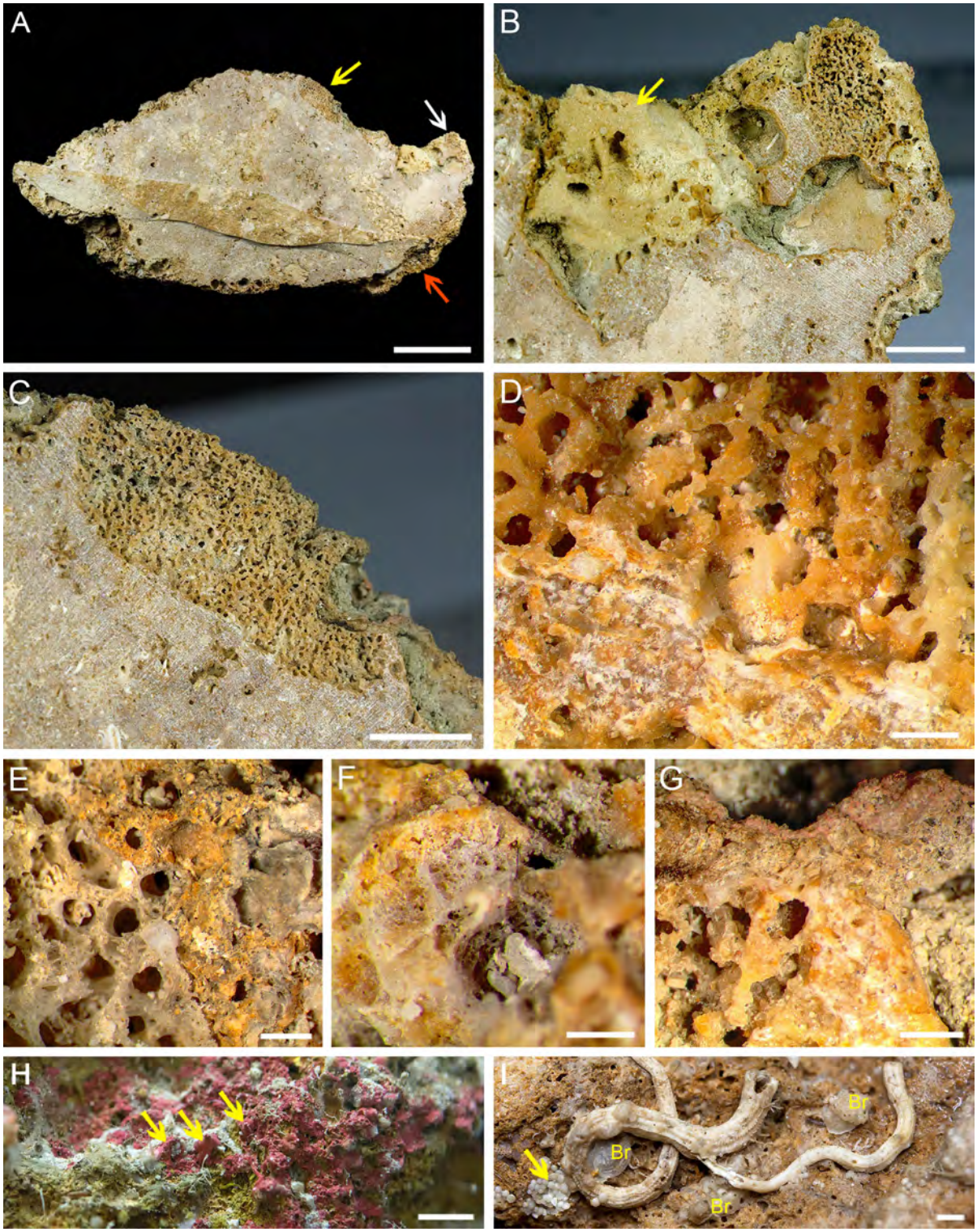

Figure 10. Section and surface of carbonate rock from 180 m depth in the Southern Sector of the ACM. (**A**) Section of the sample (orientation as at collection), with well-preserved *D. pumiceus* sponge remains (arrows). (**B**) Detail of the white arrow region in A with sponge mold (upper right) and the skeleton of the demosponge *Myrmekioderma guajajara* with siliceous spicules filling a rock cavity (yellow arrow). (**C**) Detail of sponge mold in the yellow arrow area in A, preserving the dictyonal skeletal framework with a well-defined border. (**D**) Detail of basal region of the sponge mold in C. (**E**)

View of rock surface showing a *D. pumiceus* skeleton (left) and skeletal-framework mold (right). (**F**) Skeletal architecture in different preservation, with siliceous spicules (translucent white) and carbonate coated framework (yellow). (**G**) Detail of surface (cross section) showing sponge mold (bottom left) and cemented sand grains (white colour at the top). (**H**) Living CCA growing (pink veneer) on eroded sponge mold and tests of Astrorhizids foraminifera (yellow arrows). (**I**) Serpulid tubes, benthic foraminifera (yellow arrow) and bryozoans (Br). Scale bars: A = 5 cm; B-C = 1 cm; D-E, F = 500 μm; G-H = 1 mm; I = 2 mm.

The composition of the rock sample from the southern area (with two subsamples) varies from poorly sorted bioclastic sandstone (Fig. 11A) to rudstone rich in quartz and minor feldspar grains (Table 2; Fig. 11B), with an abundant muddy matrix (Table 2). *Entobia* borings, partially lined by a thin isopachous cement, are concentrated beneath the rock surface. Non-geniculate coralline algae (Hapalidiales and *Lithophyllum* sp.), small and large benthic and planktonic foraminifera, and bryozoans are the main bioclastic components of the rudstones (Fig. 11B-D; Table 2), with *Amphiroa*, sponges, echinoderms, corals, bivalves, gastropods, barnacles, serpulids and ooids as minor components (Table 2). Some synsedimentary pores, both intra- and interskeletal, are partially lined by acicular cement, peloidal micrite and dog-tooth cement (Fig. 12A-C), which are overlain, with other pore walls by isopachous calcite, locally replacing acicular cement (Fig. 12D). Locally, *Entobia* galleries are themselves occupied by cryptic species and show characteristic concave scars in the carbonate rock (Fig. 12E-F). A mollusk shell and foraminifera in the rudstone rock sample yielded ages of 28,815 and 23,747 cal yr BP, respectively (Table 3).

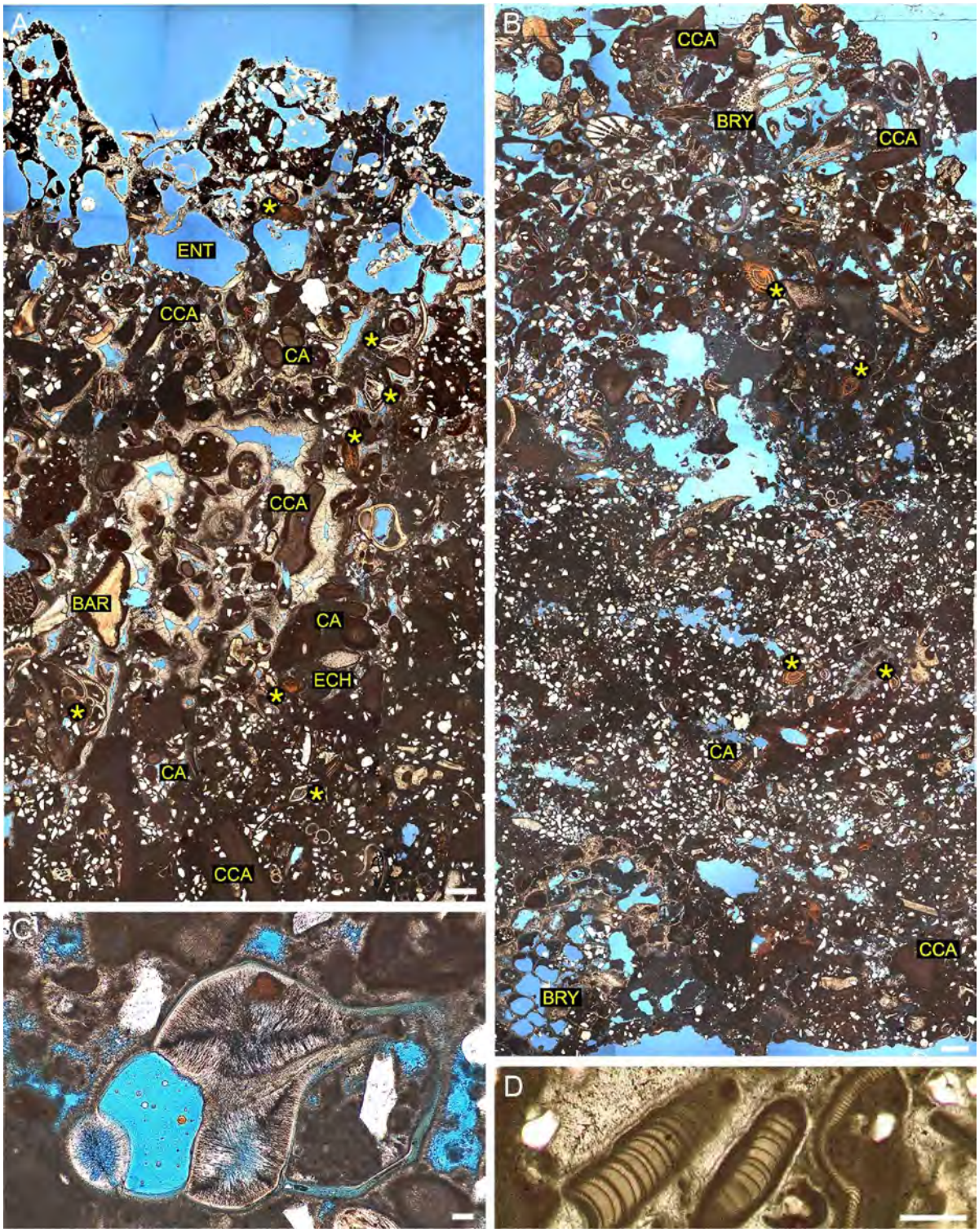

Figure 11. Micrographs of thin sections of rock sample from 180 m depth in the Southern Sector of the ACM. (**A**) Rudstone with fragments of geniculate (CA) and non-geniculate (CCA) coralline algae, barnacles (BAR), echinoderms (ECH), benthic (yellow asterisks), and planktonic foraminifera, bivalves, gastropods, and quartz grains. Some synsedimentary pores (both intra and interskeletal) are partially filled with peloidal micrite and lined by isopachous cement. *Entobia* borings (ENT) are concentrated underneath the rock surface. (**B**) Bioclastic sandstone/rudstone with abundant quartz grains and micritic matrix. Bioclasts include benthic (yellow asterisks) and planktonic foraminifers, CCA,

bryozoans (BRY), bivalves, and echinoids. (**C**) Acicular cement filling intraclast voids in a gastropod shell. (**D**) Geniculate and non-geniculate coralline algae and quartz grains with micrite envelopes fringed by fibrous cement. Scale bars: A, B = 500 µm; C = 50 µm; D = 250 µm.

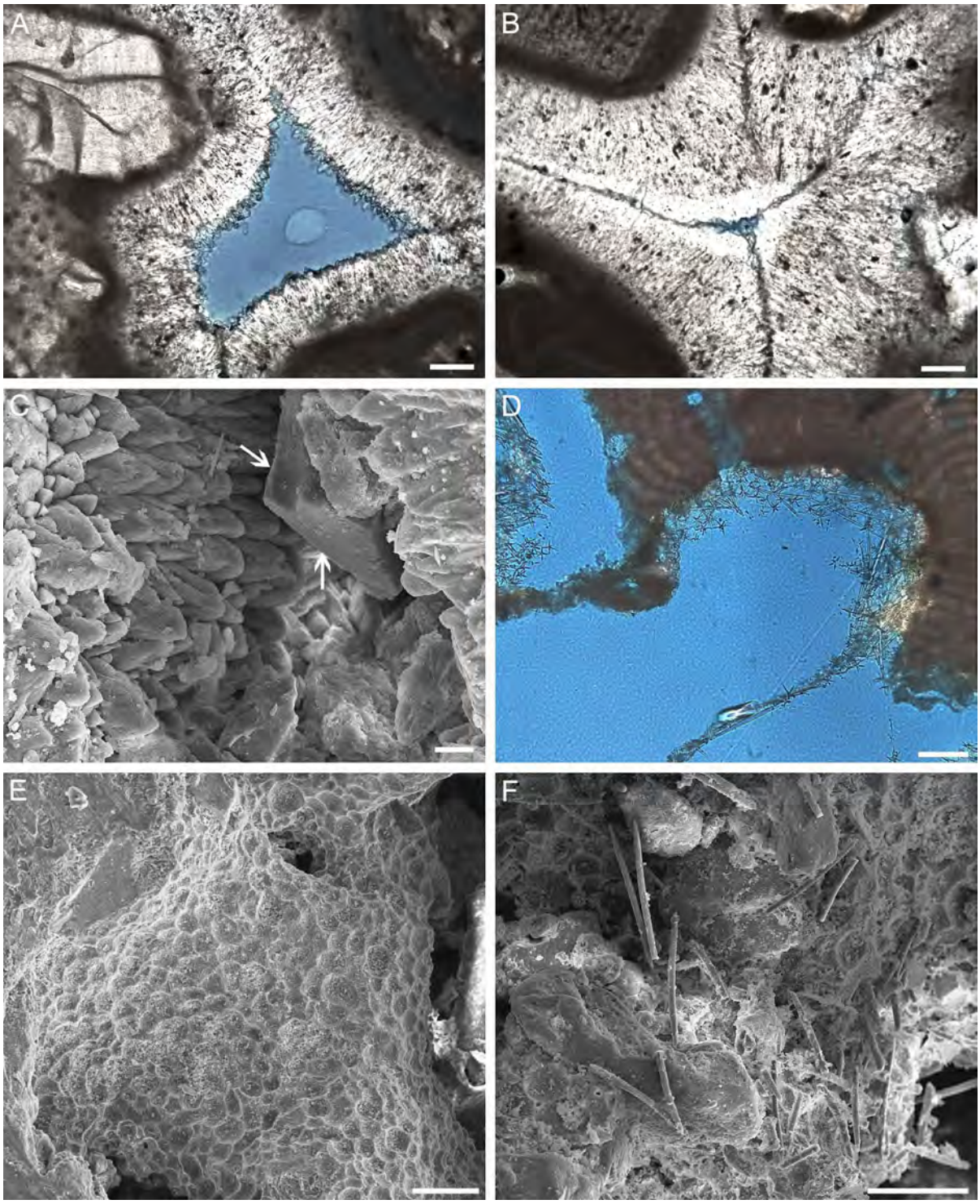

Figure 12. Optic microscopy (A-B, D) and SEM (C, E-F) images of thin sections of rudstone from 180 m depth in the Southern Sector of the ACM. (**A**) Micrite and fibrous calcite fringe cement around quartz grains and infilling interclast spaces. (**B**) Acicular cement filling an interskeletal void. (**C**) Detail of calcite cement around a quartz grain (white arrow). (**D**) Skeletal remains of siliceous spicules of a cryptic

sponge occupying voids in the rudstone excavated by *Entobia*. (**E**) Pitted surface diagnostic of excavation by bioeroding sponge (*Aka* sp.). (**F**) Small oxeas spicules of bioeroding sponge (*Aka* sp.) over pitted surface and sand grains. Scale bars: A, B, D = 50 μm; C = 10 μm; E, F = 100 μm.

Table 3. Radiocarbon ages of different components collected from rock samples used in this study. Coordinates are in SIRGAS 2000 Datum.

Sample code	Sector	Latitude	Longitude	Water depth (m)	Dated Component	Lithofacie	Conventional Age (BP)	Calibrated ^{14}C age (Cal yr BP)	95% range (cal BP)
Sa01	N	4.372717	−49.922133	117	Barnacle	Boundstone	14,630 ± 35	14,920	15,130- 14,676
Sa05	N	4.372717	−49.922133	120	Foraminifera	Rudstone	12,670 ± 30	12,160	12,383- 11,942
Sa07	N	4.372717	−49.922133	120	Barnacle	Boundstone	15,870 ± 40	16,395	16,644- 16,193
Sa08-fr	S	−0.453100	−43.983333	180	Foraminifera	Rudstone	27,400 ± 80	28,815	29,035- 28,517
Sa08-rk	S	−0.453100	−43.983333	180	Mollusk shell	Rudstone	22,300 ± 70	23,743	23,955- 23,497
V-18-18 Top[a]	N	5.420000	−51.027000	150	Oolite	–	20,090 ± 600	23,710	22,405– 25,205
X-236[a]	N	5.091000	−50.690000	133	Oolite	–	17,010 ± 400	20,037	19,025– 20,995
G-209[a]	N	4.757000	−50.419000	109	Oolite	–	14,470 ± 400	17,045	15,950– 18,060
G-210[a]	N	4.604000	−50.343000	104	Oolite	–	14,310 ± 250	16,845	16,150– 17,545
1921[a]	N	4.513000	−50.097000	146	Oolite	–	17,170 ± 1240	20,276	17,350– 23,265
G-211[a]	N	4.440000	−49.960000	191	Oolite	–	21,250 ± 400	25,063	24,145– 25,885
N01-surface[b]	N	4.369686	−49,920,442	120	Oolite	Boundstone	11,700 ± 30	13,008	11,199–10,898
N01-inner[b]	N	4.369686	−49.920442	120	Bivalve shell	Rudstone	13,480 ± 35	15,385	13,660- 13,216
N12[b]	N	4.369686	−49.920442	120	Coral polyp	Boundstone	16,640 ± 40	17,210	17,455- 16,971

Sa = sample; fr = Fragment rock; rk = Rock sample; N = Northern; S = Southern.
[a] data from Milliman and Barreto (1975);
[b] data from Vale et al. (2018).

3.5. Discussion

The mesophotic 'reefs' and rhodolith beds form the most structurally complex and biodiverse benthic habitats within the outer continental shelf and upper slope of the Brazilian portion of the ACM (Moura et al., 2016; Vale et al., 2018; Araujo et al. 2021). This carbonate domain has been known since the late 1960's (e.g., Barreto et al., 1975; Milliman et al., 1975), but the distribution, morphology and framework composition of the 'reefs' remained poorly characterized, hampering the understanding of their paleoecological evolution. Results presented here provide a detailed description of these rocky outcrops, up to 15 m high, north and south of the Amazon Cone, based on imagery and samples collected by manned submersible between about 110 and 180 m depths.

The internal compositions of the outcrops on the outer shelf and at the shelf break, indicates that they are of sedimentary rocks beneath a thin living cover. They have been

modelled by erosion and partially covered by shallow-water deposits during late Pleistocene deglaciation and the lowest sea level. The seismic profiles provided by Milliman et al. (1975) showed that the outcrops are of stratified rocks sculpted by channels and the new surface imagery provided here shows that they are lithified and, at least locally, well jointed. They are mainly well-cemented sandstones, according to the analysis of four samples recovered in this study and published data (Figueiredo et al. 2007; Cruz et al., 2019). The micrite on the sandstone surfaces is probably the result of microbial activity associated to sponges, but further study is needed to confirm any biomineralization process. Cruz et al. (2019) suggested that the sandstones are of Pleistocene age (older than the LGM), and consequently, their erosion took place during Pleistocene sea-level lowstands. The concentration of the flat tops of these features at two different depths (Fig. S1) suggests that they are relics of abrasion terraces, sculpted during at least two Pleistocene low sea-level stands. The erosion of these siliciclastic rocks and the mixed siliciclastic-carbonate deposits formed at different depths during the LGM and deglaciation.

Milliman and Barreto (1975) and Milliman et al. (1975) showed that bioclastic and oolitic sandstones with varying proportions of siliciclastics (up to 85% in some samples; Milliman and Barretto, 1975) and carbonate components (> 75%; Barreto et al., 1975) accumulated on the highs adjoining erosional channels. Leaving aside an outlier age of 41.8 cal ka BP obtained from the sample that also yielded a date of 23.7 cal ka BP (Milliman and Barretto, 1975; see also Mahiques et al., 2019), the oolitic sediments described by these authors occur from 191 to 104 m depth with ages from 25 to 16.8 cal ka BP (Table 3). Ooids in a rudstone from 120 m depth analyzed by Vale et al. (2018) yielded a younger age of 13,008 cal yr BP. The presence of ooids and shallow-water fossils suggests that the detrital sediments overlying the eroded bedrocks were deposited during low sea level in the late Pleistocene (Barreto et al., 1975; Milliman and Barretto, 1975; Milliman et al., 1975). Modern ooids

develop in shallow, warm, carbonate-saturated seawater of normal to elevated salinity and agitated water conditions, under the influence of tides and waves (Davies et al., 1978; Tucker and Wright, 1990; Duguid et al., 2010; Harris et al., 2019). The present-day depth of the overlying siliciclastic and carbonate deposits with ooids reflects a combination of global sea level at the time of their formation followed by subsidence of the shelf margin. However, no consistent rate values for subsidence since the LGM can be obtained from the age and depth of samples in the Northern Sector (Fig. 13). The data on oolites from Milliman and Barretto (1975) and Vale et al. (2018), suggest that the subsidence rate of the Northern basin floor varied between 0.40 and 3.08 mm/yr. This might reflect either uncertainties in the original depth of formation of the dated samples or errors in radiocarbon dating.

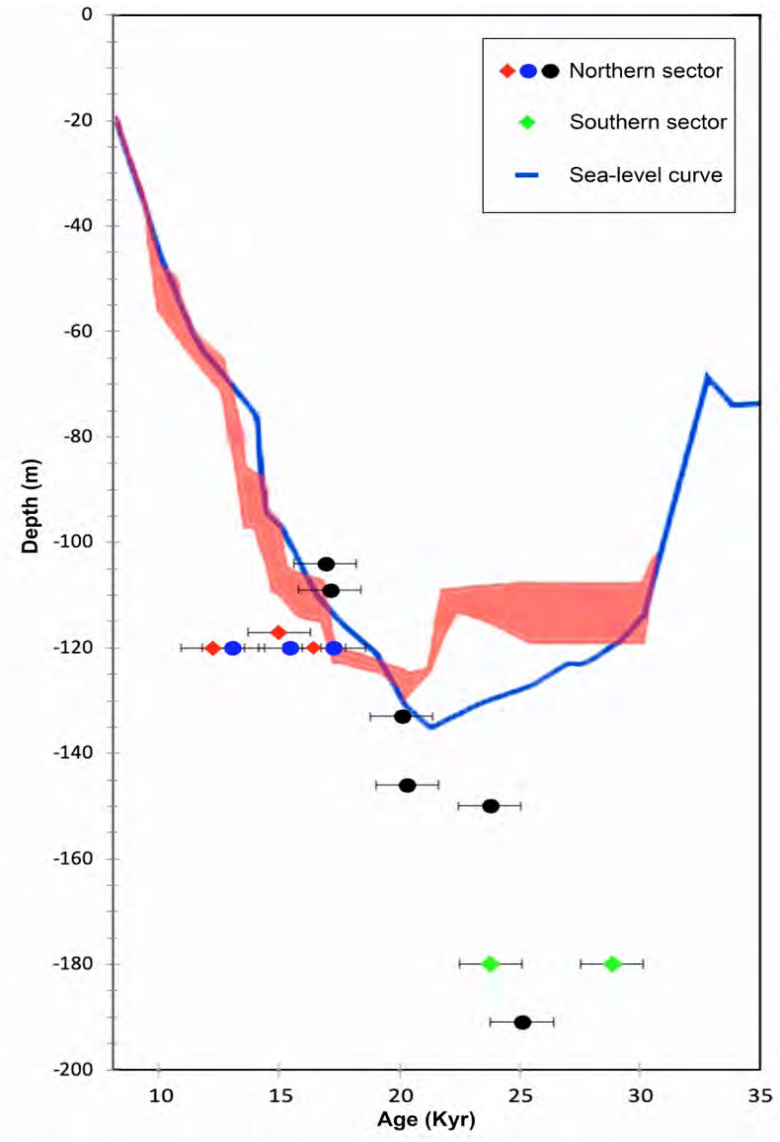

Figure 13. Age vs water depth summary of samples from the ACM: Red and green diamonds (this study, Northern and Southern sectors), black circles (Milliman and Barretto, 1975, Northern Sector), and blue circles (Vale et al., 2018, Northern Sector). The blue line is a Global Mean Sea Level (GMSL) curve (with confidence interval) of 10 to 35 ka based on Yokoyama et al. (2018). The horizontal black lines indicate 2-sigma confidence interval of calibrated ages.

The radiometric ages of boundstones rich in barnacles and sabellarids analyzed in this study (14,920 and 16,395 cal yr BP) indicate that the antecedent hard bottoms were colonized by benthic organisms that generated a relatively thin layer of calcified bioconstruction since the LGM. The main builders (barnacles, bryozoans, coralline algae and corals) thrive in a wide range of depths. However, the occurrence of a late phase of *Sabellaria* tubes in the boundstone from 120 m depth suggests formation at depths of only a few meters. On modern Brazilian shores, sabellarids grow in intertidal and shallow subtidal environments forming nodular structures and large encrusting banks (e.g., Aviz et al., 2021). Although the sabellarids recorded here did not build large monospecific structures, they probably still required shallow water to be part of the boundstone components. The present depth and age of the samples, combined with the sea-level curve of Yokoyama et al. (2018), point to a maximum depth of formation of less than 10 m. Whatever the rate on the Northern Sector margin (see discussion above), subsidence would have increased the difference between the present-day sample depth and sea level at the corresponding age. Thus, the plotted depth difference in Fig. 13 (18 m) is the maximum possible paleodepth of boundstone formation.

In the Southern Sector, the occurrence of shallow-water bioclasts (such as *Amphiroa* and barnacles) and the ages of bioclasts in the rudstone (23,747 and 28,815 cal yr BP) on the outcrop at 180 m indicate that the rock forming the substrate of the ‘reefs’ probably formed in shallow water and potentially with some terrigenous sediment input, considering the presence of 18% of siliciclastic grains. The acicular cements and isopachous calcite in the intra and interskeletal pores also suggest a shallow-marine environment for the early diagenesis of those rocks (Flügel, 2009). The bioclastic components, specifically the coralline algae in the rudstone, are compatible with deposition in a mid-shelf setting at depths of some tens of meters (Brasileiro et al., 2018). During deglaciation, sea level rose, and the substrate was colonized by organisms living in deeper water (such as encrusting to massive demosponges, *Hexactinellid*

sponges and benthic foraminifera). Plots of present-day depths and ages of the rudstone samples on the sea-level curve of Yokoyama et al. (2018) (Fig. 13) indicate a maximum paleodepth of 65 m. As in samples in the Northern Sector, any subsidence would mean a shallower paleoenvironment of formation.

The surface of these mixed carbonate-siliciclastic rocks, predating the LGM, is overlain by a benthic community dominated by sponges. Skeletons and skeletal molds of these are attached to the Pleistocene rock surface but the observed accretion is only a few centimeters (Fig. 10) and the bioconstruction potential of the living community is small. The Amazon 'reefs' in the Central Sector bear a different living community on exposed bedded and jointed Pleistocene rocks, devoid of CCA and thinly encrusting sponges. The presence of hexactinellid sponges (*D. pumiceus*) is shared with the Southern Sector, but only with scattered specimens (Moser et al., 2022).

The Amazon 'reefs' are unique and complex structures that congregate rich biodiversity living on outcrops of existing sedimentary rocks with a veneer of organic construction characterized by a relatively high abundance of calcareous algae, sponges and bryozoans, mostly in the Northern and Southern sectors (Moura et al., 2016). These mesophotic communities are able to thrive on hard substrates and rhodolith beds under only moderate influence of the Amazon River plume. They include organisms with potential building capacity provided both by mineralized skeletons (calcareous algae, bryozoans, foraminifers and serpulids), and baffling/ binding capacities (sponges). However, the outcrops in the Northern Sector are the result of Pleistocene processes of shelf sediment accumulation and erosion, with only a short episode of bioconstruction after the low sea level in the LGM and deglaciation (e.g., Milliman et al., 1975). The community of sessile benthic organisms seems to contribute to the incorporation of small amounts of sediment (micrite and quartz grains) on the rock surface but net accretion is negligible. In the Southern Sector, accretion is due to the

accumulation of sponge skeletons and their molds but is only observed on the surface layer of the rock and is also negligible. No comparable accretion was observed on the deep rock outcrops of the Central Sector of the ACM, where living communities are devoid of potential builders.

3.6. Conclusions

The rocky outcrops of the 'Amazon reefs' are the most prominent structures observed in the Northern Sector of the ACM and originated by erosion of Pleistocene sandstones during sea-level lowstands, forming a complex seafloor morphology. Mixed siliciclastic and carbonate deposits, including ooids, accumulated on these erosion surfaces in shallow water during the LGM and early deglaciation locally together with shallow-water barnacle-bryozoan-coralline algal boundstones with sabellarids. These deposits were submerged by rising sea level and subsidence and were heavily bioeroded mainly by boring sponges and polychaetes. A thin layer of encrusting organisms, mainly calcareous algae, sponges, bryozoans, and serpulids, grew on the rocky surfaces. This living cover seems to have contributed to capturing and cementing small amounts of very fine-grained quartz, and to the precipitation of very thin patches of micrite.

Similar Pleistocene bioclastic sandstones to rudstones, rich in quartz grains, outcrop along the shelf break and in a canyon head in the Southern Sector. The living mesophotic community at 180 m forms a cover and is dominated by sponges and calcareous algae that contribute to the accumulation of a thin patchy layer of micrite and siliciclastic grains. In the Central Sector, in front of the Amazon River mouth, a different benthic community develops with absence of CCA.

CRediT authorship contribution statement

Nicholas F. L. Vale: Conceptualization, Investigation, Formal analysis, Writing – Original Draft. **Juan C. Braga:** Investigation, Writing – Review & Editing, Supervision.

Leonardo T. Salgado: Resources, Writing – Review & Editing, Project administration, Funding acquisition, Supervision. **Rodrigo L. Moura:** Conceptualization, Investigation, Field Work, Project administration, Funding acquisition, Review. **Fernando C. Moraes:** Investigation, Field Work, Writing – Review & Editing, Visualization. **Cláudia S. Karez:** Formal analysis, Review & Editing, Visualization. **Rodrigo T. de Carvalho:** Formal analysis, Review & Editing, Visualization. **Paulo S. Salomon:** Investigation, Field Work, Visualization. **Pedro S. Menandro:** Acquisition data, Formal analysis, Visualization. **Gilberto M. Amado-Filho (*in memoriam*):** Conceptualization, Investigation, Resources, Supervision, Project administration, Field Work, Funding acquisition. **Alex C. Bastos:** Conceptualization, Field Work, Acquisition data, Writing – Review & Editing, Supervision.

Declaration of Competing Interest

None.

Acknowledgements

This study was funded by the International Ocean Discovery Program (IODP/ *Coordenação de Aperfeiçoamento de Pessoal de Nível Superior* – CAPES Brazil (Project 38/2014), *Agência Nacional do Petróleo, Gás Natural e Biocombustíveis* (ANP/PetroRio) (Project 48610.011013/2014-66) and Dalio Philanthropies/OceanX Initiative (oceanx.org) (grant to RLM). NFLV received grants from CAPES (Finance Code 001) and International Mobility Program. ACB, RLM, LTS and PSS acknowledge long-term funding from the Conselho Nacional de Desenvolvimento Científico e Tecnológico (CNPq) and Fundação Carlos Chagas de Amparo à Pesquisa do Estado do Rio de Janeiro (FAPERJ). Research permits were granted by *Marinha do Brasil* and *Instituto Chico Mendes de Conservação da Biodiversidade* (ICMBio). Fabio S. Motta (UNIFESP), Laís S. Araujo (UFRJ) and Leonardo M. Neves (UFRRJ) helped in the field. Patricia L. Yager (UGA) helped with project conceptualization and funding acquisition. Ricardo Gama Bahia (IPJBRJ) helped with CCA identification, Guilherme Muricy and Julia Moser (MNRJ-UFRJ) helped with hexactinellid identification. We also thank the editor Edward Anthony, together with reviewer for their attention to detail, which has helped improve the paper considerably. We dedicate this work to the memory of our dear leader, Teacher Dr. Gilberto M. Amado-Filho (IPJBRJ).

Supplementary data

Supplementary Material to this article presents high-quality photographs of main samples, a list of the voucher samples of coralline algae and sponges deposited in the Herbarium of Instituto

de Pesquisas Jardim Botânico do Rio de Janeiro (RB) and Museu Nacional - Universidade Federal do Rio de Janeiro (MN) and a link to a video showing the dive operations in the three sites.

Data Availability Statement

All data produced as part of this research is included in the article and supplementary material.

Declaration of Competing Interest

The authors declare that they have no known competing financial interests or personal relationships that could have appeared to influence the work reported in this paper.

3.7. References

Allersma, E., 1971. Mud on the oceanic shelf off Guiana. In: Symposium on investigations and resources of the Caribbean Sea and adjacent regions, UNESCO, Paris, pp. 193-203.

Alencar, M.F.V.V., 2020. The Environmental Dimension of the "Brazilian Blue Amazon": Environmental Rights and Duties on the Continental Shelf. In: Environmental Jurisdiction in the Law of the Sea. Springer, Cham, pp. 247-296. https://doi.org/10.1007/978-3-030-50543-1.

Allison, M.A., Lee, M.T., Ogston, A.S., Aller, R.C., 2000. Origin of Amazon mudbanks along the north-eastern coast of South America. Marine Geology. 163, 241-256.

Araújo, L.S., Magdalena, U.R., Louzada, T.S., Salomon, P.S., Moraes, F.C., Ferreira, B.P., Paes, E.T.C., Bastos, A.C., Pereira, R.C., Salgado, L.T., Lorini, M.L., Yager, P., Moura, R.L., 2021. Growing industrialization and poor conservation planning challenge natural resources' management in the Amazon shelf off Brazil. Marine Policy. 128, 104465. https://doi.org/10.1016/j.marpol.2021.104465.

Aviz, D., Santos, C.R.M., Rosa Filho, J.S., 2021. Sabellariid (Polychaeta: Annelida) reefs as nursery ground for the hermit crab *Clibanarius symmetricus* (Randall, 1840) on the Amazonian coast of Brazil. Marine Biology Research. 17(1), 21-30. https://doi.org/10.1080/17451000.2021.1887494.

Bahia, R.G., 2014. Algas coralináceas formadoras de rodolitos da plataforma continental tropical e ilhas oceânicas do Brasil: levantamento florístico e taxonomia. Escola Nacional de Botânica Tropical, Rio de Janeiro, PhD thesis, 221 pp.

Barreto, L.A., Milliman, J.D., Amaral, C.A.B., Francisconi, O., 1975. Northern Brazil. Contr. Sedimentology. 4, 11-43.

Brasileiro, P.S., Braga, J.C., Amado-Filho, G.M., Leal, R.N., Bassi, D., Franco, T., Bastos, A.C., Moura, R.L., 2018. Burial rate determines Holocene rhodolith development on the Brazilian Shelf. Palaios. 33 (10), 464-477.

Coles, V. J., Brooks, M.T., Hopkins, J., Stukel, M.R., Yager, P.L., Hood, R.R., 2013. The pathways and properties of the Amazon River Plume in the tropical North Atlantic Ocean. Journal of Geophysical Research: Oceans, 118 (12), 6894-6913.

Cruz, A.M., Reis, A.T., Suc, J.P., Silva, C.G., Praeg, D., Granjeon, D., Rabineau, M., Popescu, S.M., Gorini, C., 2019. Neogene evolution and demise of the Amapá carbonate platform, Amazon continental margin, Brazil. Marine and Petroleum Geology. Elsevier. 105, 185-203.

Damuth J.E., Kumar N., 1975. Amazon cone: morphology, sediments, age, and growth pattern. Geological Society of America Bulletin. 86, 863-878.
Davies, P.J., Bubela, B., Ferguson, J., 1978. The formation of ooids. Sedimentology. 25, 703–30.
Döbelin, N., Kleeberg, R., 2015. Profex: A graphical user interface for the Rietveld refinement program BGMN, Journal of Applied Crystallography. 48, 1573-1580.
Doré, A.G., 1991. The structural foundation and evolution of Mesozoic seaways between Europe and the Arctic. Palaeogeography, Palaeoclimatology, Palaeoecology. 87, 441-492.
Duguid, S.M.A., Kyser, T.K., James, N.P., Rankey, E.C., 2010. Microbes and ooids. Journal of Sedimentary Research. 80, 236–51. https://doi.org/10.1111/sed.12218.
Dunham, R.J. 1962. Classification of carbonate rocks according to depositional texture. In Ham, W.E. (Eds.). Classification of Carbonate Rocks. American Association of Petroleum Geologists Memoir. 1, 108–121.
Embry, A.F., Klovan, J.E., 1972. Absolute water depth limits of late Devonian paleoecological zones. Geologishe Rundschau. 61(2), 672–686.
Figueiredo, J.J.P., Zalán, P.V., Soares, E.F., 2007. Bacia da Foz do Amazonas. Boletim de Geociências da Petrobrás, Rio de Janeiro. 15(2), 299–309.
Flügel, E., 2009. Microfacies of carbonate rocks. Elsevier. 983p.
Francini-Filho, R.B., Asp, N.E., Siegle, E., Hocevar, J., Lowyck, K., D'Avila, N., Vasconcelos, A.A., Baitelo, R., Rezende, C.E., Omachi, C.Y., Thompson, C.C., Thompson, F.L., 2018. Perspectives on the Great Amazon Reef: Extension, Biodiversity, and Threats. Front. Marine Science. 5,142. https://doi.org/10.3389/fmars.2018.00142.
Gorini, C., Haq, B.U., Reis, A.T., Silva, C.G., Cruz, A., Soares, E., Grangeon, D., 2013. Late Neogene sequence stratigraphic evolution of the Foz do Amazonas Basin, Brazil. Terra Nova. 26(3), 179-185. https://doi.org/10.1111/ter.12083.
Harris, P.M., Diaz, M.R., Eberli, G.P., 2019. The Formation and Distribution of Modern Ooids on Great Bahama Bank Paul. Annual Review of Marine Science. 11, 1–26. https://doi.org/10.1146/annurevmarine-010318- 095251.
Heaton, T.J., Köhler, P., Butzin, M., Bard, E., Reimer, R.W., Austin, W.E.N., Bronk Ramsey, C., Hughen, K.A., Kromer, B., Reimer, P.J., Adkins, J., Burke, A., Cook, M.S., Olsen, J., Skinner, L.C., 2020. Marine20-the marine radiocarbon age calibration curve (0-55,000 cal BP). Radiocarbon. 62(4), 779-820.
Hottinger, L., 1983. Neritic macroid genesis, an ecological approach. In: Peryt, T.M. (Ed.), Coated Grains. Springer, Berlin, pp. 38–55.
Kuehl, S.A., Nittrouer, C.A., Allison, M.A., Faria, L.E.C., Dukat, D.A., Jaeger, J.M., Pacioni, T.D., Figueiredo, A.G., Underkoffler, E.C., 1996. Sediment deposition, accumulation and seabed dynamics in an energetic fine-grained coastal environment. Continental Shelf Research. 16, 283-302.
Lavagnino, A.C., Bastos, A.C., Amado-Filho, G.M., Moraes, F.C., Araújo, L.S., Moura, R.L., 2020. Geomorphometric Seabed Classification and Potential Megahabitat Distribution in the Amazon Continental Margin. Frontiers Marine Science. 7, 190. https://www.frontiersin.org/articles/10.3389/fmars.2020.00190/full.
Lesser, M.P., Slattery, M., Leichter, J., 2009. Ecology of mesophotic coral reefs. Journal of Experimental Marine Biology and Ecology. 375, 1–8. http://doi.org/10.1016/j.jembe.2009.05.009.
Mahiques, M.M., Siegle, E., Francini-Filho, R.B., Thompson, F.L., Rezende, C.E., Gomes, J.D., Asp, N.E., 2019. Insights on the evolution of the living Great Amazon Reef System, equatorial West Atlantic. Science Reports. 9, 13699. https://doi.org/10.1038/s41598-019-50245-6.

Maneveldt, G.W., Van der Merwe, E., 2012. *Heydrichia cerasina* sp. nov. (Sporolithales, Corallinophycidae, Rhodophyta) from the southernmost tip of Africa. Phycologia. 51(1), 11–21. https://doi.org/10.2216/11-05.1.

Milliman, J.D., Barretto, H.T., 1975. Relict magnesian calcite oolite and subsidence of the Amazon shelf. Sedimentology, 22, 137-145.

Milliman, J.D., Summerhayes, C.P., Barretto, H.T., 1975. Quaternary sedimentation on the Amazon continental margin: a model. Geological Society of America Bulletin. 86, 610–614.

Moraes F.C., 2011. Esponjas das Ilhas Oceânicas Brasileiras. Rio de Janeiro: Museu Nacional, Série Livros 44. pp. 253.

Moser, J., Moraes, F.C., Castello-Branco, C., Pequeno, C.B., Muricy, G., 2022. Manned submersible dives reveal a singular assemblage of Hexactinellida (Porifera) off the Amazon River mouth, Northern Brazil. Zootaxa. 5105 (1), 2.

Moura, R.M., Amado-Filho, G.M., Moraes, F.C., Brasileiro, P.S., Salomon, P.S., Mahiques, M.M., Bastos, A.C., Almeida, M.G., Silva-Jr, J.M., Araujo, B.F., Brito, F.P., Rangel, T.P., Oliveira, B.C.V., Bahia, R.G., Paranhos, R.P., Dias, R.J.S., Siegle, E., Figueiredo-Jr, A.G., Pereira, R.C., Leal, C.V., Hajdu, E., Asp, N.E., Gregoracci, G.B., Neumann-Leitão, S., Yager, P.L., Francini-Filho, R.B., Fróes, A., Campeão, M., Silva, B.S., Moreira, A.P.B., Oliveira, L., Soares, A.C., Araujo, L., Oliveira, N.L., Teixeira, J.B., Valle, R.A.B., Thompson, C.C., Rezende, C.E., Thompson, F.L., 2016. An extensive reef system at the Amazon River mouth. Science Advances. 2(4), e1501252. https://doi.org/10.1126/sciadv.1501252.

Muricy, G., Esteves, E.L., Moraes, F.C., Santos, J.P., Silva, S.M., Klautau, M., Lanna, E., 2008. Biodiversidade Marinha da Bacia Potiguar: Porifera. Rio de Janeiro: Museu Nacional, Série Livros 29, pp. 156.

Nittrouer, C.A., Kuehl, S.A., DeMaster, D.J., Kowsmann, R.O., 1986. The deltaic nature of Amazon shelf sedimentation. Geological Society of America Bulletin. 97, 444-458.

Nittrouer, C.A., DeMaster, D.J., 1996. The Amazon shelf setting: tropical, energetic, and influenced by a large river. Continental Shelf Research. 16(5), 553–573. https://doi.org/10.1016/0278-4343(95)00069-0.

Nittrouer, C.A., DeMaster, D.J., Kuehl, S.A., Figueiredo Jr, A.G., Sternberg,, R.W,, Faria, L.E.C., Fricke, A.T., 2021. Amazon sediment transport and accumulation along the continuum of mixed fluvial and marine processes. Annu. Rev. Mar. Sci. 13, 501-536. https://doi.org/10.1146/annurev-marine-010816-060457.

Omachi C.Y., Asp, N.E., Siegle, E., Couceiro, M.A.A., Francini-Filho, R., Thompson, F. 2019. Light availability for reef-building organisms in a plume-influenced shelf. Continental Shelf Research. 181, 25-33. https://doi.org/10.1016/j.csr.2019.05.005.

Pérez-Diaz, L., Eagles, G. 2017. South Atlantic paleobathymetry since early Cretaceous. Scientific Reports. 7, 11819. http://doi.org/10.1038/s41598-017-11959-7.

Pettijohn, F.J., Potter, P.E., Siever, R., 1987. Sand and Sandstone. Springer Science & Business Media, New York, pp. 553.

Reis, A. T., Araújo, E., Silva, C.G. Cruz, A.M., Gorini, C., Droz, L., Migeon, S., Perovano, R., King I, Bache, F., 2016. Effects of a regional décollement level for gravity tectonics on late Neogene to recent large-scale slope instabilities in the Foz do Amazonas Basin, Brazil. Marine and Petroleum. Geology. 75, 29-52.

Sandes J., Moraes F., Pinheiro U., Muricy, G., 2021. Taxonomy and distribution of Didiscus and Myrmekioderma (Demospongiae: Axinellida) off the mouths of the two largest rivers in Brazil, with description of four new species. Marine Biodiversity. 51, 27. https://doi.org/10.1007/s12526-021-01168-x.

Silva, A.C., Araújo, M., Bourles, B. 2005. Variação sazonal da estrutura de massas de água na Plataforma Continental do Amazonas e área oceânica adjacente. Revista Brasileira de Geofísica. 23(2), 1-13.

Stuiver, M., Reimer, P.J., Reimer, R.W., 2020. CALIB 8.2 at [http://calib.org]. Accessed 2020-3-20.

Syvitski, J. M. P., Vörösmarty, C. J., Kettner, A. J., Green, P., 2005. Impact of humans on the flux of terrestrial sediment to the global coastal ocean. Science. 308, 376–380.

Tetteh, J.T., 2016. The Cretaceous Play of Tano Basin, Ghana. International Journal of Applied Science and Technology. 6 (1), 1004-2221.

Tucker, M.E., Wright, V.P., 1990. Carbonate Sedimentology. New York: Wiley-Blackwell. pp. 496.

Vale, N.F.L., Amado-Filho, G.M., Braga, J.C., Brasileiro, P.S., Karez, C.S., Moraes, F.C., Bahia, R.G., Bastos, A.C., Moura, R.L., 2018. Structure and composition of rhodoliths from the Amazon River mouth, Brazil. Journal of South American Earth Sciences. 84, 149-159. https://doi.org/10.1016/j.jsames.2018.03.014.

Varona, H.L., Veleda, D., Silva, M., Cintra, M., Araújo, M., 2019. Amazon River plume influence on Western Tropical Atlantic dynamic variability. Dynamics of Atmospheres and Oceans. 85, 1–15.

Vital, H., 2014. The north and northeast Brazilian tropical shelves. *In:* Chiocci, F.L., Chivas, A.R. (Eds). Continental Shelves of the World: Their Evolution During the Last Glacio-Eustatic Cycle. Geological Society, London, Memoirs. 41, 35–46.

Yokoyama, Y., Esat, T.M., Thompson, W.G., Thomas, A.L., Webster, J.M., Miyairi, Y., Sawada, C., Aze, T., Matsuzaki, H., Okuno, J., Fallon, Stewart, Braga, J.C., Humblet, M., Iryu, Y., Potts, D.C., Fujita, K., Suzuki, A., Kan, H., 2018. Rapid glaciation and a two-step sea level plunge into the Last Glacial Maximum. Nature. 559, 603–607. https://doi.org/10.1038/s41586-018-0335-4.

3.8. Supplementary data

Distribution, morphology and composition of mesophotic 'reefs' on the Amazon Continental Margin

Nicholas F. Vale, Juan C. Braga, Rodrigo L. de Moura, Leonardo T. Salgado, Fernando C. de Moraes, Claudia S. Karez, Rodrigo T. de Carvalho, Paulo S. Salomon, Pedro S. Menandro, Gilberto, M. Amado-Filho, Alex C. Bastos

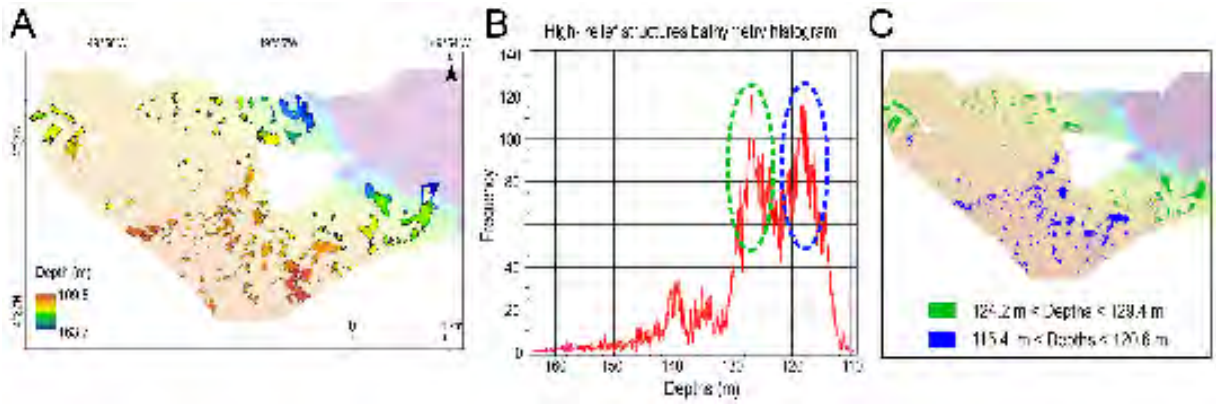

Figure S1. (**A**). The bathymetry cut inside the polygons representing the high-relief structures (HRS) in the Northern Sector. (**B**) Histogram of the depths of the HRS' polygons, with indications of two well-defined depth ranges. (**C**). Distribution of the depth ranges marked in the histogram.

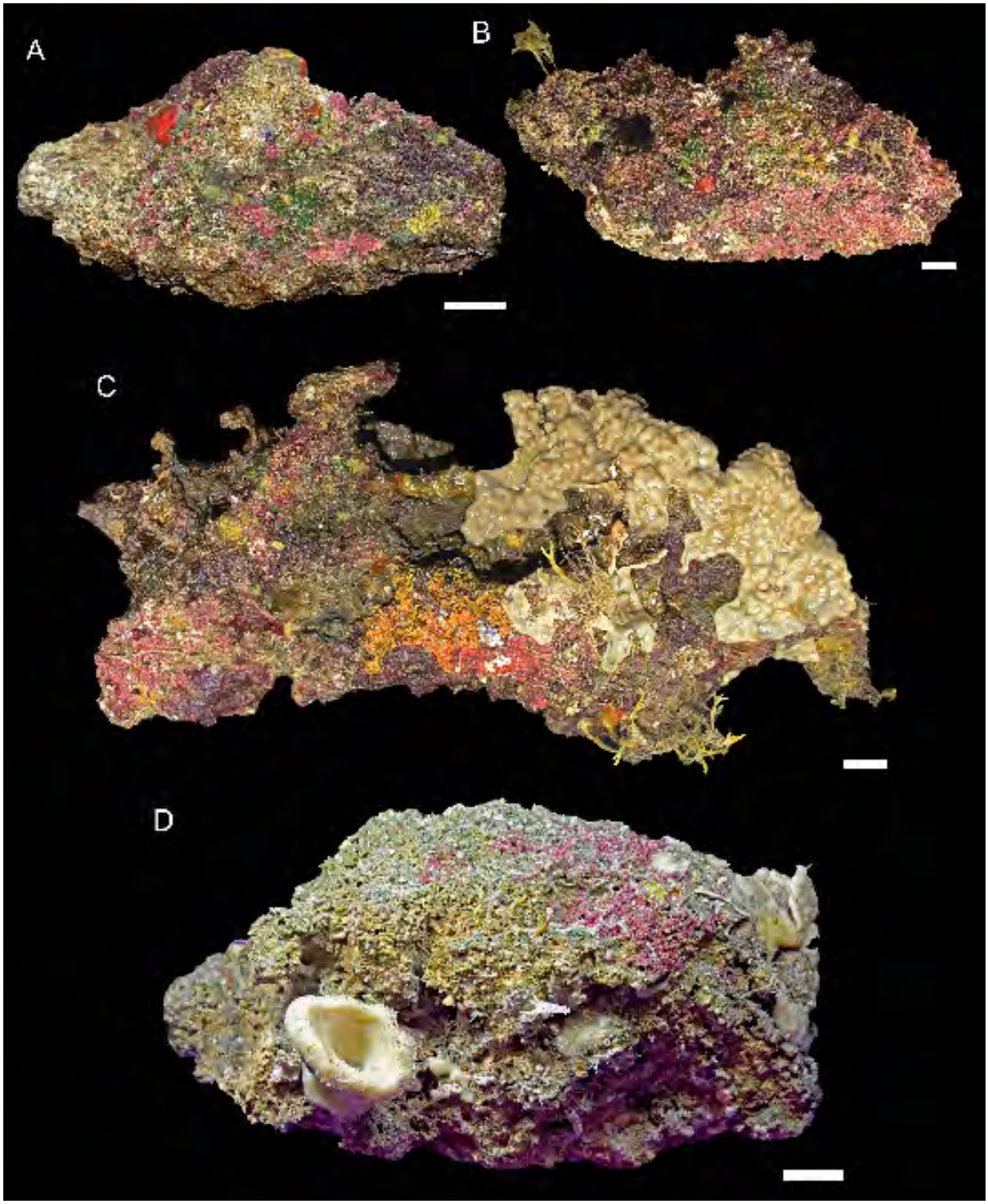

Figure S2. Carbonate samples collected in different sectors and depths of the ACM, showing most common living organisms on the surfaces, such as living ascidians, green algae, non-geniculate corallines, sponges and Peyssonneliales. (**A**). Boundstone sample 1 (from Northern Sector at 117 m depth). (**B**). Rudstone sample 5 (from Northern Sector at 120 m depth). (**C**). Boundstone sample 7 (from Northern Sector at 120 m depth). (**D**). Rudstone sample 8 (from Southern Sector at 180 m depth). Scale bars = 2 cm..

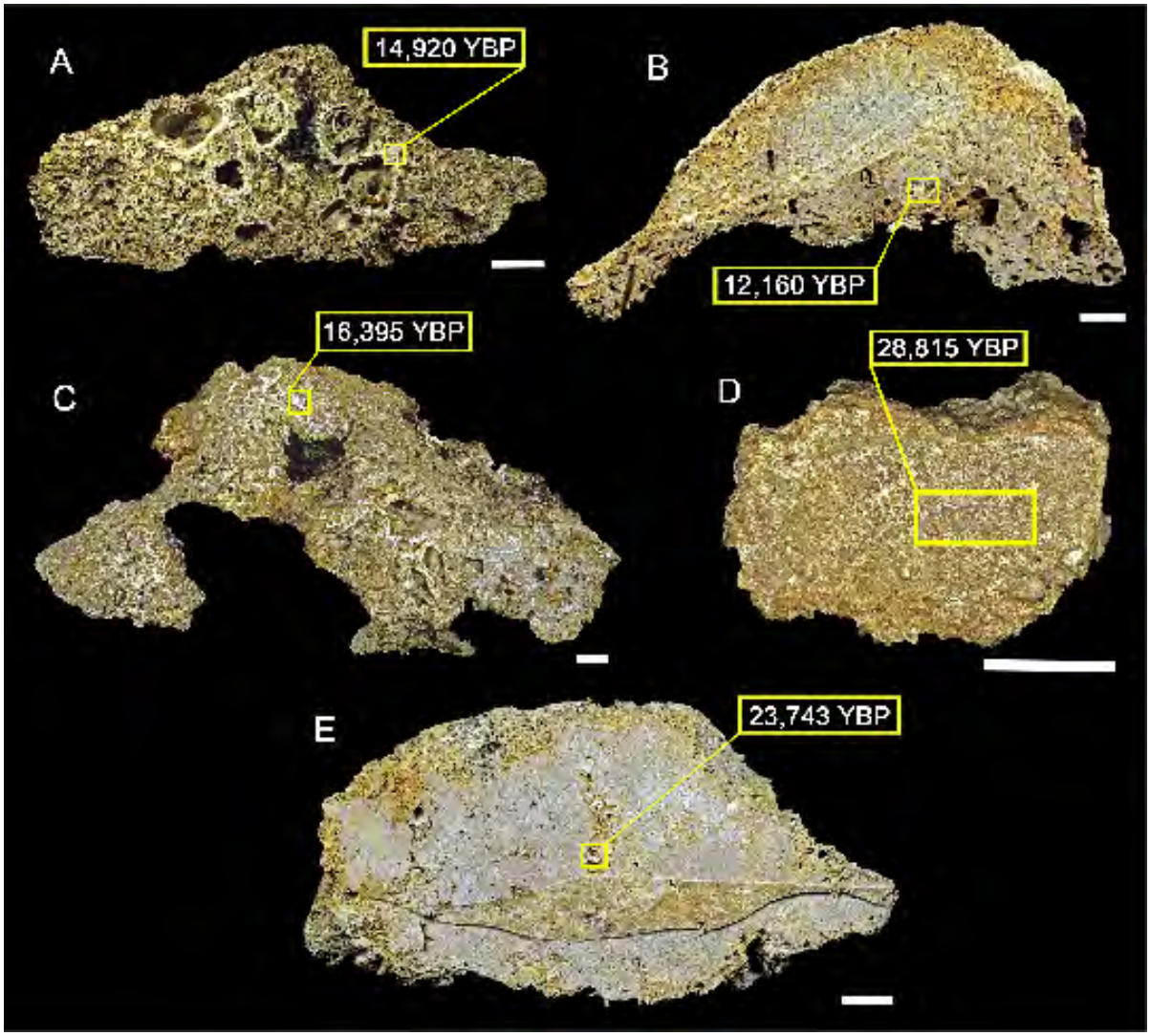

Figure S3. Radiocarbon dated carbonate samples collected in different zones and depths of the ACM. Yellow squares indicate the dated organisms. (**A**). Barnacle in sample 1 (Northern Sector at 117 m depth). (**B**). Foraminifera in sample 5 (Northern Sector at 120 m depth). (**C**). Barnacle in sample 7 (Northern Sector at 120 m depth). (**D**). Mollusk shell in fragment rock of sample 8 (Southern Sector at 180 m depth). (**E**). Foraminifera in sample 8 (Southern Sector at 180 m depth). Scale bars = 2 cm.

Table S1.

Voucher samples of coralline algae and sponges deposited in the Herbarium of Instituto de Pesquisas Jardim Botânico do Rio de Janeiro (RB) and Museu Nacional - Universidade Federal do Rio de Janeiro (MN), respectively. Coordinates in SIRGAS 2000 Datum.

Phylum	Family	Genus	Latitude	Longitude	Depth (m)	Voucher
Rhodophyta	Corallinaceae	*Harveylithon* sp.	4.372717	-49.922133	117	RB 822624

Rhodophyta	Corallinaceae	*Harveylithon* sp.	-0.453100	-43.983333	180	RB 822623
Rhodophyta	Corallinaceae	*Lithophyllum* sp.	4.372717	-49.922133	120	RB 822620
Rhodophyta	Hapalidiaceae	*Mesophyllum* sp.	4.372717	-49.922133	117	RB 822617
Rhodophyta	Hapalidiaceae	*Mesophyllum* sp.	4.372717	-49.922133	120	RB 822619
Rhodophyta	Hapalidiaceae	*Mesophyllum* sp.	4.372717	-49.922133	120	RB 822621
Rhodophyta	Sporolithaceae	*Sporolithon* sp.	4.372717	-49.922133	117	RB 822618
Rhodophyta	Sporolithaceae	*Sporolithon* sp.	-0.453100	-43.983333	180	RB 822622
Porifera	Ancorinidae	*Jaspis* sp.	4.372.717	-49.922.133	120	MNRJ21570A
Porifera	Chalinidae	*Haliclona* sp.	4.372.717	-49.922.133	120	MNRJ21570B
Porifera	Corallistidae	*Corallistes* sp.	-0.453100	-43.983.333	180	MNRJ21293
Porifera	Dactylocalycidae	*Dactylocalyx pumiceus*	1.521.682	-46.737.600	260	MNRJ21299
Porifera	Dactylocalycidae	*Dactylocalyx pumiceus*	-0.454082	-43.990.878	210	MNRJ21284
Porifera	Heteroxyidae	*Myrmekioderma guajajara*	-0.453100	-43.983.333	180	MNRJ21285

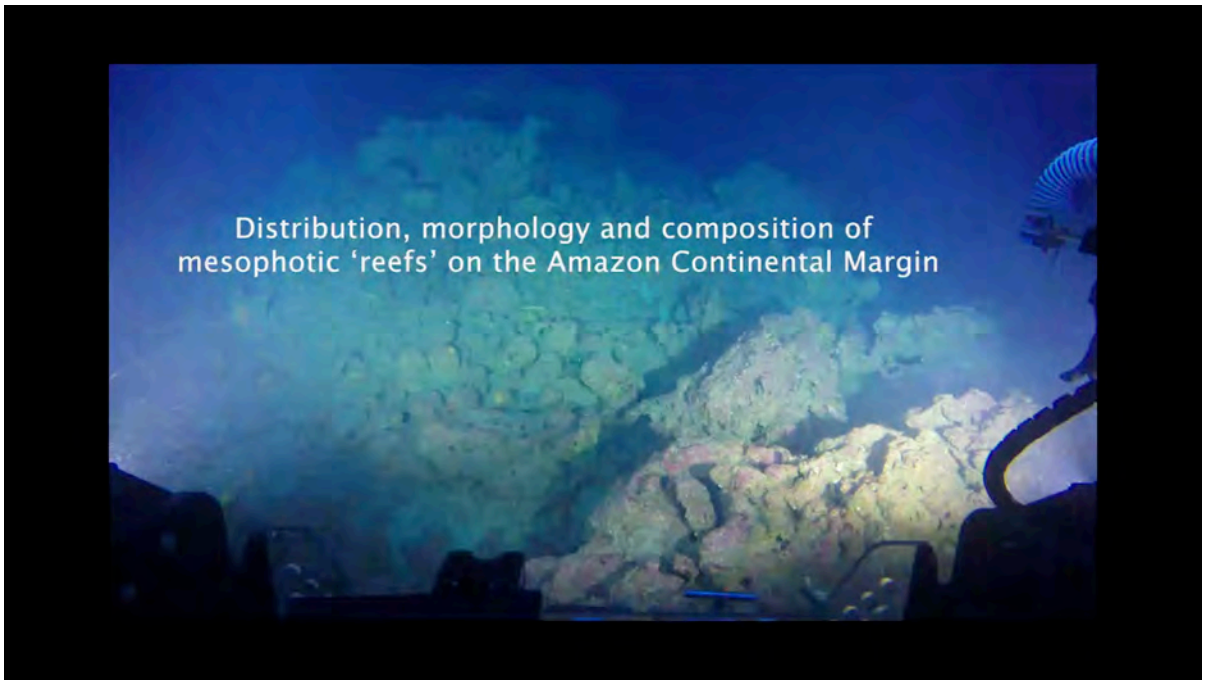

Video S1. Video obtained by submersible operations with R/V *Alucia* on July/17 showing three areas from the outer shelf of the Amazon Continental Margin that are typically dominated by High-Relief Structures (Northern Sector between 100-120 m depth) and outcrops (Central Sector between 250-378 m depth and Southern Sector between 180-230 m depth).

4. Structure and composition of rhodolith beds from the Sergipe-Alagoas Basin (NW Brazil, Southwestern Atlantic)

Published in the Journal of *Diversity* **2022**, v. 14(4), 282. (Appendix 2)

AUTHORS: Nicholas F. Vale, Juan C. Braga, Alex C. Bastos, Fernando C. de Moraes, Claudia S. Karez, Ricardo G. Bahia, Luis A. Leão, Renato C. Pereira, Gilberto M. Amado-Filho, Leonardo T. Salgado

Abstract

Rhodolith beds are biogenic benthic habitats mainly formed by unattached, non-geniculate coralline algae, which can be inhabited by many associated species. The Brazilian continental shelf encompasses the largest continuous rhodolith bed in the world. This study was based on samples obtained from seven sites and videos taken by a Remotely Operated Vehicle (ROV) at four transects off the Sergipe-Alagoas Coast on the northeast Brazilian shelf. ROV operations and bottom trawl sampling revealed the occurrence of rhodolith beds between 25 and 54 m depths. At the shallower depths, fruticose (branching) rhodoliths (maërl) appear in troughs of ripples, and other non-branching rhodoliths occur associated with corals and sponge patches surrounded by bioclastic sand. Rhodoliths also occur in patches from 30 to 39 m depth; some are fused, forming larger, complex tridimensional structures. At deeper depths, from 40 to 54 m, the abundance of rhodoliths increases and occur associated with fleshy macroalgae on a smooth seafloor; some rhodoliths are fused into complex structures, locally some are fruticose (maërl), and others are partially buried by fine-grained sediment. The collected rhodoliths vary from fruticose in two sites to encrusting to lumpy, concentric and boxwork nodules in the rest; their size ranges from small (<1.5 cm) to large (~6 cm) and are mostly sub-spheroidal to spheroidal. A total of 16 red algal morpho-taxa were identified in the study sites. Two phases of growth can be distinguished in some rhodoliths by changes in color. The brownish inner cores yielded ages of 1600–1850 cal years before the present, whereas outer layers were much younger (180–50 years BP old). Growth layers appeared to have been separated by a long period of burial in the seafloor sediment. Other rhodoliths have ages of hundreds of years.

Keywords: non-geniculate coralline red algae; rhodolith beds; maërl; morpho-anatomy; ROV; Brazilian Northeast continental shelf.

4.1. Introduction

Throughout their evolutionary history, non-geniculate coralline algae have been present in carbonate platforms as well as siliciclastic and mixed carbonate-siliciclastic systems [1]. Living and fossil non-geniculate coralline algae occur as crusts of varying thickness on both hard and soft substrates and free-living (unattached) nodules, also called rhodoliths and maërl, which can occur in large concentrations on the seafloor, known as rhodolith beds [2]. The rhodoliths occur worldwide from polar to tropical seas in a wide depth range on marine shelves [3,4] and are generally found where light is weak but sufficient for non-geniculate coralline algal growth and water motion and/or bioturbation are sufficient to move the rhodoliths [5]. Rhodoliths develop, in many cases, around a nucleus (bioclast or rock fragment) and can be composed of one or several non-geniculate coralline algal species, which can be intergrown with other encrusting organisms, such as bryozoans, gastropods, serpulids and encrusting foraminifera [6]. The rhodolith beds form three-dimensional complex biogenic benthic habitats [5] inhabited by a diverse biota of macroalgae and invertebrates [7–9], in particular crustaceans, polychaetes [10], cnidarians and chitons [11]. Some species of the associated fauna seem to be rhodolith-specific [12], influenced by rhodolith-forming species and rhodolith morphologies [13,14]. Furthermore, the phytobenthic community from the Sergipe-Alagoas (SEAL) Basin was characterized by a rich flora with a predominance of red algae (Rhodophyta) [15], showing an increasing gradient from the coast to the deepest regions, with lower values in the coastal areas under the influence of the São Francisco, Sergipe and Vaza-Barris rivers, and higher values in the deeper areas, characterized by the occurrence of more stable sediments [15], consisting of rhodolith beds.

Analyses of growth forms (e.g., lumpy, warty or encrusting) and the taxonomic composition of the non-geniculate coralline algae from the nucleus to the surface of the rhodoliths can provide valuable information on paleoenvironmental conditions during their

development [1]. Rhodoliths and rhodolith beds do not grow continuously, as their growth could be interrupted by burial [16], sometimes making paleoenvironmental inferences from their growth record difficult [1].

The Brazilian continental shelf encompasses the largest continuous rhodolith beds in the world [17]. The fauna associated with rhodolith beds indicates high diversity of species across extensive areas of the continental shelf, but the main geographical gap of knowledge about rhodolith beds in Brazil is the northeast coast, specifically the continental shelf between Sergipe and Pernambuco, including the region of the São Francisco River mouth [18]. The marine sedimentation of the Sergipe-Alagoas continental shelf was analyzed in some studies that characterized Holocene sedimentation [19,20]. These studies show the spatial distribution of the main carbonate and siliciclastic components of the seabed [20,21] and their contributions to the formation of superficial sediment, comparing biotic and abiotic characteristics [22,23].

In this study, we aimed to (a) determine the distribution, structure and composition of rhodolith beds from the middle and outer shelf of the Sergipe-Alagoas Basin and (b) know their temporal evolution by establishing rhodolith ages obtained at different depths through carbon radiometric dating.

4.2. Study area

The SEAL Basin on the northeast shelf of Brazil is subdivided into the Alagoas sub-basin, Sergipe sub-basin, Cabo sub-basin and Jacuípe sub-basin [24]. The study area (35◦ to 37◦ W and 10◦ to 11◦ S) is located within the Sergipe sub-basin and northern Jacuípe sub- basin, between the mouths of the Coruripe and Piaui-Real rivers (Figure 1). The Sergipe and south Alagoas continental shelf is considered shallow and narrow, with an average depth of 45 m and an average width of 28 km in Alagoas, 33 km in north Sergipe and 22 km in south Sergipe [23,25], with the shelf break beginning between 36 and 51 m depth in the center of the study

area. It presents a gentle slope of approximately 1:570 and is characterized by a series of incised-shelf valleys, which have a northwest–southeast direction [23]. The main hydrographic basins of the study area are Coruripe, São Francisco, Japaratuba, Sergipe, Vaza Barris, Piauí and Real [26]. The continental shelf has different geomorphological settings along its 380 km length. These include five different areas, namely smooth areas or areas with little roughness, rough areas, canyons, incised valleys and aligned banks [27]. Rough areas are located south of Alagoas, between the São Francisco and Japaratuba rivers and south of Sergipe and correspond to the carbonate domain with calcareous algae [27]. We subdivided the carbonate domain into north, central and south sectors (Figure 1), which are separated by the two largest canyons, formed by the influence of the São Francisco and the Japaratuba rivers. The outer shelf of the north sector shows a reduced width and a soft and smooth relief in the southern part and a rugged and steeper relief in the northern one. The outer zone starts at the 30 m isobath and continues until the shelf break [23]. The incised valleys were partially filled with fine sediments, and carbonate deposition at the outer edge of the shelf is segmented by muddy zones adjacent to the river mouths. During the last deglaciation, the continental shelf of the SEAL was quickly flooded by the rapid rise in sea level. The shelf flooding started around 10,000 years BP and was completed 3000 years later [28,29]. The presence of sediments deposited over a geological history that extends from the penultimate marine regression represents the last marine transgression and records the stage of the current marine regression [21].

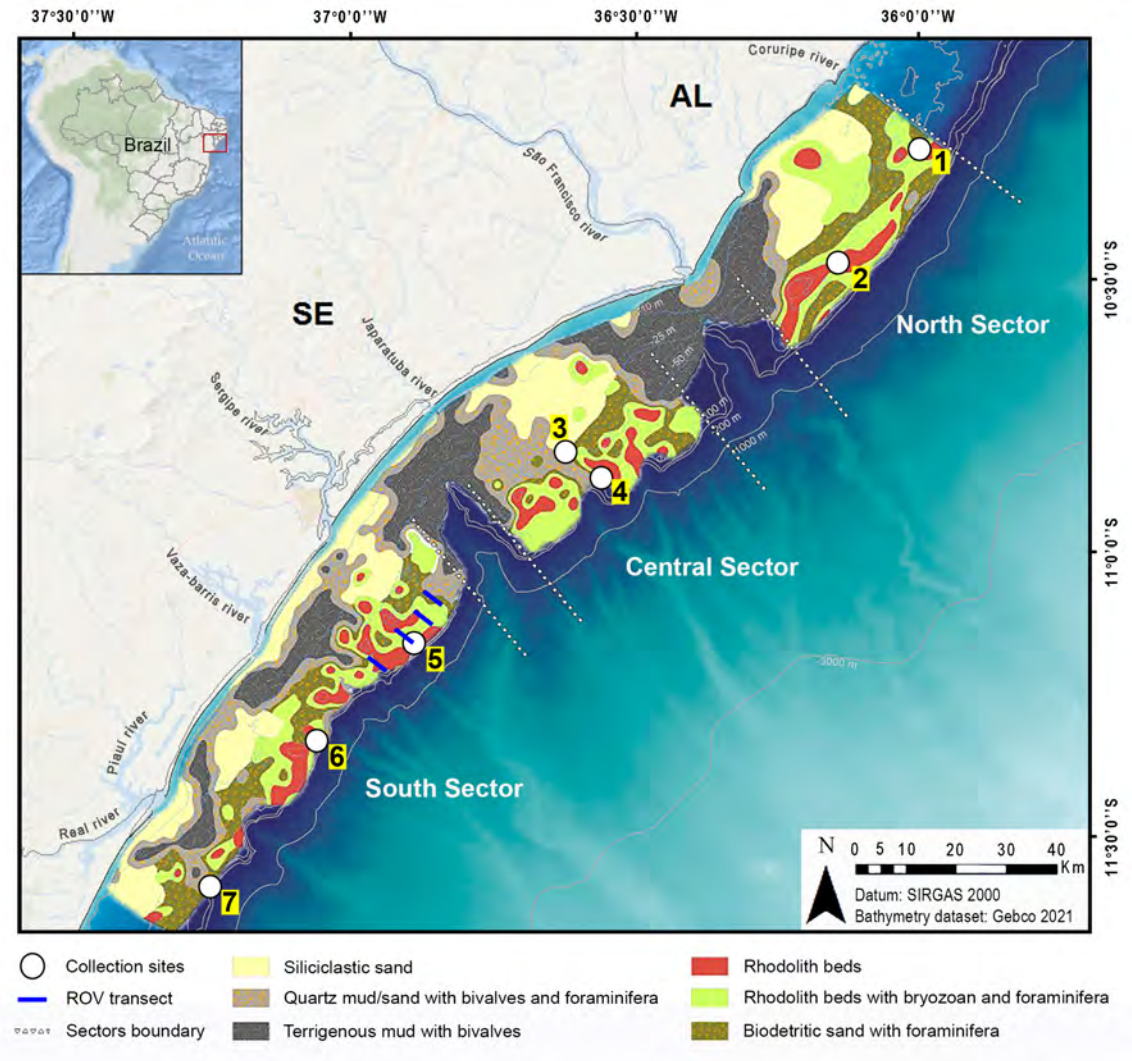

Figure 1. Sergipe-Alagoas (SEAL) Basin and collection sites (white circles with numbers 1–7) along the three carbonate domain sectors (North, Central and South) on the middle/outer shelf collected in 2011 and transects surveyed by a remotely operated vehicle (ROV) from the south sector obtained in 2014 (blue lines) with biofacies data [21] and the bathymetry dataset [22].

The tidal regime in the study area is semi-diurnal, with amplitude between 1.0 to 3.0 m [26], and the wave regime is high energy, predominating from NE and E in January to May (summer–autumn) and September to November (spring), and SE waves occur from March to August [26,30]. The normal sea surface temperature (SST) values vary between 25 and 28 ◦C and show a discrete decrease from north to south [26]. The SST in the summer and winter periods oscillates around 27–28 ◦C and 25–26 ◦C, respectively. Salinity (36–37‰) increases in the north and south, from the coastal region to the outer shelf, except near the river mouths, where salinity can reach values as low as 32–33‰ [26]. The primary productivity varies from

1.6–2.0 mg C/m2/day, and surface chlorophyll A concentrations vary from 0.7 and 5 mg/m3, with the highest values recorded in the coastal zone, which presented the potential of effective littoral drift with a predominant direction to the south [30]. The São Francisco River Basin discharges at the border between Sergipe and Alagoas and is the largest drainage basin in the Brazilian territory [29]. It is also one of the most regulated rivers in the country, and the discharge of the São Francisco River was drastically altered by the construction of six large dams built to generate energy and regulate flow [29]. Its average annual flow of more than 3000 m3/s declined by 80%. Its natural seasonal pulsation has been regulated to an almost constant flow of ~600 m3/s [25], and approximately 95% of the river's total solids in suspension (TSS) are retained within the dam reservoirs [22,29,30]. The impact of the dams has considerably modified the main estuarine processes and sediment transportation; coastal erosion has also been drastically increased [31–34]. The São Francisco River and its delta have been featured in global compilations on the effects of sediment retention in dams and the risks represented by climate change [35]. Since 1960, rainfall has declined by approximately 27%, and average annual precipitation is projected to decrease up to 35% by 2080, compared to the average of 1961–1990, using the A1B scenario of the IPCC [35].

Currently, the continental shelf is characterized by low fluvial input and greater influence of the tropical surface waters (TSW) of the South Equatorial Current (SEC) that flows from east to west across the Atlantic Ocean [26,30]. In the proximity of the São Francisco and Japaratuba canyons during the summer months (December), there are lower temperatures and nutrient-rich waters due to the seasonal upwelling of the South Atlantic Central Water [26]. These environmental conditions promote the predominance of carbonate features from 30 m to 60 m depth, dominated by gravel and biogenic carbonate components [19,21,36] with an associated biota [19].

Coastal sediment transport along the Sergipe coast is 790,000 m3/year, with about 658,000 m3/year in the NE–SW direction and 132,000 m3/year in the opposite direction [37]. These processes influence the coastal region, either through coastal erosion in certain places or through deposition in others, as observed on the coast of the Sergipe State [38]. Large areas of smooth mud surfaces have been identified in front of the mouths of the São Francisco and Japaratuba rivers [39]. The middle and outer shelf, ca. 10,000 km2 of the Sergipe–Alagoas shelf, are mainly characterized by carbonate deposits [39]. In southern Alagoas, these carbonate sediments are also found near the coastline [27]. Rough surfaces were found in the north sector, in the central sector, between the mentioned rivers, and in a larger area in the south sector. Siliciclastic components (quartz and rock fragments) are present along the inner shelf, up to 30 m depth, while carbonate contents that are predominate on the middle to outer shelf consist of rhodolith beds (Figure 1) that comprise non-geniculate coralline algae, foraminifera, bivalves and bryozoans (82%), while green algae *Halimeda* sp., echinoderms (spines and tests of urchins), spicules of sponges, fragments of crustaceans, gastropods, scaphopods, serpulids and corals are minor components, representing the remaining 18% [19,21].

4.3. Materials and Methods

4.3.1. Sampling

Data were collected within the framework of the SEAL Basin Regional Characterization Project carried out by Petrobras (Brazilian Petroleum S.A., Rio de Janeiro, RJ, Brazil) and the Federal University of Sergipe (UFS) from 2008 to 2018. A total of 53 high-definition video images, comprising 33 h of video inspections, was recorded from February to March 2014 [40] with a remotely operated vehicle (ROV) along four transects with a length of 4 km per transect, ranging from 25 to 46 m depth in the south sector of the study area (Figure 1, Supplementary Material Table S1 and Video S1). The cover percentage of rhodoliths was estimated by the proportion of the total video time spent on rhodolith concentrations.

Due to the high facies complexity of the continental margin of the Sergipe and Alagoas shelf and the distribution patterns of the biota along environmental gradients, the strategy for selecting the collection sites considered longitudinal, latitudinal and bathymetric gradients [41]. Rhodolith samples (404 rhodoliths) were obtained from two expeditions: the first carried out from 29 January to 6 February 2011 aboard the R/V *Luke Thomas* and the second from 24 June to 3 July 2011 aboard the R/V *Seward Johnson*, using a trawl [41]. The samples were stored in the Laboratory of Benthos from UFS and later ceded to the Instituto de Pesquisas Jardim Botânico do Rio de Janeiro (IPJBRJ). Rhodolith sampling sites and ROV video transects are shown in Figure 1. A total of seven sites between 27 and 54 m in depth were sampled along the middle and outer shelf of the SEAL Basin (Figure 1 and Table 1). The geomorphological features of the shelf evaluated by high-resolution mapping in other studies [21,22], combined with the biofacies classes, sedimentological data [21] and the bathymetry dataset [22], were incorporated into a geographic information system (GIS) environment on the QGIS platform to produce the map in Figure 1.

Table 1. Sampling site locations, water depth and number (n = 404) of samples collected and analyzed in the present study. Coordinates are in SIRGAS 2000 Datum.

Site	Sector	Water depth (m)	Latitude	Longitude	Samples (n)
1	North	30	-10.2789	-35.9792	07
2	North	30	-10.4875	-36.1245	173
3	Central	27	-10.8223	-36.6118	04
4	Central	47	-10.8694	-36.5472	141
5	South	47	-11.1642	-36.8839	05
6	South	54	-11.3389	-37.0556	18
7	South	50	-11.5989	-37.2384	56

4.3.2. Sample characterization

The non-geniculate coralline algal growth forms were classified based on their morphology as encrusting, encrusting warty, lumpy and fruticose, according to [42,43]. The latter are monospecific rhodoliths lacking a macroscopic nucleus and characterized by a high prevalence of protuberances [44]. Based on their longest axes, rhodoliths were divided into large (d > 3 cm), medium (d = 1.5–3 cm) and small (d < 1.5 cm) size classes. Rhodolith sphericity was determined by measuring the longest, intermediate and shortest axes [45,46], and the triangular diagram plotting spreadsheet (TRI-PLOT) was used to separate ellipsoidal, discoidal or spheroidal shapes [46]. Species identification of crusts on the outermost surface of rhodoliths was conducted solely through the morpho-anatomical observation of histological sections (Supplementary Material Figure S1) of fertile material [44,47–50]. A permutational multivariate analysis of variance (PERMANOVA) with the software Primer (v.6) + PERMANOVA was used to evaluate possible significant differences in rhodolith size between the different sites and depths. Images of fruticose (branching) rhodoliths were used to derive a morphological parameter, the mean solidity index (degree of complexity of the thalli, which is reflected as values between 0—fully complex shape—and 1—no ramifications) of the thalli, corresponding to the surface of a given thallus of the fruticose rhodoliths on the image plane divided by its convex surface [51]. These analyses were performed using ImageJ 1.53 free software [51].

To characterize the inner structure of rhodoliths, 15 samples were selected and sectioned along their longest axis with a tungsten handsaw (Dremel 3000, Dremel, Bosch Power Tools). Both halves of the rhodoliths were then photographed using a digital camera (Nikon D7000, Nikon). The inner structure was defined as a boxwork, asymmetrical or concentric arrangement [42]. Small blocks (3 × 3 cm) were cut from 10 selected samples and were sent to the National Petrographic Service Inc. (Rosenberg, TX, USA) to make thin

sections. The carbonate texture [52,53] was identified, and the Bioerosion Index (BI) was determined [54] to estimate the extent to which the primary features were bioeroded. Fossil marine macroinvertebrates, foraminifera and borings were identified to the most precise taxonomic level possible. The average proportions (%) of the main rhodolith com- ponents, trace fossils, voids and sediment were estimated by counting on images taken from each thin section (10 images per sample (n = 10), with 50 points randomly distributed on each image) using the CoralNet program ([55], https://coralnet.ucsd.edu/; accessed on 12 March 2021). Voids include constructional voids (intraskeletal and spaces among encruster skeletons) and bioerosion [56]. Voucher specimens of algae were deposited in the Herbarium of the Rio de Janeiro Botanical Garden (RB) (Supplementary Material Table S2).

To determine the radiocarbon age, eight subsamples of fossils in rhodoliths were selected. About 10–20 mg of carbonate powder was obtained from each subsample with a tungsten handsaw (Dremel 3000, Bosch Power Tools) and then chemically pretreated with HCl. They were analyzed at the Center for Applied Isotope Studies (University of Georgia, Athens, GA, USA) using an Accelerator Mass Spectrometer (AMS, nuPlasma II multi-collector). All conventional radiocarbon ages (between 603 and 50,779 years before present (BP)) were recalibrated using the software CALIB 8.2 ([57], http://calib.org/; accessed on 28 August 2020), using the Marine20 calibration curve [58] and a global reservoir effect. Dates are reported as calendar years before present (cal year BP; “present” = 1950 CE) with a 2-sigma confidence interval.

4.4. Results

4.4.1. Seabed Characterization in the Examined ROV Transect Lines

In the south sector (around site 5), living rhodoliths were always associated with fleshy macroalgae and were recorded along the four ROV transects (totaling 16 km in length, 4 km

per transect). At the shallower depths (25–30 m) in this sector, fruticose (branching) rhodoliths (maërl) appeared in troughs of ripples on bioclastic sands (1.6 km; 10% of ROV transect length, Figure 2A, B). At the same depth range, patches of encrusting to lumpy rhodoliths (Figure 2C, D) were associated with corals, sponges and macroalgae (Figure 3A, C, D) and were surrounded by bioclastic sand occupying another 1.6 km (10%) of the transect length (Figure 2C, D). At depths between 30 and 39 m, rhodoliths patches extended for 4.8 km (30%) of the transect length and included small fused rhodoliths creating larger complex 3D structures together with corals and sponges (Figure 2E) associated with fleshy macroalgae (Figure 3B). From 40 to 54 m, the abundance of rhodoliths increased. They occurred in association with fleshy macroalgae on a smooth seafloor (6.4 km; 40% of transect length, Figure 2F), and some include fused rhodolith structures (Figure 2G). At this depth interval, 5% (0.8 km) of the transect length was occupied by rhodoliths partially buried by fine-grained sediment (Figure 2H). Fruticose (branching) rhodoliths (maërl) also occurred locally at 47 m. A reef fish community was observed associated with rhodolith patches between 36 and 44 m depth, including *Holocentrus adscensionis*, *Gymnothorax moringa* and *Cephalopholis fulva* (Figures 2E, and 3B, E, F) as the main species. Massive sponge species were recorded attached to rhodoliths, including *Aplysina* sp. and *Ircinia strobilina* (Figures 2D and 3C). The videos showed differences in rhodolith distribution between the northeast (green colour in Figure 1) and southwest (red colour in Figure 1). Rhodoliths were sparsely grouped, and some of them fused (Figure 2A–D) in the former transect, whereas rhodolith patches were larger with larger aggregates of fused rhodoliths (Figure 2E–H) in the latter.

Figure 2. *In situ* images of the explored sites on the middle and outer shelf of the south sector of the SEAL Basin: (**A**) Zoom-out of fruticose rhodoliths on ripple troughs (darker colours) at 30 m depth; (**B**) Zoom-in of the seafloor dominated by living fruticose rhodoliths at 30 m depth (vinaceous colours);

(**C**, **D**) Rhodolith patches at 30 m depth, depicting the sponge *Aplysina* sp.; (**E**) Reef formed by fused rhodoliths associated to corals (*Montastraea cavernosa*), macroalgae and encrusting sponges (*Monanchora arbuscula*) at 32 m depth; (**F**, **G**) Coalescent rhodoliths forming complex three-dimensional structures covered by macroalgae, at 41 and 43 m depths, respectively; (**H**) Rhodoliths partially buried by fine-grained sediment with living coralline algae covered by green macroalgae at 43 m depth. Scale bars = ~5 cm.

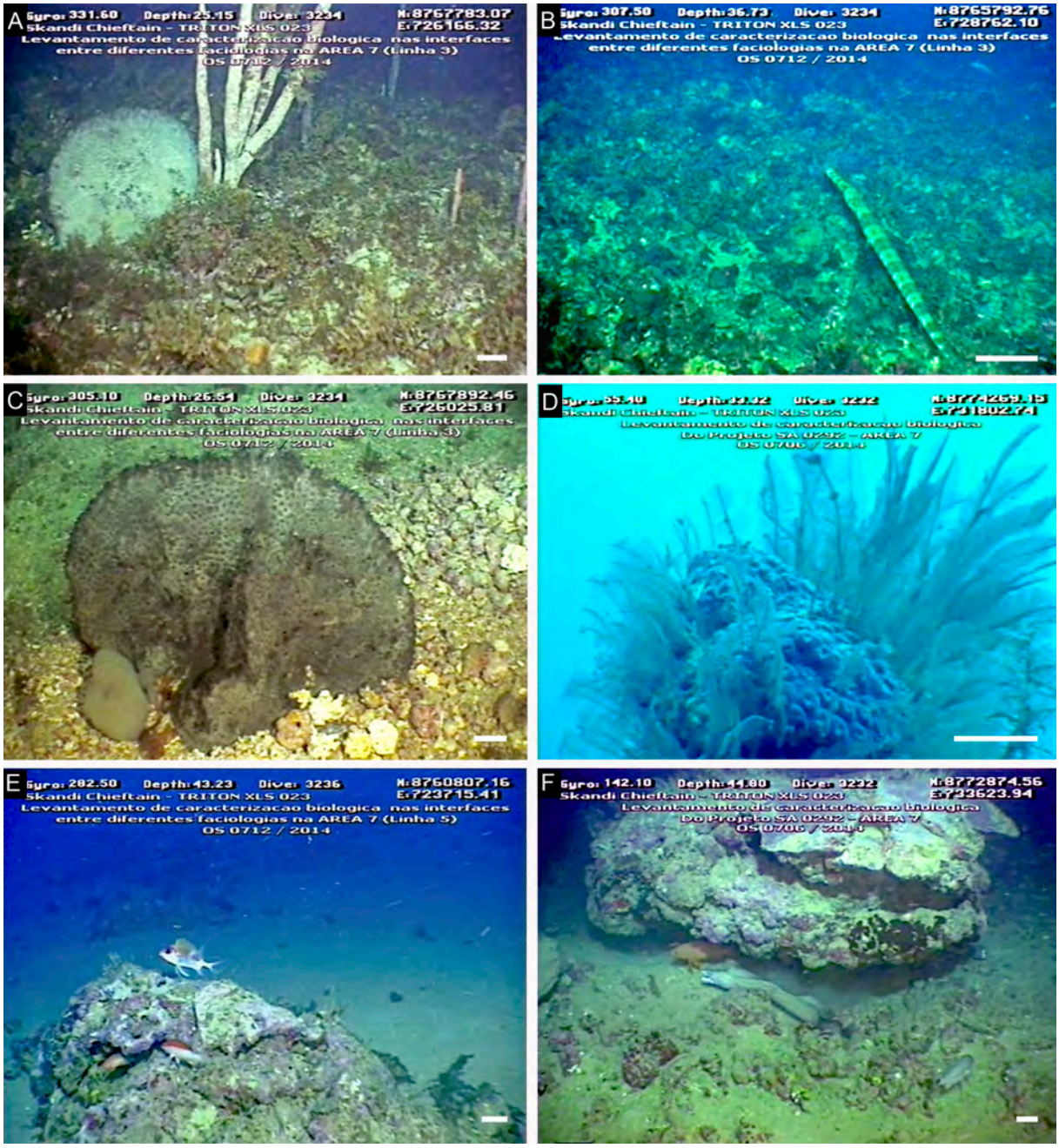

Figure 3. *In situ* images of the benthic community associated with the rhodolith beds on the south sector of the SEAL Basin: (**A**, **C**, **D**) Fleshy macroalgae, corals (*Montastraea cavernosa*) and sponges (*Aplysina* sp. and *Ircinia strobilina*) occur from 25 m to 30 m depth; (**B**, **E**, **F**) A reef fish community

(*Aulostomus maculatus*, *Holocentrus adscensionis*, *Gymnothorax moringa* and *Cephalopholis fulva*) occurs from 36 to 44 m depth. Scale bars = ~5 cm.

4.4.2. North Sector

The rhodoliths collected in the middle shelf at 30 m depth from site 1 were large (5.7–20.4 cm at the longest axis and mean diameter that ranged from 4.2–14.3 cm; Figures 4A and 5A), en- crusting and encrusting warty with mostly sub-discoidal (42.8%) to sub-spheroidal (28.5%) shapes (Figure 5B and Table 2). The rhodoliths examined from this site had living encrusting coralline algae (*Harveylithon* sp., *Sporolithon* sp.) and sponges partially covering their surfaces (Figure 4A). The nuclei consisted of coral fragments (Figure 6A) or other bioclasts. Coralline algae intergrown with bryozoans, corals and serpulids formed an asymmetrical cover with a boxwork structure. Coralline algae included *Mesophyllum* sp., *Lithophyllum* sp., *Harveylithon* gr. *catarinense* (I.O. Costa, P.A. Horta & J.M.C. Nunes 2019) and an unidentified Hapalidiales species (Figure 6C and Table 2). The three rhodoliths examined were heavily bored (Bioerosion Index is 4) by sponges (*Entobia*) and bivalves (*Gastrochaenolites*). Constructional voids and bio- erosion traces varied from empty to partially filled by wackestone rich in sponge spicules and micrite-rich packstone. Geniculate coralline algae, benthic and planktonic foraminifera, and solitary corals appeared in the fillings (Figure 6B and Table 3). Radiocarbon dating of a coral in the innermost part of a rhodolith sample yielded an age of 789 cal yr BP (Figure 7A), and a non-geniculate coralline alga in the outermost part of another rhodolith sample yielded an age of 180 cal yr BP (Figure 7B and Table 4).

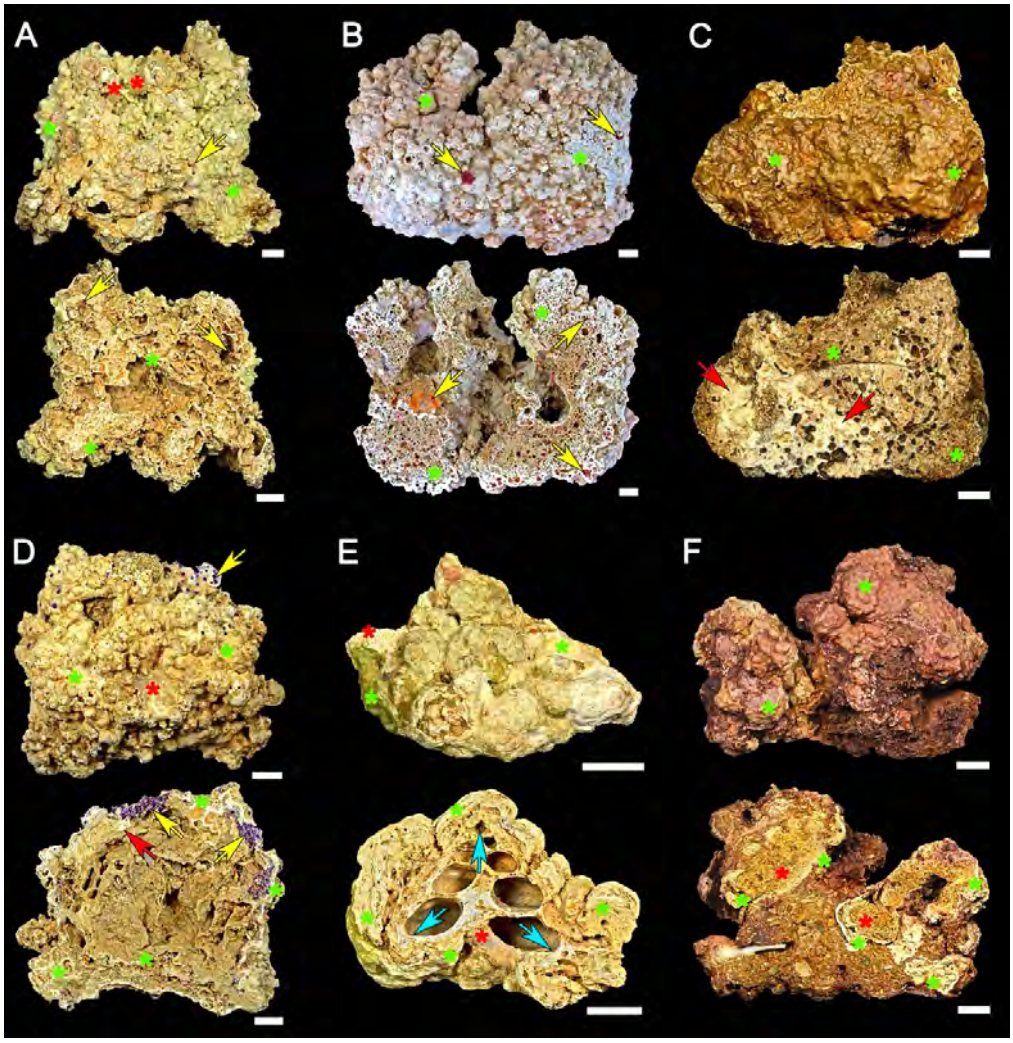

Figure 4. Surface and inner portion of rhodoliths analyzed in this study (upper and lower images, respectively): North sector: (**A**) rhodolith from site 1; (**B**) rhodolith from site 2; Central sector: (**C**) rhodolith from site 3; South sector: (**D**) rhodolith from site 5; (**E**) rhodolith from site 6; (**F**) rhodolith from site 7. Non-geniculate coralline algae (green asterisks), bryozoan (red asterisks), coral (red arrows), sponge *Cliona* cf. *schmidtii* (yellow arrows), gastropod (blue arrows). Scale bars = 1 cm.

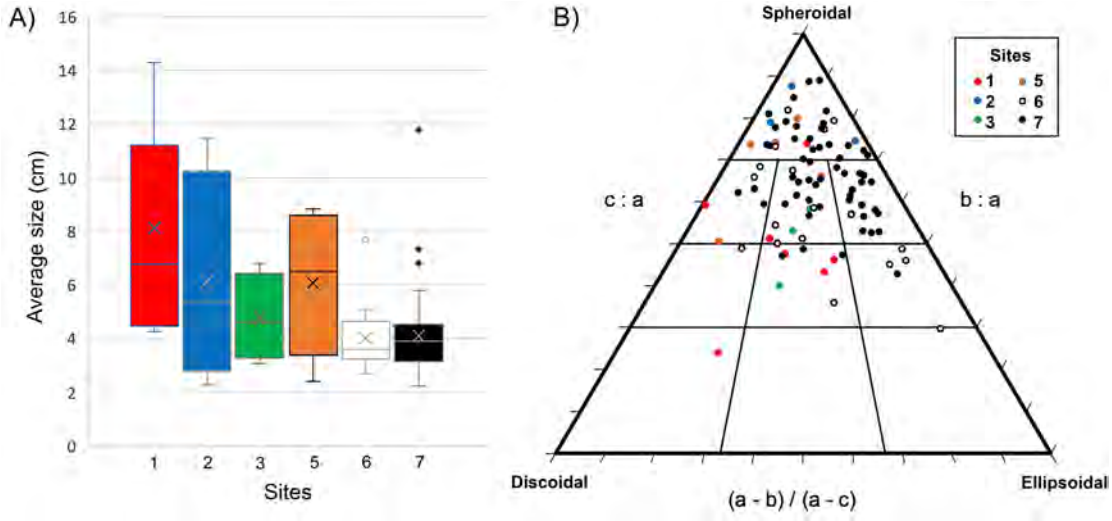

Figure 5. Graphical analyses of rhodolith (n = 94) size and shape: (**A**) Box plot showing average size range of rhodoliths (average axes value), considering them as ellipsoidal structures (with long, intermediate and short axes); (**B**) Shape classification of rhodoliths using a TRIPLOT diagram [40,41]: Long (a), intermediate (b) and short (c) axes of rhodoliths. Hence, branching rhodoliths were not considered for size and sphericity measurements.

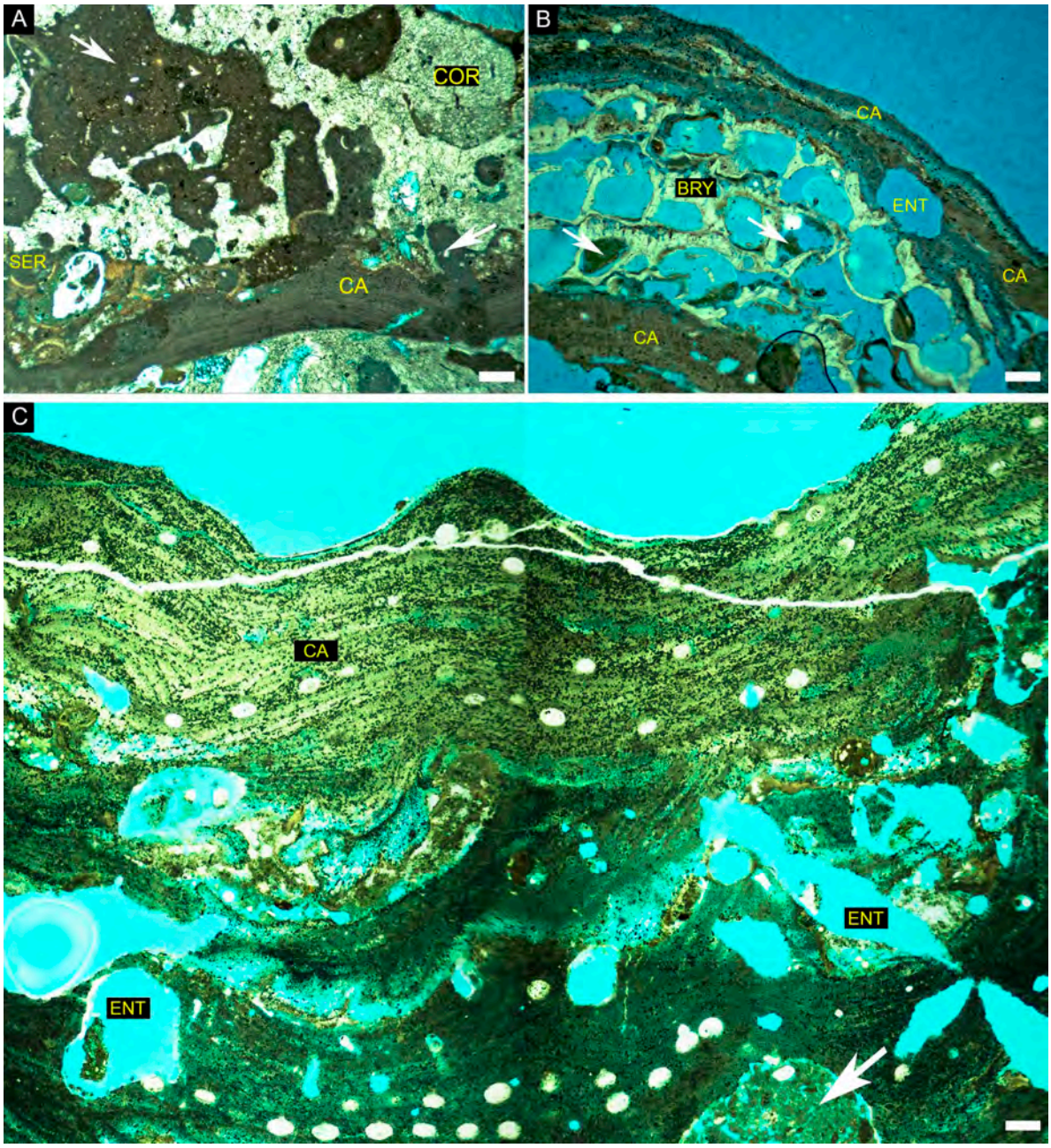

Figure 6. Thin-section images of rhodoliths from site 1 of the North Sector of the SEAL Basin (30 m depth). (**A**) Innermost portion of rhodolith sample 1 composed of coral (COR), coralline algae (CA) and serpulid (SER) with borings filled by micrite (white arrow) and siliciclastic grains (quartz-white grains); (**B**) Outermost portion of rhodolith sample 2 composed mainly by coralline algae (CA) intergrown with bryozoans (BRY) with sponge borings (*Entobia*-ENT), some filled by packstone (white arrow); (**C**) Middle to outermost portion of rhodolith sample 3 with dominance of *Harveylithon* gr. *catarinense* (CA) and sponge borings (*Entobia*-ENT), some filled by packstone (white arrow). Scale bars = 200 µm.

Table 2. Rhodolith size, coralline algal growth-form, rhodolith shape (%) and rhodolith-forming coralline algal species from the SEAL Basin. Surface (x-blue); outermost portion (x-green); innermost portion (x-red).

Site	Sector	(n)	Size			CCA growth-forms				Rhodolith shapes (%)						Rhodolith-forming coralline algae species													
			L	M	S	EN	EW	FR	L	SP	SSP	EL	SEL	DI	SDI	H	HR	HC	Hsp	Lisp	PF	Spsp	LtP	Ltsp	Lsp	Rs	ME	Msp	SFr	Ssp	Psp
1	N	7	7	0	0	4	1	0	2	14.29	28.57	0	0	14.29	42.86	x		x	x					x				x		x	
2	N	173	3	1	169	2	0	169	2	75	25	0	0	0	0		x							x	x	x	x	x			
3	C	4	4	0	0	4	0	0	0	0	50	0	0	0	50							x									x
4	C	141	0	0	141	2	7	130	2	0	0	0	0	0	0									x	x					x	
5	S	5	4	1	0	4	0	0	1	60	40	0	0	0	0	x	x		xx		x		x		x				x	xx	xx
6	S	18	18	0	0	11	1	0	6	22.22	38.89	5.56	16.67	0	16.67				x	x		x	x	x	xx	xx				x	x
7	S	56	54	2	0	36	8	0	12	39.29	53.57	0	1.79	0	5.36	x			x	xx		x	xx	xx	xx	x	x			x	xx

N = North sector; C = Central sector; S = South sector; L = Large (d > 3 cm); M = Medium (d = 1.5–3 cm); S = Small (d< 1.5 cm); EN = Encrusting; EW = Encrusting warty; FR = Fruticose; L = Lumpy; SP = Spheroidal; SSP = Sub-spheroidal; EL = Ellipsoidal; SEL = Sub-ellipsoidal; DI = Discoidal; SDI = Sub-discoidal; H = unidentified Hapalidiales; HR = *Harveylithon* gr. *rupestre*; HC = *Harveylithon* gr. *catarinense*; Hsp = *Harveylithon* sp.; Lisp = *Lithoporella* sp.; PF = *Pneophyllum* gr. *fragile*; Spsp = *Spongites* sp.; LtP = *Lithophyllum* gr. *pustulatum*; Ltsp = *Lithophyllum* sp.; Lsp = *Lithothamnion* sp.; Rs = *Roseolithon* sp.; ME = *Melyvonnea erubescens*; Msp = *Mesophyllum* sp.; SFr = *Sporolithon franciscanum*; Ssp = *Sporolithon* sp.; Psp = *Peyssonnelia* sp.

Table 3. Main components (%) in ten analyzed rhodolith samples from the SEAL Basin. 1gp = first growth phase (innermost portion); 2gp = second growth phase (outermost portion).

	North Sector (Site 1)			Central Sector (Site 3)	South Sector (Site 5)		South Sector (Site 6)			South Sector (Site 7)		
Sample number	**1**	**2**	**3**	**4**	**5**	**6**	**7**	**8-1gp**	**8-2gp**	**9**	**10-1gp**	**10-2gp**
Bryozoan	3.94	12.29	7.54	0.58	8.4	5.62	47.4	17.26	37.27	16.38	26.25	7.75
Coral	20.15	0	0.91	52.15	2.31	8.51	0	0	0	0	0	0
Geniculate coralline algae	1.34	0	0	0	0.8	0.35	0	0	0	0	0	0
Non-geniculate coralline Algae	19.28	56.53	48.36	6.92	31.36	52.7	21.46	23.47	32.38	38.19	28.75	59.41
Echinodermata	2.13	0.45	0.88	0	0	0	0	0	0	0	0	0
Foraminifera	0.42	0.44	0.46	0	1.38	0	0	0.39	0.71	0	0	0.64
Gastropod	0	0	0.24	0.1	0	0	0	13.4	0.36	9.93	7.5	1.57
Serpulid	0	1.67	0	0.83	0.83	0.6	0	0	0.7	0.42	0	0
Sponge spicules	0	0	0.54	3.44	0	5.03	0	0	0	0	0	1.77
Filling sediments	33.16	6.69	5.54	9.15	13.02	5.36	1.9	6.28	3.68	5.15	17.5	9.95
Siliciclastic grains	5.48	2.23	0	3.68	4.65	0	1.83	2.14	0	0	0	0
Borings	13.7	24.17	16.25	18.06	20.6	32.5	11.67	19.6	17.5	16.67	17.5	17.3
Constructional voids	0	0	9.51	0.91	0.9	0.42	14.47	16.32	4.71	11.04	2.5	0.21

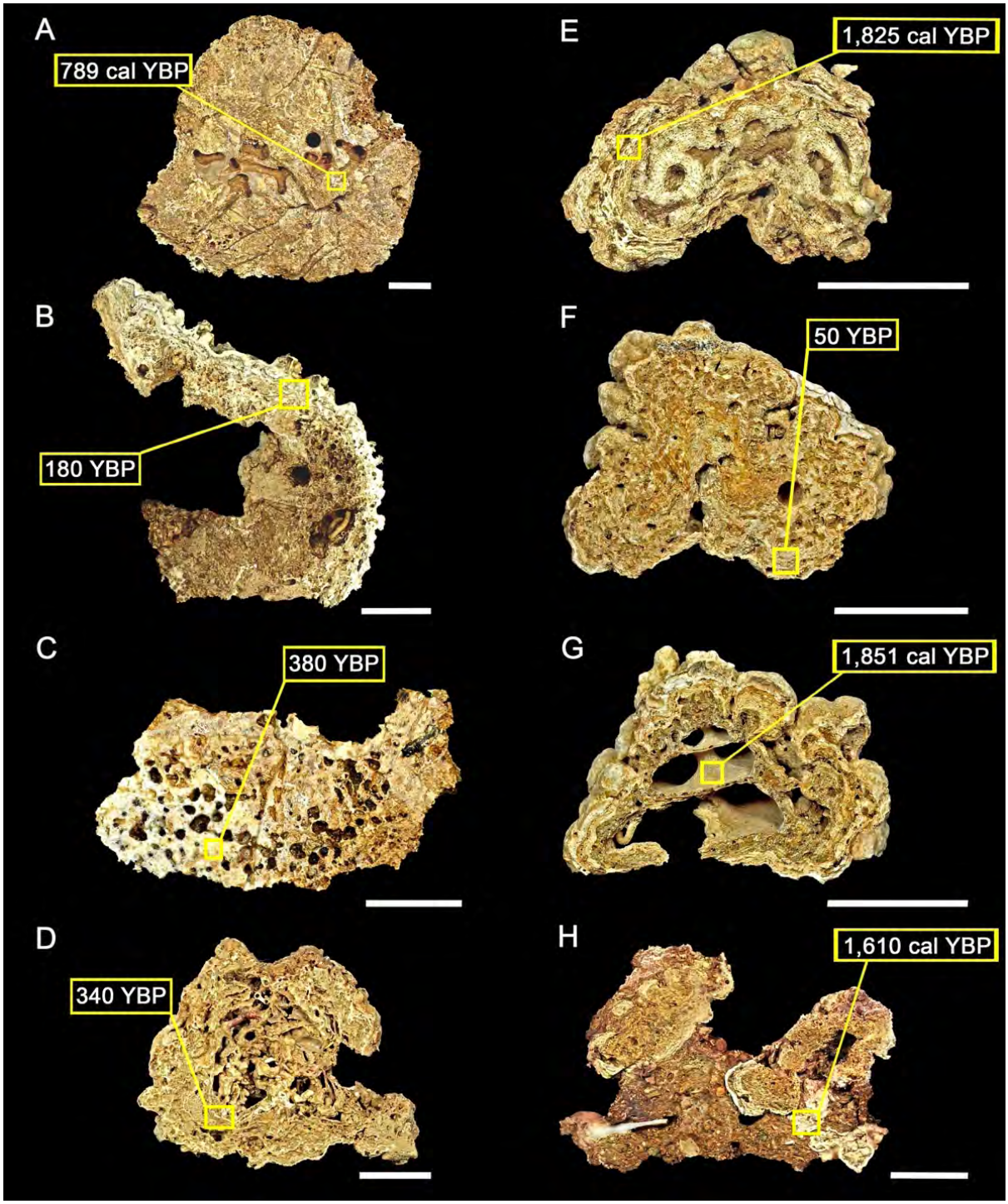

Figure 7. Radiocarbon dated samples collected in different sectors of the SEAL Basin. The yellow squares indicate location of the dated fossils in the sample: North sector: (**A**) Coral from site 1 (30 m depth); (**B**) Coralline algae from site 1 (30 m depth); Central sector: (**C**) Coral from site 3 (27 m depth); South sector: (**D**) Coralline algae from site 5 (47 m depth); (**E**) Coralline algae from site 6 (54 m depth); (**F**) Coralline algae from site 7 (50 m depth); (**G**) Gastropod shell from site 7 (50 m depth); (**H**) Bryozoan from site 7 (50 m depth). Scale bars = 2 cm.

Table 4. Radiocarbon age of different components in rhodoliths collected at different sites from 3 sectors (N, North; C, Central; and S, South) of the SEAL Basin. Coordinates are in SIRGAS 2000 Datum. * Values < 433 yr BP cannot be calibrated at the curve Marine20; BP = before present.

Site	Sector	Latitude	Longitude	Water depth (m)	Dated component	Conventional Age (BP)	Calibrated ^{14}C age (Cal yr BP)	95% range (cal BP)
1	N	-10.2789	-35.9792	30	Coral	1,840 ± 200	789	666- 922
1	N	-10.2789	-35.9792	30	Coralline algae	180* ± 200	-	-
3	C	-10.8223	-36.6118	27	Coral	380* ± 250	-	-
5	S	-11.1642	-36.8839	47	Coralline algae	340* ± 200	-	-
6	S	-11.3389	-37.0556	54	Coralline algae	760 ± 200	1,825	1,700- 1,950
7	S	-11.5989	-37.2384	50	Coralline algae	50* ± 200	-	-
7	S	-11.5989	-37.2384	50	Gastropod	4,040 ± 250	1,851	1,690- 2,014
7	S	-11.5989	-37.2384	50	Bryozoans	960 ± 250	1,610	1,476- 1,755

Rhodoliths from site 2 were mostly fruticose (branching) less than 2 cm in length (Figure 8A). They exhibited complex shapes with branches varying from small to medium (Solidity Index = 0.386–0.937). Together with bryozoans, specimens of *Harveylithon* gr. *rupestre*, *Roseolithon* sp., *Lithothamnion* sp., *Lithophyllum* sp., *Melyvonnea* gr. *erubescens* and *Mesophyllum* sp. were identified at the rhodolith surfaces (Figure 8A and Table 2). Larger rhodoliths with asymmetrical boxwork to the concentric inner arrangement also occurred. They were medium to large (2.1–13.7 cm; Figures 4B and 5A), encrusting and lumpy with mostly spheroidal (75%) shapes (Figure 5B and Table 2). Rhodolith were formed mainly by non-geniculate coralline algae with bryozoans and corals as secondary components.

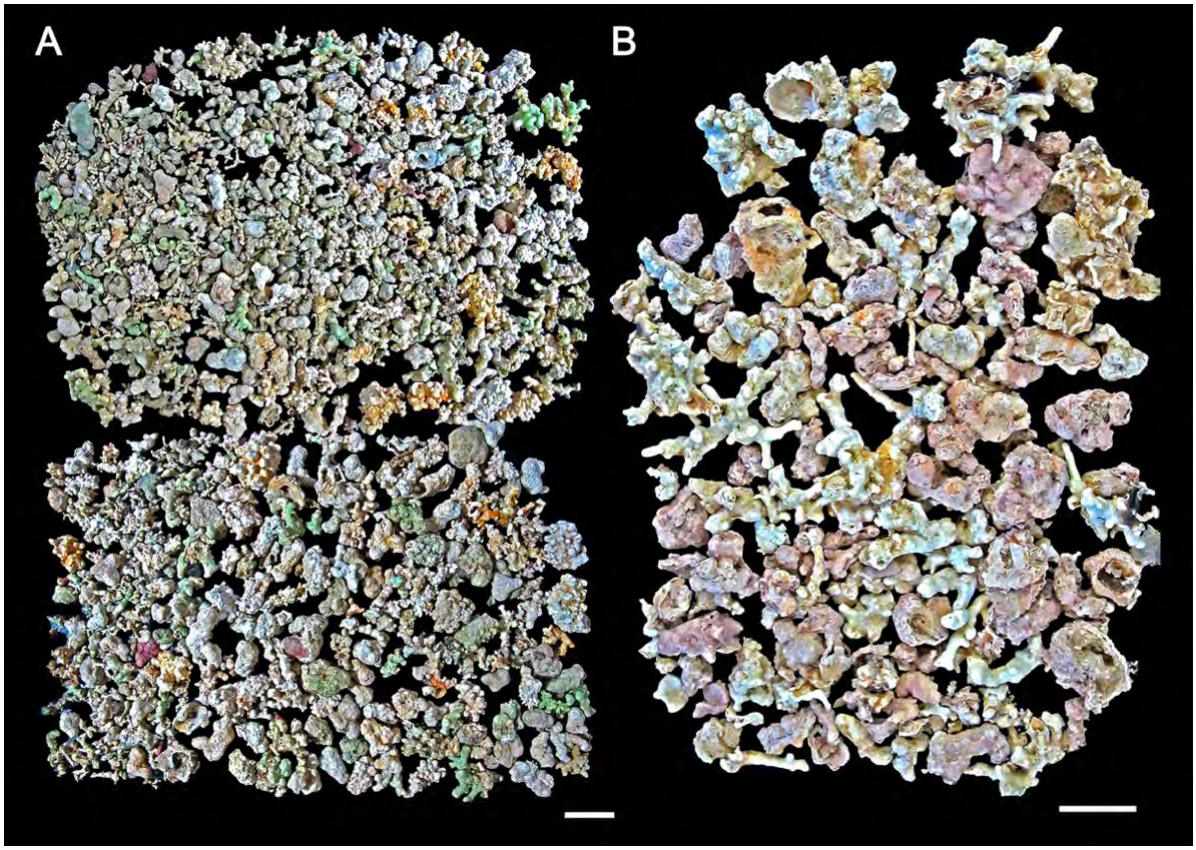

Figure 8. Fruticose (maërl) and small encrusting rhodoliths with associated shells: (**A**) from site 2 of the North Sector, at 30 m depth; (**B**) from site 4 of the Central Sector, at 47 m depth. Scale bars = 1 cm.

4.4.3. Central Sector

Rhodoliths from site 3 at 27 m depth were large in size (4–9.5 cm at the longest axis and mean diameter that ranged from 3.0-6.8 cm; Figures 4C and 5A), encrusting with sub-spheroidal (50%) and sub-discoidal (50%) shapes (Figure 5B and Table 2). Four rhodoliths examined had surfaces partially covered by red algae (*Spongites* sp., *Peyssonnelia* sp.). They were characterized by a highly asymmetrical boxwork inner arrangement, with nuclei formed mostly by corals. The covers consist of non-geniculate coralline algae, serpulids, bryozoans and encrusting foraminifers (Figure 9A, B and Table 3). Both nuclei and covers are bored by sponges (*Entobia*), and the Bioerosion Index is 3. The borings were partially filled by wackestone and packstone rich in micrite, with bioclasts of echinoids and mollusks, sponge

spicules, and siliciclastic grains, mainly quartz (Figure 9C). Radiocarbon dating of a coral nucleus of a rhodolith yielded an age of 380 yr BP (Figure 7C and Table 4).

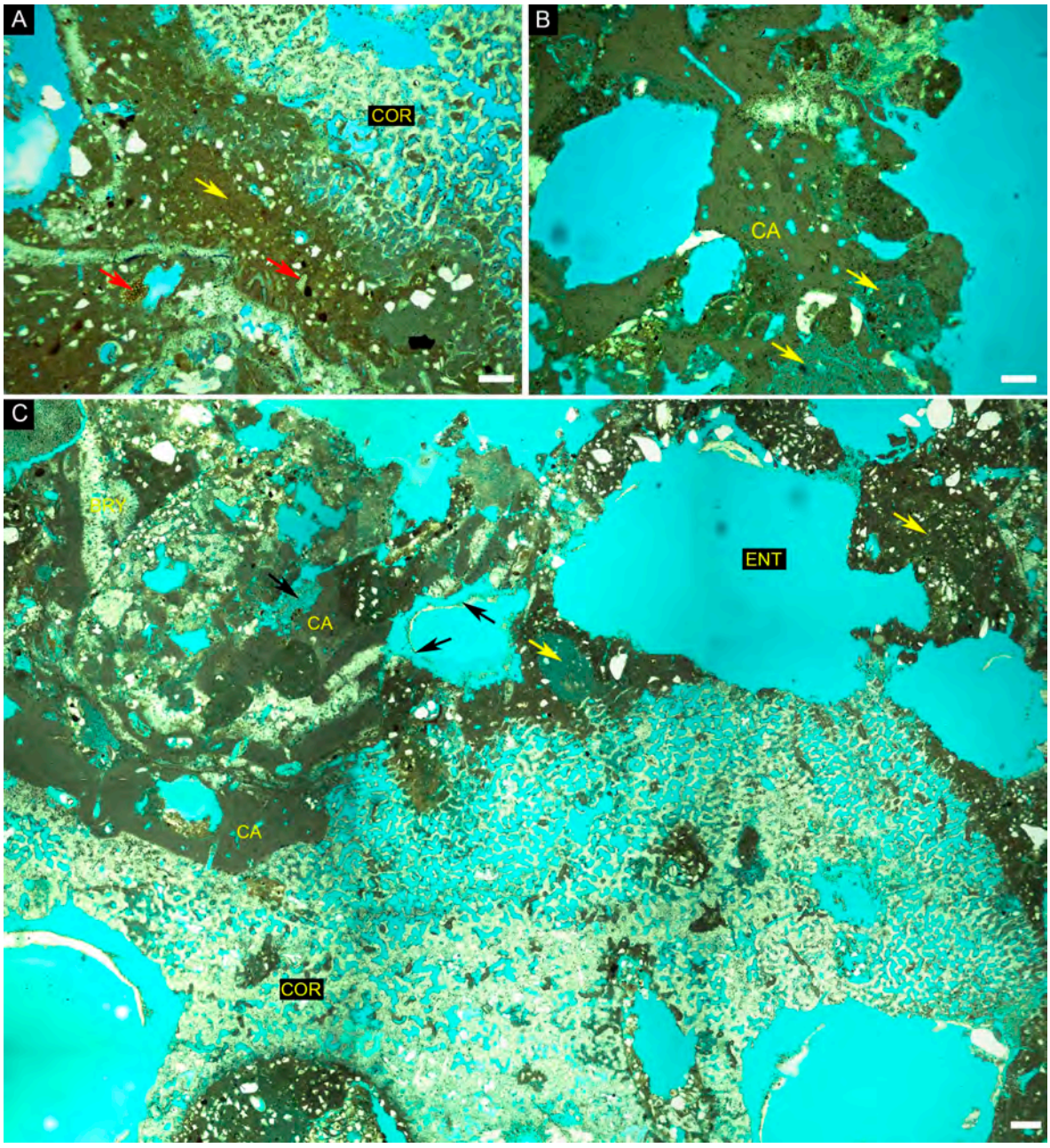

Figure 9. Thin-section images of rhodolith sample 4 from site 3 of the Central sector of the SEAL Basin (27 m depth). (**A**) Middle portion of a rhodolith with coral (COR) with borings partially filled by packstone (yellow arrow) and siliciclastic grains, mainly quartz (white color) and bioclasts of echinoids (red arrow); (**B**) Outermost portion of a rhodolith with coralline algae (CA) with some voids filled by wackestone (yellow arrow); (**C**) Rhodolith with coral (COR) nucleus overgrown by coralline algae (CA), with boring and intraskeletal voids partially filled by wackestone (yellow arrow), siliciclastic grains (white) and sponge spicules (black arrows). Borings are attributed to *Entobia* borings (ENT). Scale bars = 200 µm.

The rhodoliths collected in the outer shelf at 47 m depth from site 4 were mainly fruticose, and a few were small encrusting warty. Fruticose rhodoliths were less than 3 cm in size (Figure 8B), with low complexity, i.e., exhibit medium branches and no branching (Solidity Index = 0.614–1.000). They were mainly made up of *Lithothamnion* sp. and *Lithophyllum* sp., whereas bryozoans were secondary components. *Sporolithon* sp. was identified at the surface of small encrusting warty rhodoliths (Figure 8B).

4.4.4. South Sector

Rhodoliths from site 5 at 47 m depth were medium to large (2.7–10.3 cm at the longest axis and mean diameter that ranged from 2.4-8.8 cm; Figures 4D and 5A), encrusting, encrusting warty, and lumpy with mostly spheroidal (60%) shapes (Figure 5B and Table 2). The rhodolith surfaces were partially covered by living encrusting red algae (*Harveylithon* gr. *rupestre*, *Harveylithon* sp., *Pneophyllum* gr. *fragile*, *Sporolithon franciscanum*, *Sporolithon* sp. and Peyssonneliaceans, Figure 4D) and *Cliona* cf. *schmidtii* sponges. The rhodoliths had an asymmetrical boxwork inner arrangement, formed mostly by non-geniculate coralline algae, bryozoans, encrusting foraminifera and serpulids. *Lithothamnion* sp. and unidentifiable Hapalidiales, *Harveylithon* sp., *Lithophyllum* gr. *pustulatum*, thin unidentifiable laminar thalli, *Sporolithon* sp. and Peyssonneliaceans are the algal components (Table 2). The skeletal framework was heavily bored by sponges (*Entobia*), and the Bioerosion Index is 4. Intraskeletal and constructional voids, as well as sponge borings (Figure 10A and Table 3), varied from empty to partially filled by wackestone to packstone. Geniculate coralline algae, benthic and planktonic foraminifera appear with echinoid and mollusk fragments and siliciclastic grains, mainly quartz, in the fillings. Sponge spicules are common in the empty spaces in the outer part. Radiocarbon dating of non-geniculate coralline alga in the middle part of a rhodolith yielded an age of 340 yr BP (Figure 7D and Table 4).

Rhodoliths from site 6 at 54 m depth were large (3.3–13.8 cm at the longest axis and mean diameter that ranged from 2.6–7.6 cm; Figures 4E and 5A), encrusting, encrusting warty, and lumpy with sub-spheroidal (38%) and spheroidal (22%) shapes (Figure 5B and Table 2). The surfaces were partially covered by Peyssonneliaceans, *Roseolithon* sp. and thin unidentifiable non-geniculate coralline algae. The examined rhodoliths consist of brownish bioclastic nuclei, commonly bryozoan nodules or gastropod shells (Figures 4D, 7E, G and 10B, C), and covers made of non-geniculate coralline algae intergrown with bryozoans with an asymmetrical concentric arrangement. Serpulids and encrusting foraminifers were secondary framework builders. *Roseolithon* sp., *Lithothamnion* sp., *Spongites* sp., *Harveylithon* sp., *Lithoporella* sp., *Lithophyllum* gr. *pustulatum*, *Lithophyllum* sp., *Sporolithon* sp., unidentifiable thin laminar thalli and Peyssonneliaceans are the algal components (Table 2). The rhodoliths were slightly bioeroded (Bioerosion Index is 2) by sponges and worms. Most intraskeletal and constructional voids and borings are empty (Figure 10B), with a small proportion partially filled by wackestone and packstone rich in micrite with siliciclastic grains, mainly quartz (Table 3). Radiocarbon dating of non-geniculate coralline alga in the middle part of a rhodolith yielded an age of 1825 cal yr BP (Figure 7E and Table 4).

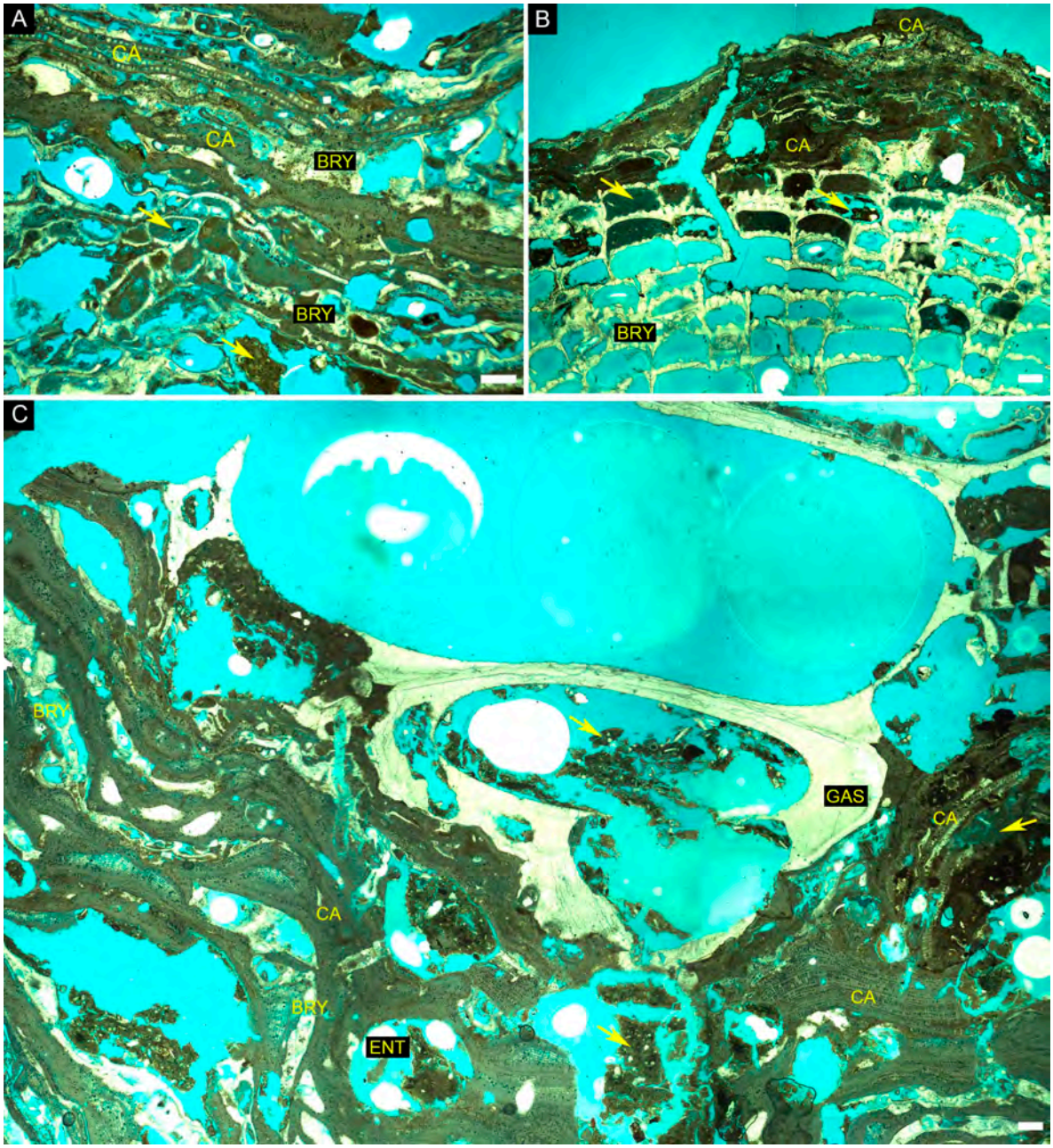

Figure 10. Thin-section images of rhodoliths from the South sector of the SEAL Basin. (**A**) Inner portion of a rhodolith sample 5 from site 5 (at 47 m depth) formed by coralline algae (CA) and bryozoans with some voids filled by micrite (yellow arrow); (**B**) Outer portion of a rhodolith sample 7 from site 6 (at 54 m depth) with bryozoan (BRY) in the nucleus covered by coralline algae (CA) with some voids filled by packstone rich in micrite (yellow arrow); (**C**) Rhodolith sample 10 from site 7 (at 50 m depth) with gastropod shell (GAS) in the nucleus covered by coralline algae (CA) and bryozoan (BRY) with some voids partially filled by wackestone (yellow arrow). Scale bars = 200 µm.

Rhodoliths from site 7 at 50 m depth were medium to large (3.4–14.5 cm at the longest axis and mean diameter that ranged from 2.3–11.7 cm; Figures 4F and 5A), encrusting, en-

crusting warty, and lumpy with mostly sub-spheroidal (53%) shapes (Figure 5B and Table 2). The surfaces are partially covered by thin crusts of *Melyvonnea* gr. *erubescens*, *Lithothamnion* sp., *Lithophyllum* gr. *pustulatum* and Peyssonneliaceans (Table 2). Most rhodoliths show two distinct phases of growth. The inner phases, brownish in color, are made of bioclastic nuclei, such as gastropod shells and bryozoan fragments, or frameworks of bryozoans, serpulids and small oysters with a small proportion of non-geniculate coralline algae, including *Lithophyllum* sp. and *Lithoporella* sp. (Figure 10C and Table 3). These inner phases are bored by sponges. Borings and intraskeletal voids are partially filled by mudstone to packstone. The outer phases consist of non-geniculate coralline algae intergrown with bryozoans and minor serpulids and encrusting foraminifers with an asymmetrical concentric arrangement. *Roseolithon* sp., *Lithothamnion* sp., unidentifiable Hapalidiales, *Spongites* sp., *Harveylithon* sp., *Lithoporella* sp., *Lithophyllum* gr. *pustulatum*, *Lithophyllum* sp., *Sporolithon* sp., unidentifiable thin laminar thalli and Peyssonneliaceans are the algal components (Table 2). The outer and inner phases, including the boring fillings, are bioeroded by sponges, and most of the voids are empty. A gastropod shell and a bryozoan in the inner phases of two rhodoliths were dated as 1851 and 1610 cal yr BP, respectively. Radiocarbon dating of non-geniculate coralline alga from the outer phase of another rhodolith yielded an age of 50 years BP (Figure 7F–H and Table 4).

4.4.5. Comparison of rhodolith distribution and characteristics among sectors

According to the biofacies distribution at SEAL (See Section 2 Figure 1), the different bottom features of the rhodolith beds in the south sector of the SEAL Basin, observed in ROV video, extend to the middle and outer shelf of the north and central sectors.

The size of rhodoliths differs among sites (PERMANOVA; $F = 6.8764$; $p = 0.0002$). A posteriori test, pairwise, showed that rhodoliths of site 1 were larger than those of deeper sites 6 ($p = 0.0014$) and 7 ($p = 0.0002$) (Figure 5A). Small fruticose rhodoliths (maërl) occurred both

in ripple troughs in shallow settings in the south sector and the deeper sampling sites in the north and central sectors. The rest of the rhodoliths exhibited concentric and boxwork inner arrangements made up of encrusting to lumpy coralline algae in all sites. In the south sector, however, the proportion of constructional void is higher, and a concentric arrangement was prevalent in rhodoliths at the two deepest sampling sites. In these sites, a two-phase development of analyzed rhodoliths was observed. The nuclei of shallowest rhodoliths are commonly formed by corals, which are absent in deeper rhodoliths from the south sector.

The number of coralline morpho-taxa involved in rhodolith formation was higher in the south sector than in the other two. The nuclei of rhodoliths in the north and central sectors include coral fragments, which are absent in the south sector, where the nuclei are formed either by mollusk shells or bryozoan skeletons.

4.5. Discussion

The rhodoliths analyzed in this study started to grow between 1.9 and 1.8 ka cal BP, a long time after the Holocene flooding of the SEAL shelf [35]. The bathymetry of the investigated rhodolith beds lies within the large range of rhodolith beds in Brazil, which occur between 12 and 95 m depth [59–65]. Temperature, nutrients, sedimentation and water current velocity are considered the main environmental drivers of rhodolith development in the Brazilian ecoregions [65]. Specifically, sediment influx depends on discharge from large rivers and directly influences the distribution of bottom sediments and rhodolith beds [59]. On the inner SEAL shelf, rhodolith growth is inhibited by riverine sediment influx (mud/sand siliciclastic sediments), but rhodolith beds can occur locally (See Section 2 Figure 1). Rhodolith beds on the SEAL shelf were concentrated north and south of the São Francisco river mouth. A similar distribution can be observed in the Rio Doce shelf, where rhodoliths are most abundant in two discontinuous areas at depths between 45 and 65 m. The area south of the Rio

Doce mouth is larger and shows higher rhodolith cover, while the area north of the mouth shows very low rhodolith cover (<10%), which was interpreted as a consequence of long-term deposition of fine sediments [59].

Rhodolith beds on the SEAL shelf are widespread in the middle-outer shelf, following the same trend observed along the Brazilian margin, but their distribution is interrupted by the presence of shelf-incised valleys and canyons, such as the Sao Francisco canyon, and minor incisions dissecting the shelf (Figure 1). In narrow mixed continental shelves, such as the SEAL shelf, transitions from terrigenous sediments to carbonates occur laterally due to lateral variation in environmental controls, such as sediment input and carbonate production [66]. Moreover, the presence of canyon systems in narrow shelves favor the possibility of discontinuities in sediment distribution even during high stands [67]. Shelf-incised valleys, canyons and riverine plumes led to the patchy distribution in large-scale rhodolith beds on the SEAL shelf (Figure 1). On wider shelves, such as the Abrolhos shelf, which also has low sediment input, rhodolith beds are extensive and more continuous [63,66]. At a smaller scale, within individual rhodolith beds mapped on the SEAL shelf (Figure 1), the distribution of rhodoliths is patchy with varying rhodolith density. This uneven distribution has been reported for deep rhodolith beds and seems to be mainly related to seafloor morphology and/or bottom currents [59,68–70].

The video surveys confirmed the occurrence of patches of fused rhodoliths in depths between 30 and 50 m, creating complex large three-dimensional structures with up to 10% of cover (Figures 2F and 3F). Similar structures occur in deeper waters in other regions in Brazil, i.e., from around 50 to 80 m depths on the Rocas Atoll shelf [69] and from 65 to 105 m on the Doce River shelf [59]. On the latter shelf, carbonate concretions, including rhodoliths, occur in areas with a high density of rhodoliths, suggesting that the concretions were formed by rhodolith fusions, later overgrown by coralline algae and other encrusters, mainly bryozoans

[59]. In the Mediterranean Sea, the so-called coralligenous de plateau (tridimensional build-ups of calcareous encrusting algae growing on flat surfaces) is common on almost all shelves, at low irradiance levels and in relatively calm waters [71,72]. In some cases, they were interpreted as frameworks developed from a coalescence of rhodoliths [71,73,74], and, therefore, the patches of fused rhodoliths on the SEAL shelf can be considered initial steps of the formation of frameworks similar to coralligenous banks. However, fossil examples from the early Miocene in Sardinia [75] and the late Miocene in SE Spain [76] showed that fused rhodoliths do not necessarily promote further development of coralline algal frameworks.

The shallowest rhodoliths (27 m depth) in the north and central sectors commonly have large nuclei of coral fragments, which is in accordance with the occurrence of corals in the rhodolith patches observed by the ROV between 25 and 30 m depth. Similar nuclei characterize the rhodoliths collected at 20 m depth in the Queimada Grande Island [64] and at 23 m depth in the southern zone of the Amazon continental margin, which has the lowest riverine influx in the region off the Amazon mouth [62]. In the north sector of the SEAL shelf, the coral nuclei have an age of nearly 800 years BP, while the dated coralline algae cover is only a few hundred years old.

Beds of small fruticose rhodoliths (maërl) are uncommon on the Brazilian shelf. The fruticose rhodoliths in sites 2 and 4 exhibit low to medium branching or no ramification in some cases, which corresponds to low habitat complexity. The development and distribution of maërl are controlled by various environmental factors that remain difficult to discern [77,78]. Maërl beds can be shaped by the swell to form megaripples, but wave energy can rapidly limit the vitality of the maërl-forming species in contrast to encrusting coralline algae that can live in highly hydrodynamic environments [78]. The mobility of branching rhodoliths depends on wave agitation and currents, and they may only move occasionally due to bioturbation and severe storms [79]. If hydrodynamic conditions are too low, fine sediment particles can stifle

algal growth [80], whereas under strong energy, the fine sediments are re-suspended, inhibiting photosynthetic activity, and coarser particles such as sand or broken shells bury the thalli [78]. Well-developed maërl beds occur in areas swept by currents, preventing the burial of rhodoliths by fine-grained sediment [42,81], although they also occur in areas with no significant energy but with reduced sediment influx [82]. Maërl beds are consequently very sensitive to sediment input and sediment mobility. On the north Atlantic coasts, maërl beds usually occur in shallow and sheltered bays [77,78]. In contrast, in the Spencer Gulf in South Australia, fruticose rhodolith pavements develop at depths of several tens of meters under the influence of moderate to high-energy currents of tidal origin that remove fine sediments [83]. In the Mediterranean Sea, fruticose rhodoliths are found in deeper settings, from 30 to 100 m [81,84–86]. In fossil examples, fruticose rhodoliths also tend to occur in paleoenvironments deeper than those of nodules formed by encrusting to lumpy thalli [87]. The occurrence of the two beds of maërl in the deeper sites of the north and central sectors of the SEAL seems to be favored by calm conditions in deep shelf settings sheltered from sediment influx. In the south sector, however, fruticose rhodoliths occur in higher energy areas in the troughs of ripples.

The concentric arrangement and high proportions of constructional void in rhodolith covers in sites of the south sector of the SEAL shelf are common in shallow-water rhodoliths in the south Espirito Santo and Rio Doce shelves [59,63]. High proportions of constructional voids were interpreted as reflecting low energy conditions [63], whereas concentric arrangements with little destruction by bioerosion indicate relatively short residence times of rhodoliths on the seafloor before burial. In the deepest sites of the south sector, a two-phase development of rhodoliths was observed. Nuclei are highly bored by sponges, whilst bioerosion in the covers is very low. In these rhodoliths, there is a large difference in age between growth phases: the inner phases yielded ages of 1600–1850 cal years BP, whereas the dated outer phase was only 50 years BP. The difference in bioerosion density and age can be explained by two

phases of growth separated in time by a long period of burial in the seafloor sediment. Such a burial of rhodoliths by fine-grained sediments was recently observed in the ROV transects at site 5, between 40 and 46 m depths. A similar two-phase development of rhodoliths was observed in the central zone of the Amazon River mouth, at 50–55 m depth [62]. In this location, the growing gap was much shorter, about 400 years from the oldest age of the darkened interior [62]. The burial by sediment, subsequent exhumation and regrowth are probably related to variations in riverine dis- charge to the shelf [62]. Some deep-water rhodoliths of the Abrolhos Continental Shelf also show multiphasic growth with growth gaps of thousands of years caused by temporary burial and exhumation [63]. Rhodoliths with well-differentiated growth phases have also been described in different regions [88–92], with time gaps between growth phases of several hundred years. Multistory rhodoliths with two to several growth phases have also been described in the fossil records [1,93], suggesting that temporary burial is a common phenomenon in rhodolith beds.

The 15 rhodolith-forming coralline taxa recorded in this study are commonly found in the beds of northeast and southeast Brazil [18,59]. Among the identified taxa, the multispecific genus *Roseolithon* (previously recognized as the single species *Lithothamnion crispatum* in Brazil) occurs on surfaces and inner portions of rhodoliths from sites in the north and south sectors of the SEAL Basin. This is considered one of the main rhodolith-forming non-geniculate coralline algae of the Brazilian continental shelf [17,18,94]. The number of morphoanatomically identified taxa in the SEAL shelf is similar to that of the Abrolhos continental shelf (14 taxa) but substantially higher than numbers recorded in the Rio Doce shelf (10 taxa), Campos Basin (2 taxa), Amazon continental margin (6 taxa) and Fernando de Noronha Archipelago (6 taxa) [17,18,48,62,95]. However, all these taxon accounts based on morpho-anatomical identifications do not reflect the higher richness of phylogenetic species of coralline algae delimited in the different ecoregions of the Brazilian shelf by DNA-based

methods [65]. In particular, in the northeastern Brazil ecoregion to which the SEAL shelf belongs, 23 phylogenetic species of coralline algae have been identified [65].

The extension and composition of the SEAL rhodolith beds show the importance of these ecosystems on the Brazilian continental shelf. This region has great economic importance due to its extensive areas of carbonate accumulation [22] and is subjected to multiple disturbances as direct and indirect consequences of human activities, such as mineral extraction of calcium carbonate for commercial use, bottom trawl fishing, and oil and gas extraction [21,96]. Knowledge about rhodolith beds is becoming even more urgent to support local conservation and management actions and assess the environmental impacts that the exploitation of its resources can generate on this rich marine ecosystem.

4.6. Conclusions

Rhodolith beds on the SEAL shelf mainly occur on the middle-outer shelf, at depths between 25 and 55 m. Sediment influx from the major rivers in the area and incision of the shelf by submarine canyons determine the large-scale areal distribution of rhodolith beds on the shelf. The spatial variability of rhodolith beds reveals living rhodoliths grouped in patches interspersed with bioclastic sediments and associated with fleshy macroalgae and a reef fish community; some rhodoliths are fused, forming coralline algal concretions; fruticose rhodoliths (maërl) occur both in ripple troughs in shallow waters and deeper sites of the north and central sectors. Coralline algal identification recorded a total of 15 in the study sites, where some sites supported up to 11 different morphospecies; some species occur at five sites along the three sectors of the SEAL shelf. The rhodoliths from the north and central sectors commonly have large nuclei of coral fragments hundreds of years old. In the south sector, the rhodoliths have old nuclei (about 1800–1600 cal years BP) of gastropod and bryozoan fragments or coralline algae-bryozoan-serpulid boundstones. In this sector, rhodoliths show two growth phases with a difference in age of more than 1500 years, which can be explained

by a long period of burial in the seabed sediment and later exhumation and resuming of growth. Increased knowledge about the role of these rhodolith beds in the benthic ecosystems is important to provide support for marine spatial planning programs, which could lead to more sustainable use of these habitats.

Supplementary Materials

The following are available online at https://www.mdpi.com/article/10.3390/d14040282/s1; **Figure S1**: External morphology and the anatomy of identified coralline algae species; **Table S1**: Remotely operated vehicle (ROV) log sheet at different depths on the south sector of the SEAL shelf; **Table S2**: Voucher samples of the coralline algae deposited in the Herbarium of the Rio de Janeiro Botanical Garden (RB); **Video S1**: Video obtained from ROV surveys on the middle to outer shelf of the SEAL shelf (south sector).

Author Contributions

N.F.L.V.: Conceptualization, Investigation, Writing—Original Draft, Visualization. **J.C.B.**: Investigation, Writing—Review & Editing, Supervision. **A.C.B.**: Formal analysis, Writing—Review & Editing, Supervision. **F.C.M.**: Review & Editing, Visualization. **C.S.K.**: Formal analysis, Writing—Review & Editing, Visualization. **R.G.B.**: Formal analysis, Review & Editing, Visualization. **L.A.L.**: Formal analysis, Visualization. **R.C.P.**: Formal analysis, Visualization. **G.M.A.-F.** (in memoriam): Conceptualization, Investigation, Supervision. **L.T.S.**: Writing—Review & Editing, Visualization, Supervision. All authors have read and agreed to the published version of the manuscript.

Funding

This study was funded by the Coordenação de Aperfeiçoamento de Pessoal de Nível Superior (CAPES- Finance Code 001) and Fundação de Amparo à Pesquisa do Estado do Rio de Janeiro- Jovem Cientista do Nosso Estado (FAPERJ/JCNE- Fellow to Leonardo T. Salgado).

Institutional Review Board Statement

Not applicable.

Data Availability Statement

All data produced as part of this research is included in the manuscript and supplementary material.

Acknowledgments

We are grateful to Maria Eulália R. Carneiro (Petrobras) and the Federal University of Sergipe for provided the samples and for the collaboration with the IPJBRJ; to the 3 reviewers for their comments that improved the final version of the manuscript. We dedicate this work to the memory of our dear leader, Professor Dr. Gilberto M. Amado-Filho.

Conflicts of Interest:

The authors declare no conflict of interest.

4.7. References

1. Aguirre, J.; Braga, J.C.; Bassi, D. Rhodoliths and rhodolith beds in the rock record. In*: Rhodolith/Maërl Beds: A Global Perspective,* Riosmena-Rodríguez, R., Nelson, W., and Aguirre, J., Eds.; Springer International Publishing: Geerbestrasse, Switzerland, 2017; Volume 15, pp. 105-138.
2. Basso, D.; Babbini, L.; Kaleb, S.; Bracchi, V.; Falace, A. Monitoring deep Mediterranean rhodolith beds. *Aquat. Conserv* **2016**, *26*, 549–561. https://doi.org/10.1002/aqc.2586.
3. Foster, M.S. Rhodoliths: between rocks and soft places - Minireview. *J. Phycol.* **2001**, *37,* 659-667. https://doi.org/10.1046/j.1529-8817.2001.00195.x.
4. Kamenos, N.A.; Heidi, L.B.; Darrenougue, N. Coralline algae as recorders of past climatic and environmental conditions. In*: Rhodolith/Maërl Beds: A Global Perspective,* Riosmena-Rodríguez, R., Nelson, W., and Aguirre, J., Eds.; Springer International Publishing: Geerbestrasse, Switzerland, 2017; Volume 15, pp. 27–53.
5. Foster, M.S.; Amado-Filho, G.M.; Kamenos, N.A.; Riosmena-Rodriguez, R.; Steller, D.S. Rhodolith and rhodolith beds. In*: Contribution of SCUBA diving to research and discovery in marine environments*, Lang, M. Org.; Smithsonian Institution Scholarly Press, Washington DC, 2013; pp. 143-156.
6. Harvey, A.S.; Woelkerling, W.J. A guide to non-geniculate coralline red algal (Corallinales, Rhodophyta) rhodolith identification. *Ciencias Marinas* **2007**, *33(4),* 411–426. http://doi.org/10.7773/cm.v33i4.1210.
7. Hily, C.; Potin, P.; Floch, J.Y. Structure of subtidal algal assemblages on soft bottom sediments: fauna/flora interactions and role of disturbances in the Bay of Brest, France. *Mar. Ecol. Prog. Ser.* **1992**, *85,* 115–130.
8. Birkett, D.A.; Maggs, C., Dring, M.J. Maërl: An overview of dynamic and sensitivity characteristics for conservation management of marine SACs. *Scott. Assoc. Mar. Sci.* **1998**, *5,* 1–90.
9. Nelson W.A.; Neill, K.; Farr, T.; Barr, N.; D'Archino, R.; Miller, S.; Stewart, R. Rhodolith Beds in Northern New Zealand: Characterization of associated biodiversity and vulnerability to environmental stressors. *New Zealand Aquatic Environments and Biodiversity Report* **2009**, *99,* p. 102.
10. Harvey, A.S.; Bird, F.L. Community structure of a rhodolith bed from cold temperate waters (southern Australia). *Aust. J. Bot.* **2008**, *56,* 437–450. http://doi.org/10.1071/BT07186.

11. Konar, B.; Riosmena-Rodriguez, R.; Iken, K. Rhodolith bed: a newly discovered habitat in the North Pacific Ocean. *Bot. Mar.* **2006**, *49,* 355–359. https://doi.org/10.1515/BOT.2006.044.

12. Steller, D.L.; Riosmena-Rodriguez, R.; Foster, M.S.; Roberts, C. Rhodolith bed diversity in the Gulf of California: the importance of rhodolith structure and consequences of anthropogenic disturbances. *Aquat. Conserv. Mar. Freshw. Ecosyst.* **2003**, *13,* S5–S20. http://doi.org/10.1002/aqc.564.

13. Hinojosa-Arango, G.; Riosmena-Rodriguez, R. Influence of rhodolith-forming species and growth-form on associated fauna of rhodolith beds in the central-west Gulf of California, México. *Mar. Ecol.* **2004***, 25,* 109–127. http://doi.org/10.1111/j.1439-0485.2004.00019.x.

14. Sañé, E.; Chiocci, F.L.; Basso, D.; Martorelli, E. Environmental factors controlling the distribution of rhodoliths: An integrated study based on seafloor sampling, ROV and side scan sonar data, offshore the W-Pontine Archipelago. *Cont. Shelf Res.* **2016**, *129,* 10–22. http://dx.doi.org/10.1016/j.csr.2016.09.003.

15. Concentino, A.L.M.; Vieira, I.B.; Reis, T.N.V.; Vasconcelos, E.R.T.P.P.; Paes, E.T. Fitobentos da Plataforma Continental de Sergipe e de Alagoas. In: *Plataforma Continental de Sergipe e Alagoas: Geoquímica Sedimentar e Comunidade Bêntica*. Carneiro, M.E.R., Arguelho, M.L.P.M., Org.; Editora UFS; Coleção Projeto MARSEAL: São Cristóvão, Brazil, 2018; Volume 2, pp. 196-220.

16. Figueiredo, M.A.O.; Eide, I.; Reynier, M.; Villas-Bôas, A.B.; Tâmega, F.T.S.; Ferreira, C.G.; Nilssen, I.; Coutinho, R.; Johnsen, S. The effect of sediment mimicking drill cuttings on deep-water rhodoliths in a flow-through system: experimental work and modeling. *Mar. Pollut. Bull.* **2015**, *95,* 81–88. http://doi.org/10.1016/j.marpolbul.2015.04.040.

17. Amado-Filho, G.M.; Moura, R.L.; Bastos, A.C.; Salgado, L.T.; Sumida, P.Y.G.; Guth, A.Z.; Francini-Filho, R.B.; Pereira-Filho, G.H.; Abrantes, D.P.; Brasileiro, P.S.; Bahia, R.G.; Leal, R.N.; Kaufman, L.; Kleypas, J.; Farina, M.; Thompson, F.L. Rhodolith beds are major CaCO3 bio-factories in the tropical South West Atlantic. *PLoS One,* **2012**, *7 (4)*, e35171. https://doi.org/10.1371/journal.pone.0035171.

18. Amado-Filho, G.M.; Bahia, R.G.; Pereira-Filho, G.H.; Longo, L.L. South Atlantic rhodolith beds: latitudinal distribution, species composition, structure and ecosystem functions, threats and conservation status. In*: Rhodolith/Maërl Beds: A Global Perspective,* Riosmena-Rodríguez, R., Nelson, W., and Aguirre, J., Eds.; Springer International Publishing: Geerbestrasse, Switzerland, 2017; Volume 15, pp. 299-317.

19. Guimarães, C.R.P. Composição e distribuição dos sedimentos superficiais e da fauna bêntica na plataforma continental de Sergipe. PhD Thesis, Instituto de Geociências, Universidade Federal da Bahia. Salvador-Bahia. 2010.

20. Nascimento, A.A. Sedimentação holocênica na plataforma continental de Sergipe, nordeste do Brasil. Dissertation (Master Degree) Instituto de Geociências, Universidade Federal da Bahia. Salvador–Bahia. 2011.

21. Fontes, L.C.S.; Santos, J.R.; Santos, L.A.; Mendonça, J.B.S.; Santos, M.S. Sedimentos superficiais da plataforma continental de Sergipe-Alagoas. In*: Geologia e Geomorfologia da Bacia de Sergipe-Alagoas*; Carneiro, M.E.R., Ed.; Editora UFS; Coleção Projeto MARSEAL: São Cristóvão, Brazil, 2017; Volume 1, pp. 64-96.

22. Santos, J.R.; Souza, R.M.; Andrade, E.; Fontes, L.C.S. Biogenic components as environmental indicators of the Continental Platform of the state Sergipe and south of Alagoas. *Geociências* **2019***, 38 (2)*, 409–425.

23. Santos, R.S.; Santos, L.A.; Fontes, L.C.S. Geomorphological and sedimentary mapping of paleo-lines of coast in the continental platform South of Alagoas. *GeoNordeste Journal* **2019**, 1, 60-79. http://doi.org/10.33360/RGN.2318-2695.2019.i1p60-79.

24. Souza-Lima W.; Andrade A.J.; Bengtson P.; Galm P.C. A Bacia de Sergipe-Alagoas: evolução geológica, estratigrafia e conteúdo fóssil. *Fundação Paleontológica Phoenix, Aracaju* **2002***, 1 (1)*, 1-34.

25. Coutinho, P.N. Geologia marinha da plataforma continental Alagoas-Sergipe. PhD Thesis, Centro de Tecnologia, Universidade Federal de Pernambuco. Recife. 1976.

26. Santos, J.R. Feições morfológicas e biofacies como indicadores evolutivos da Plataforma Continental de Sergipe e sul de Alagoas. PhD Thesis, Centro de Tecnologia, Universidade Federal de Sergipe. Recife. 2019.

27. Knoppers, B.A.; Carneiro, M.E.R.; Fontes, L.C.S.; Souza, W.F.L.; Medeiros, P.R.P. Plataforma Continental de Sergipe e Alagoas. In: *Plataforma Continental de Sergipe e Alagoas: Geoquímica Sedimentar e Comunidade Bêntica*. Carneiro, M.E.R., Arguelho, M.L.P.M., Org.; Editora UFS; Coleção Projeto MARSEAL: São Cristóvão, Brazil, 2018; Volume 2, pp. 11-38.

28. Bezerra, F.H.R.; Barreto, A.M.F.; Suguio, K. Holocene sea level history on the Rio Grande do Norte State Coastal, Brazil. *Mar. Geol.* **2003**, 196, 73-89. http://doi.org/10.1016/S0025-3227(03)00044-6.

29. Caldas, L.H.O.; Stattegger, K.; Vital, H. Holocene sea-level history and coastal evolution: evidences from coastal sediments of the northern Rio Grande do Norte coast, NE Brazil. *Mar. Geol.* **2006**, 228, 39-53. http://doi.org/10.1016/j.margeo.2005.12.008.

30. Medeiros, P.R.P.; Knoppers, B.A.; Santos, R.C.; Souza, W.F.L. Aporte fluvial e dispersão de matéria particulada em suspensão na zona costeira do rio São Francisco (SE/AL). *Geochimica Brasiliensis* **2007***, 21 (2),* 212-231.

31. Oliveira, E.N.; Knoppers, B.A.; Lorenzzetti, J.A.; Medeiros, P.R.P.; Carneiro, M.E.; Souza, W.F.L. A satellite view of riverine turbidity plumes on the NE-E Brazilian coastal zone. *Braz. J. Oceanogr.* **2012***, 60 (3)*, 283-298. https://doi.org/10.1590/S1679-87592012000300002.

32. Knoppers, B.; Medeiros, P.R.P.; Souza, W.F.L.; Jennerjahn, T. The São Francisco Estuary, Brazil. In: *Estuaries, Pollution.* Wangersky, P., Ed.; Springer Handbook of Environmental Chemistry: Berlin, 2006; Volume 5, pp. 51-70.

33. Bittencourt, A.C.S.P.; Dominguez, J.M.L.; Fontes, L.C.S.; Sousa, D.L.; Silva, I.R.; Silva, F.R. Wave refraction, river damming and episodes of severe shoreline erosion: The Sao Francisco River Mouth, Northeastern Brazil. *Journal of Coastal Research* **2007***, 23 (4),* 930-938. http://doi.org/10.2112/05-0600.1.

34. Medeiros, P.R.P.; Knoppers, B.; Souza, W.F.L.; Oliveira, E.N. Aporte de material em suspensão no Baixo Rio São Francisco (SE/AL), em diferentes condições hidrológicas. *Braz. J. Aquat. Sci. Technol.* **2011***, 15 (1),* 42-53.

35. Dominguez, J.M.L.; Guimarães, J.K. Effects of Holocene climate changes and anthropogenic river regulation in the development of a wave-dominated delta: The São Francisco River (Eastern Brazil). *Mar. Geol.* **2021**, 435, 106456. https://doi.org/10.1016/j.margeo.2021.106456.

36. Coutinho, P.N. Oceanografia Geológica. In: *Levantamento do Estado da Arte da Pesquisa dos Recursos Vivos Marinhos do Brasil (Programa REVIZEE).* Coutinho, P.N. Ed.; Ministério do Meio Ambiente dos Recursos Hídricos e da Amazônia Legal, Secretaria de Coordenação dos Assuntos do Meio Ambiente: Brasília, Brazil, 2000; pp. 75.

37. Oliveira, M.B. Caracterização Integrada da Linha de Costa do Estado de Sergipe – Brasil. Dissertation (Master Degree), Instituto de Geociências, Universidade Federal da Bahia. Salvador, Brazil. 2003.

38. Bittencourt, A.C.S.P.; Oliveira M.B.; Dominguez J.M.L. Erosão e Progradação do Litoral Brasileiro – Sergipe. In: *Erosão e Progradação do Litoral Brasileiro.* Muehe, D. Org.; Ministério do Meio Ambiente, Brasília, Brazil, 2006; Volume 2, pp. 213-218.

39. Fontes, L.C.S.; Santos, J.R.; Santos, L.A.; Mendonça, J.B.S.; Santos, M.S. Geomorfologia da Plataforma Continental de Sergipe-Alagoas. In: *Geologia e geomorfologia da bacia de Sergipe-Alagoas*, Fontes, L.C.S., Kowsmann, R.O., Puga-Bernabéu, A. Eds.; Editora UFS, São Cristóvão, Brazil, 2017; Volume 1, pp. 25-61.

40. PETROBRAS. Projeto de Caracterização Regional da Bacia de Sergipe-Alagoas, Relatório IBAMA; Etapa 3; Volume 3, Algas Calcárias, Corais e Moluscos da Bacia Sergipe-Alagoas; PETROBRAS: Rio de Janeiro, Brasil, 2015.

41. Carneiro, M.E.R.; Moreira, D.L.; Oliveira, P.; Omena, E.; Garcia, C.A.B.; Alexandre, M.R.; Carreira, R.; Santos, N.C., Politano, A.T. Delineamento amostral, métodos de campo e análise dos dados In: *Plataforma Continental de Sergipe e Alagoas: Geoquímica Sedimentar e Comunidade Bêntica*. Carneiro, M.E.R., Arguelho, M.L.P.M., Org.; Editora UFS; Coleção Projeto MARSEAL: São Cristóvão, Brazil, 2018; Volume 2, pp. 40-59.

42. Basso, D. Deep rhodolith distribution in the Pontian Islands, Italy: a model for the paleoecology of a temperate sea. *Palaeogeogr. Palaeoclimatol. Palaeoecol.* ***1998****, 137,* 173–187. http://doi.org/10.1016/S0031-0182(97)00099-0.

43. Woelkerling, W.J.; Irvine, L.M.; Harvey, A.S. Growth-forms in non-geniculate coralline red algae (Corallinales, Rhodophyta). *Aust. Syst. Bot.* **1993***, 6*, 297-293. http://doi.org/10.1071/SB9930277.

44. Basso, D.; Nalin, R.; Nelson, C.S. Shallow-water *Sporolithon* rhodoliths from North Island (New Zealand). *Palaios* **2009**, *24,* 92–103. https://doi.org/10.2110/palo.2008.p08-048r.

45. Bosence, D.W.J. Description and classification of rhodoliths (rhodoids, rhodolites). In*: Coated grains,* Peryt, T.M. Eds.; Springer, Berlin, 1983; pp. 217–224.

46. Graham, D.J.; Midglay, N.G. Graphical representation of a particle shape using triangular diagrams: An Excel spread sheet method. *Earth Surf. Processes Landforms* **2000***, 25 (13),* 1473-1477.

47. Maneveldt, G. W.; VanDer Merwe, E. *Heydrichia cerasina* sp. nov. (Sporolithales, Corallinophycidae, Rhodophyta) from the southernmost tip of Africa. *Phycologia* **2012***, 51 (1),* 11–21. https://doi.org/10.2216/11-05.1.

48. Bahia, R.G. Algas coralináceas formadoras de rodolitos da plataforma continental tropical e ilhas oceânicas do Brasil: levantamento florístico e taxonomia. PhD Thesis, Escola Nacional de Botânica Tropical, Rio de Janeiro, Brazil, 2014.

49. Leão, L.A.S.; Bahia, R.G.; Jesionek, M.B.; Adey, W.H.; Johnson, G.; Salgado, L.T.; Pereira, R.C. *Sporolithon franciscanum* sp. nov. (Sporolithales, Rhodophyta), a New Rhodolith-Forming Species from Northeast Brazil. *Diversity* **2020***, 12:* 199. http://doi.org/10.3390/d12050199.

50. Costa, I.O.; Jesus, P.B.; Jesus, T.S.; Souza, P.S.; Horta, P.A.; N, J.M.C. Reef-building coralline algae from the Southwest Atlantic: filling gaps with the recognition of Harveylithon (Corallinaceae, Rhodophyta) on the Brazilian Coast. *J. Phycol.* **2019**, 55, 1370–1385. http://doi.org/10.1111/jpy.12917.

51. Bernard, G.; Romero-Ramirez, A.; Tauran, A.; Pantalos, M.; Deflandre, B.; Grall, J.; Grémare, A. Declining maerl vitality and habitat complexity across a dredging gradient: insights from in situ sediment profile imagery (SPI). *Sci. Rep.* **2019***, 9*, 16463. https://doi.org/10.1038/s41598-019-52586-8.

52. Dunham, R.J. Classification of carbonate rocks according to depositional texture. In*: Classification of Carbonate Rocks*, Ham, W.E. Eds.; AAPG Mem, Tulsa, 1962; pp. 108–121.

53. Embry, A.F.; Klovan, J.E. Absolute water depth limits of late Devonian paleoecological zones. *Geol. Rundsch.* **1972***, 61 (2),* 672–686.

54. Bassi, D.; Iryu, Y.; Humblet, M.; Matsuda, H.; Machiyama, H.; Sasaki, K.; Matsuda, S.; Arai K.; Inoue, T. Recent macroids on the Kikai-jima shelf, Central Ryukyu Islands, Japan. *Sedimentology* **2012***, 59,* 2024-2041. https://doi.org/10.1111/j.1365-3091.2012.01333.x.

55. Beijbom, O.; Edmunds, P.J.; Roelfsema, C.; Smith, J.; Kline, D.I.; Neal, B.; Dunlap, M.J.; Moriarty, V.; Fan, T-Y.; Tan, C-J.; Chan, S.; Treibitz, T.; Gamst, A.; Mitchell, B.G.; Kriegman, D. Towards automated annotation of benthic survey images: variability of human experts and operational modes of automation. *PLoS ONE* **2015***, 10 (7):* e0130312. https://doi.org/10.1371/journal.pone.0130312.

56. Nitsch, F.; Nebelsick, J.H.; Bassi, D. Constructional and Destructional patterns—Void classification of rhodoliths from Giglio Island, Italy. *Palaios* **2015**, 30, 680–91. http://dx.doi.org/10.2110/palo.2015.007.

57. Stuiver, M.; Reimer, P.J.; Reimer, R.W. 2020. CALIB 8.2. Available online: http://calib.org. (Accessed on 2020-8-28).

58. Heaton, T.J.; Köhler, P.; Butzin, M.; Bard, E.; Reimer, R.W.; Austin, W.E.N.; Bronk Ramsey, C.; Hughen, K.A.; Kromer, B.; Reimer, P.J.; Adkins, J.; Burke, A.; Cook, M.S.; Olsen, J.; Skinner, L.C. Marine20-the marine radiocarbon age calibration curve (0-55,000 cal BP). *Radiocarbon* **2020**, *62.* http://doi:10.1017/RDC.2020.68.

59. Holz, V.L.; Bahia, R.G.; Karez, C.S.; Vieira, F.V.; Moraes, F.C.; Vale, N.F.; Sudatti, D.B.; Salgado, L.T.; Moura, R.L.; Amado-Filho, G.M.; et al. Structure of Rhodolith Beds and Surrounding Habitats at the Doce River Shelf (Brazil). *Diversity* **2020**, 12, 75. http://doi.org/10.3390/d12020075.

60. Stelzer, P.S.; Mazzuco, A.C.A.; Gomes, L.E.; Martins, J.; Netto, S.; Bernardino, A.F. Taxonomic and functional diversity of benthic macrofauna associated with rhodolith beds in SE Brazil. *PeerJ* **2021**, 9, e11903. https://doi.org/10.7717/peerj.11903.

61. Moura, R.L.; Amado-Filho, G.M.; Moraes, F.C.; Brasileiro, P.S.; Salomon, P.S.; Mahiques, M.M.; Bastos, A.C.; Almeida, M.G.; Silva, J.M.; Araujo, B.F.; Brito, F.P.; Rangel, T.P.; Oliveira, B.C.V.; Bahia, R.G.; Paranhos, R.P.; Dias, R.J.S.; Siegle, E.; Figueiredo, A.G.; Pereira, R.C.; Leal, C.V.; Hajdu, E.; Asp, N.E.; Gregoracci, G.B.; Neumann-Leitão, S.; Yager, P.L.; Francini-Filho, R.B.; Fróes, A.; Campeão, M.; Silva, B.S.; Moreira, A.P.B.; Oliveira, L.; Soares, A.C.; Araujo, L.; Oliveira, N.L.; Teixeira, J.B.; Valle, R.A.B.; Thompson, C.C.; Rezende, C.E.; Thompson, F, L. An extensive reef system at the Amazon River mouth. *Science Advances* **2016**, 2, 1–11.

62. Vale, N.F.L.; Amado-Filho, G.M.; Braga, J.C.; Brasileiro, P.S.; Karez, C.S.; Moraes, F.C.; Bahia, R.G.; Bastos, A.C.; Moura, R.L. Structure and composition of rhodoliths from the Amazon River mouth, Brazil. *J. South Am. Earth Sci.* **2018**, 84, 149–159. https://doi.org/10.1016/j.jsames.2018.03.014.

63. Brasileiro, P.S.; Braga, J.C.; Amado-Filho, G.M.; Leal, R.N.; Bassi, D.; Franco, T.; Bastos, A.C.; Moura, R.L. Burial rate determines Holocene rhodolith development on the Brazilian Shelf. Palaios **2018**, 33 (10), 464-477. https://doi.org/10.2110/palo.2017.109.

64. Pereira-Filho, G.H.; Shintate, G.S.; Kitahara, M.V.; Moura, R.L.; Amado-Filho, G.M.; Bahia, R.G.; Moraes, F.C.; Neves, L.M.; Francini, C.L.B.; Gibran, F.Z.; Motta, F.S. The southernmost Atlantic coral reef is off the subtropical island of Queimada Grande (24°S), Brazil. *Bull. Mar. Sci.* **2019**, 95(0), 000–000.

65. Sissini, M.N.; Koerich, G.; de Barros-Barreto, M.B.; Coutinho, L.M.; Gomes, F.P.; Oliveira, W.; Costa, I.O.; Nunes, J.M.C.; Henriques, M.C.; Vieira-Pinto, T.; Torrano-Silva, B.N.; Oliveira, M.C.; Le Gall, L.; Horta, P.A. Diversity, distribution, and environmental drivers of coralline red algae: the major reef builders in the Southwestern Atlantic. *Coral Reefs* **2021**. https://doi.org/10.1007/s00338-021-02171-1.

66. Vieira, F.V.; Bastos, A.C.; Quaresma, V.S.; Leite, M.D.; Costa-Jr., A.; Oliveira, K.S.S.; Dalvi, C.F.; Bahia, R.G.; Holz, V.L.; Moura, R.L.; Amado-Filho, G.M. Along-shelf changes in mixed carbonate-siliciclastic sedimentation patterns. *Cont. Shelf Res.* **2019**, 187, 103964. https://doi.org/10.1016/j.csr.2019.103964.

67. Ribeiro, R.F.; Dominguez, J.M.L.; Santos, A.A.; Rangel, A.G.A.N. Continuous canyon-river connection on a passive margin: The case of São Francisco Canyon (eastern Brazil). *Geomorphology* **2021**, 375, 107549. https://doi.org/10.1016/j.geomorph.2020.107549.

68. Pereira-Filho, G.H.; Veras, P.C.; Francini-Filho, R.B.; Moura, R.L.; Pinheiro, H.T.; Gibran, F.Z.; Matheus, Z.; Neves, L.M.; Amado-Filho, G.M. Effects of the sand tilefish *Malacanthus plumieri* on the structure and dynamics of a rhodolith bed in the Fernando de Noronha Archipelago, tropical West Atlantic. *Mar. Ecol. Progr. Ser.* **2015**, 541, 65. http://doi.org/10.3354/meps11569.

69. Amado-Filho, G.M.; Moura, R.L.; Bastos, A.C.; Francini-Filho, R.B.; Pereira-Filho, G.H.; Bahia, R.G.; Moraes, F.C.; Motta, F.S. Mesophotic ecosystems of the unique South Atlantic atoll are composed by rhodolith beds and scattered consolidated reefs. *Mar Biodiv*. **2016**, 46: 933–936. https://doi.org/10.1007/s12526-015-0441-6.

70. Prager, E.J.; Ginsburg, R.N. Carbonate nodule growth on Florida's outer shelf and its implications for fossil interpretations. *Palaios* **1989**, 4: 310-317.

71. Pérès, J.; Picard, J.M. Nouveau manuel de bionomie benthique de la mer Méditerranée. *Recueil Travaux Station Marine Endoume* **1964**, 31(47), 1-131.

72. Ballesteros, E. Mediterranean coralligenous assemblages: A synthesis of present knowledge). *Oceanography and Marine Biology: An Annual Review* **2006**, 44, 123-195.

73. Nalin, R.; Basso, D.; Massari, F. Pleistocene coralline algal build-ups (*coralligène de plateau*) and associated bioclastic deposits in the sedimentary cover of Cutro marine terrace (Calabria, southern Italy). In: *Cool-Water Carbonates: Depositional Systems and Palaeoenvironmental Controls.* Pedley, H.M., Carannante, G., Eds.; Geological Society, London, Special Publications. 2006; Volume 255, pp 11-22.

74. Basso, D.; Nalin, R.; Massari, F. Genesis and composition of the Pleistocene *Coralligène de plateau* of the Cutro Terrace (Calabria, southern Italy). *N. Jb. Geol. Paläont. Abh*. **2007**, 244, 173– 182.

75. Benisek, M.F.; Marcano, G.; Betzler, C.; Mutti, M. Facies and stratigraphic architecture of a Miocene warm-temperate to tropical fault-block carbonate platform, Sardinia (Central Mediterranean Sea). In: *Carbonate Systems during the Oligocene-Miocene Climatic Transition*, Mutti, M., Piller, W.E., Betzler, C., Eds.; IAS Spec Publ. 2010; Volume 42, pp 129-148.

76. Braga, J.C.; Martín, J.M. Neogene coralline-algal growth-forms and their palaeoenvironments in the Almanzora River Valley (Almeria, S.E. Spain). *Palaeogeogr Palaeoclimatol Palaeoecol* **1988**, 67, 285-303.

77. Wilson, S.; Blake, C.; Berges, J.A.; Maggs, C.A. Environmental tolerances of free-living coralline algae (maerl): implications for European marine conservation. *Biol. Conserv* **2004**, 120 (2), 279–289. http://doi.org/10.1016/j.biocon.2004.03.001.

78. Ehrhold, A.; Jouet, G.; Le Roy, P.; Jorry, S.J.; Grall, J.; Reixach, T.; Lambert, C.; Gregoire, G.; Goslin, J.; Roubi, A.; Penaud, A.; Vidal, M.; Siano, R. Fossil maerl beds as coastal indicators of late Holocene palaeo-environmental evolution in the Bay of Brest (Western France). *Palaeogeogr. Palaeoclimatol. Palaeoecol.* **2021**, 577, 110525. https://doi.org/10.1016/j.palaeo.2021.110525

79. Pardo, C.; Guillemin, M.L.; Pena, V.; Bárbara, I.; Valero, M.; Barreiro, R. Local coastal configuration rather than latitudinal gradient shape clonal diversity and genetic structure of *Phymatolithon calcareum* maerl Beds in north European Atlantic. *Front. Mar. Sci.* **2019**, 6, 149. https://doi.org/10.3389/fmars.2019.00149.

80. Steller, D.L.; Hernandez-Ayon, J.M.; Riosmena-Rodriguez, R.; Cabello-Pasini, A. Effect of temperature on photosynthesis, growth and calcification rates of the free- living coralline alga *Lithophyllum margaritae*. *Cienc Mar.* **2007**, 33 (4), 441–456. http://dx.doi.org/10.7773/cm.v33i4.1255.

81. Toscano, F.; Vigliotti, M.; Simone, L. Variety of coralline algal deposits (rhodalgal facies) from the Bays of Naples and Pozzuoli (northern Tyrrhenian Sea, Italy). In: *Cool-water carbonates: depositional systems and paleoenvironmental controls*. Pedley, H.M., Carannante, G., Eds.; Geological Society, Spec. Publ., London, 2006, volume 225, pp 85–94. https://doi.org/10.1144/GSL.SP.2006.255.01.07.

82. Millar, K.R.; Gagnon, P. Mechanisms of stability of rhodolith beds: sedimentological aspects. *Mar Ecol Prog Ser* **2018**, 594, 65-83. https://doi.org/10.3354/meps12501.

83. O' Connell, L.G.; James, N.P.; Doubell, M.; Middleton, J.F.; Luick, J.; Currie, D.R.; Bone, Y. Oceanographic controls on shallow-water temperate carbonate sedimentation: Spencer Gulf, South Australia. *Sedimentology* **2016**, 63, 105–135. http://doi.org/10.1111/sed.12226.

84. Basso, D. Study of living calcareous algae by a paleontological approach: the non-geniculate Corallinaceac (Rhodophyta) of the soft bottoms of the Tyrrhenian Sea (Western Mediterranean). The genera *Phymamlitum* Foslie and *Mesophyllum* Lemoine. *Riv. It. Pal. Strat.* **1994**, 100 (4), 575-596. https://doi.org/10.13130/2039-4942/8602.

85. Basso, D. Living calcareous algae by a paleontological approach: the genus *Lithothamnion* Heydrich nom. cons. from the soft bottoms of the Tyrrhenian Sea (Mediterranean). *Riv. It. Paleontol. Stratigr* **1995**, 101 (3), 349-366. https://doi.org/10.13130/2039-4942/8592.

86. Di Geronimo, R.; Giaccone, G. Le alghe calcaree nel Detritico Costiero di Lampedusa (lsole Pelagie). *Boll. Acc. Gioenia Sci. Nat*. **1994**, 27 (346), 5-25.

87. Braga, J.C. Neogene rhodoliths in the Mediterranean Basins. In*: Rhodolith/Maërl Beds: A Global Perspective,* Riosmena-Rodríguez, R., Nelson, W., and Aguirre, J., Eds.; Springer International Publishing: Geerbestrasse, Switzerland, 2017; Volume 15, pp. 169-193. https://doi.org/10.1007/978-3-319-29315-8_7.

88. McMaster, R.W.; Conover, J.P. Recent algal stromatolites from the Canary Islands. *J Geol.* **1966**, 74, 647-652

89. Focke, J.W.; Gebelein, C.D. Marine lithification of reef rock and rhodolites at a fore-reef slope locality (-50m) off Bermuda. *Geologie en Mijnbouw* **1978**, 57, 163-171.

90. Reid, R.P.; Macintyre, I. G. Foraminiferal-algal nodules from the Eastern Caribbean: Growth history and implications on the value of nodules as paleoenvironmental indicators. *Palaios* **1988**, 3: 424–435.

91. Minnery, G.A. Crustose coralline algae from the Flower Garden Banks, northwestern Gulf of Mexico: controls on distribution and growth morphology. *J. Sed. Petrology* **1990**, 60: 992–1007.

92. Littler, M.M.; Littler, D.S.; Hanisak, M.D. Deep-water rhodolith, productivity, and growth history at sites of formation and subsequent degradation. *J. Exp. Mar. Biol. Ecol.* **1991**, 150: 163–182.

93. Checconi, A.; Bassi, D.; Carannante, G.; Monaco, P. Re-deposited rhodoliths in the middle Miocene hemipelagic deposits of vitulano (Southern Apennines, Italy): coralline assemblage characterization and related trace fossils. *Sediment Geol.* **2010**, 225, 50–66. http://doi.org/10.1016/j.sedgeo.2010.01.001.

94. Coutinho, L.M.; Penelas Gomes, F.; Nasri Sissini, M.; Vieira-Pinto, T.; Muller de Oliveira Henriques, M.C.; Oliveira, M.C.; Antunes Horta, P.; Barbosa de Barros Barreto, M.B. Cryptic diversity in non-geniculate coralline algae: a new genus *Roseolithon* (Hapalidiales, Rhodophyta) and seven new species from the Western Atlantic. European Journal of Phycology, pp.1-24.

95. Tâmega, F.T.S.; Bassi, D.; Figueiredo, M.A.; Cherkinsky, A. Deep-water rhodolith bed from central Brazilian continental shelf, Campos Basin: coralline algal and faunal taxonomic composition. *Journal of Coral Reef Studies* **2014**, 16 (1), 21-31. https://doi.org/10.3755/galaxea.16.21.

96. Martin, S.; Hall-Spencer, J.M. Effects of Ocean Warming and Acidification on Rhodolith/Maërl Beds. In *Rhodolith/Maerl Beds: A Global Perspective*; Riosmena-Rodrigues, R., Nelson, W., Aguirre, J., Eds.; Coastal Research Library, Springer: New York, NY, USA, 2017; Volume 15, pp. 55–85.

4.8. Supplementary Material

Structure and composition of rhodolith beds from the Sergipe-Alagoas Basin (NW Brazil, Southwestern Atlantic)

Nicholas F. Vale, Juan C. Braga, Alex C. Bastos, Fernando C. de Moraes, Claudia S. Karez, Ricardo G. Bahia, Luís A. Leão, Renato C. Pereira, Gilberto M. Amado-Filho, Leonardo T. Salgado

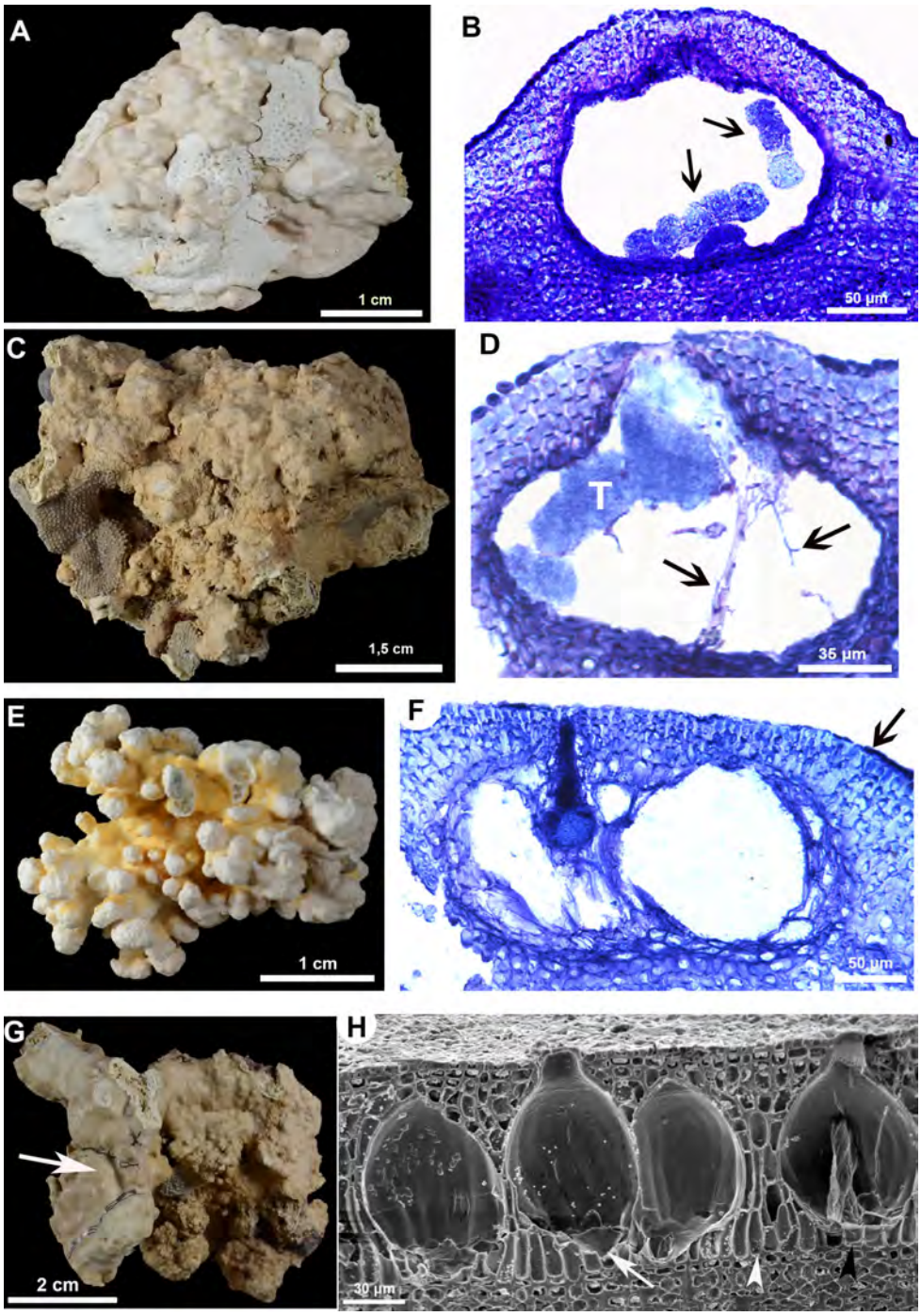

Figure S1. External morphology and anatomy of identified coralline algae species. *Harveylithon* gr. *rupestre* (A) Specimen with encrusting to warty growth form; (B) Vertical section showing an uniporate tetrasporangial conceptacle flush or slightly raised above the surrounding thallus surface, with tetrasporangia along the conceptacle floor (arrows); *Pneophyllum* gr. *fragile* (C) Specimen with encrusting growth form; (D) Vertical section of a uniporate tetrasporangial conceptacle with a tetrasporangia on the floor and interspersed filaments among the tetrasporangia (arrow); *Melyvonnea erubescens* (E) Specimen with encrusting to warty growth form; (F) Vertical section showing the flattened roof surface (arrow); note a tetrasporangia still connected to the pore canal; *Sporolithon franciscanum* (G) Habit of holotype; (H) SEM view of the upper portion of the thallus showing the paraphyses (white arrowhead) between tetrasporangial chambers, a tetrasporangia subtended by a single stalk cell (arrow) and chambers with a basal layer of elongate cells (black arrowhead).

Table S1. Remotely Operated Vehicle (ROV) log sheet at different depths close to site 5, on the South sector of the SEAL Basin. Coordinates are in SIRGAS 2000 Datum.

Line	Latitude (start)	Longitude (start)	Depth (m) start	Latitude (end)	Longitude (end)	Depth (m) end
1	-11,075816	-36,884563	29	-11,095702	-36,857933	46
2	-11,117404	-36,888315	27	-11,129388	-36,872269	44
3	-11,138520	-36,930717	25	-11,160102	-36,902968	40
5	-11,184261	-36,976190	27	-11,205673	-36,947461	42

Table S2. Voucher samples of coralline algae deposited in the in the Herbarium of the Rio de Janeiro Botanical Garden (RB). Coordinates in SIRGAS 2000 Datum.

Family	Genus	Latitude	Longitude	Depth (m)	Voucher
Corallinaceae	*Harveylithon rupestre*	-111.642	-368.839	47	RB 797663
Corallinaceae	*Harveylithon rupestre*	-111.642	-368.839	47	RB 797664
Corallinaceae	*Harveylithon rupestre*	-102.789	-359.792	30	RB 797679
Corallinaceae	*Lithophyllum sp.*	-104.875	-361.245	30	RB 797660
Corallinaceae	*Spongites* sp.	-108.223	-366.118	27	RB 797662
Hapalidiaceae	*Roseolithon* sp.	-102.789	-359.792	30	RB 797666
Hapalidiaceae	*Roseolithon* sp.	-102.789	-359.792	30	RB 797667

Hapalidiaceae	*Roseolithon* sp.	-102.789	-359.792	30	RB 797668
Hapalidiaceae	*Roseolithon* sp.	-102.789	-359.792	30	RB 797671
Hapalidiaceae	*Roseolithon* sp.	-102.789	-359.792	30	RB 797672
Hapalidiaceae	*Roseolithon* sp.	-102.789	-359.792	30	RB 797673
Hapalidiaceae	*Roseolithon* sp.	-102.789	-359.792	30	RB 797674
Hapalidiaceae	*Roseolithon* sp.	-108.223	-366.118	27	RB 797675
Hapalidiaceae	*Roseolithon* sp.	-113.389	-370.556	54	RB 797676
Hapalidiaceae	*Melyvonnea erubescens*	-102.789	-359.792	30	RB 797677
Hapalidiaceae	*Melyvonnea erubescens*	-102.789	-359.792	30	RB 797678
Mastoporaceae	*Pneophyllum fragile*	-111.642	-368.839	47	RB 797661
Sporolithaceae	*Sporolithon franciscanum*	-111.642	-368.839	47	RB 797665

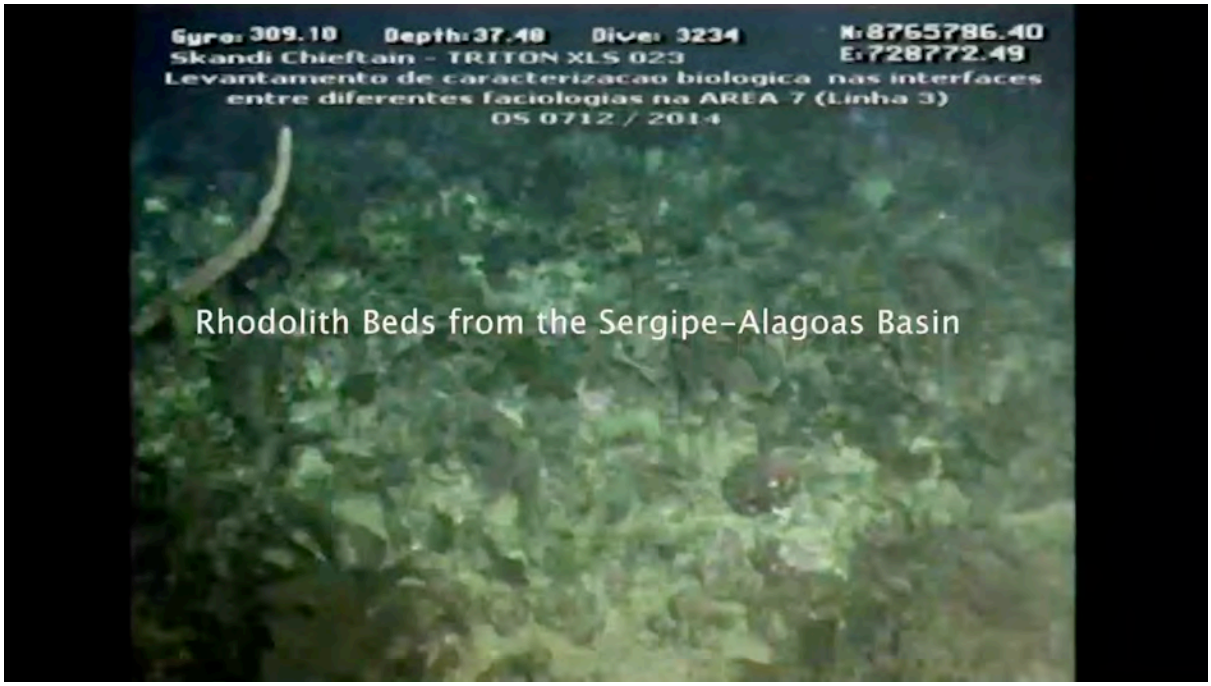

Video S1. Video obtained from ROV surveys on the middle to outer shelf of the SEAL shelf (South Sector).

.

5. Conclusões gerais

Foram estudados sistemas mesofóticos produtores de carbonato da Plataforma Continental Brasileira, nos quais as AC são importantes. O estudo se concentrou em duas áreas: a Margem Continental Amazônica (MCA) e a Baía de Sergipe-Alagoas (SEAL).

O capítulo 3 da tese forneceu a primeira descrição detalhada estruturas que se elevam até 15 m de altura do fundo do mar, ao norte do Cone Amazônico (Sector Norte), com base em mapeamento acústico realizado com *Multi-beam*, imagens em alta resolução e amostras coletadas por submersíveis tripulados entre cerca de 110 e 175 m de profundidade. As estruturas com alto relevo (*high-relief structures* -HRS) são formadas por arenito do Pleistoceno erodidas nos períodos de baixo nível do mar. Sobre elas se acumularam finos carbonatos, *boundstones* y *rudstones* com fósseis de organismos de águas rasas e ooids, durante no LGM e a deglaciação. Estas estruturas foram gradualmente submersas pela elevação do nível do mar e pelo afundamento da plataforma. Posteriormente, uma fina camada de organismos incrustantes cresceu nas superfícies rochosas e atualmente essas feições suportam uma comunidade mesofótica, que produz uma fina camada de sedimento (siliciclásticos aprisionados em micrita e esqueleto de organismos incrustantes) sobre a superfície rochosa cuja capacidade de acreção é negligente. O Setor Central, associado ao acúmulo de sedimentos do rio Amazonas carece de uma ruptura na plataforma. No entanto, comunidades bentônicas vivas ocorrem em afloramentos rochosos. O Setor Sul é menos influenciado pela pluma do rio. Os afloramentos rochosos do Pleistoceno a 180 m carregam uma comunidade bentônica dominada por esponjas e algas coralinas, que são responsáveis pelo acúmulo de um depósito fino de bioclastos, areia de quartzo e lama sobre o substrato rochoso, sem, ou pouca, capacidade de acreção.

Na Bacia SEAL a distribuição em grande escala dos bancos de rodolitos está controlada pela descarga de sedimento dos grandes sistemas fluviais da região. A variabilidade espacial dos bancos de rodolitos apresentada no capítulo 4 da tese, baseado em amostras coletadas e vídeos obtidos por um Veículo Operado Remotamente (ROV) ao longo da costa de SEAL na plataforma do Nordeste brasileiro, revelou rodolitos vivos agrupados em manchas intercaladas com sedimentos bioclásticos e associados a macroalgas com uma comunidade de peixes recifais; alguns rodolitos são fusionados, formando concreções de AC; rodolitos ramificados (maërl) ocorrem tanto nos leitos de ondulação em águas rasas quanto em locais mais profundos. A idade radiométrica mais antiga (1.850 anos) analisada nos rodolitos da Bacia SEAL sugere que sua formação se deu muito tempo após a inundação Holocênica ocorrida na região. No setor Sul alguns rodolitos apresentaram duas fases de crescimento com uma diferença de idade de mais de 1.500 anos, o que pode ser explicado por um longo período de enterro no sedimento do fundo do mar e posterior exumação e retomada do crescimento.

Em complemento aos objetivos propostos, um total de 6 morfo-taxons de algas vermelhas (rodofíceas) foram identificados na MCA e de 16 morfo-taxons na Bacia SEAL, pertencentes a Corallinales, Hapalidiales, e Sporolithales dentro das AC, e a Peyssonneliales, integradas em 04 famílias e 10 gêneros. Com isso, os registros de táxons baseados em identificações morfo-anatômicas refletem uma maior riqueza do que a quantidade de espécies filogenéticas de AC delimitadas para as ecoregiões do Norte e Nordeste do sudoeste do Atlântico por métodos em DNA. Demonstrando que a riqueza de espécies de AC pode ser ainda maior do que a quantidade registrada até o presente.

O presente estudo contribuiu com o avanço no conhecimento sobre diferentes aspectos dos ambientes mesofóticos no Brasil, foi possível obter informações consideradas consistentes sobre a distribuição em pequena e média escala, estrutura dos bancos de rodolitos e “recifes”, organismos associados, composição de espécies de algas vermelhas coralináceas. Contudo,

estudos futuros explorando novos locais dentro da MCA e Bacia SEAL contribuirão para descobrir novos ambientes e espécies de algas coralináceas. Um maior conhecimento sobre o papel desses bancos de rodolitos e ambientes recifais mesofóticos nos ecossistemas bentônicos é importante para dar apoio aos programas de planejamento espacial marinho, o que poderia levar a uma utilização mais sustentável desses habitats.

Referências Bibliográficas

Abbey, E., Webster, J.M., Braga, J.C., et al. 2011a. Variation in deglacial coralgal assemblages and their paleoenvironmental significance: IODP Expedition 310, "Tahiti Sea Level". *Global and Planetary Change*.

_____, Webster, J.M., Beaman, R.J. 2011b. Geomorphology of submerged reefs on the shelf edge of the Great Barrier Reef: The influence of oscillating Pleistocene sea levels. *Marine Geology* 288: 61-78.

_____, Webster, J.M., Braga, J.C., et al. 2013. Deglacial mesophotic reef demise on the Great Barrier Reef. *Paleogeography, Paleoclimatology, Paleoecology* 392: 473-494.

Alencar, M.F.V.V. 2020. The Environmental Dimension of the "Brazilian Blue Amazon": Environmental Rights and Duties on the Continental Shelf. *In* Ventura, V.A.M.F. (ed). *Environmental Jurisdiction in the Law of the Sea*. Springer, Cham: 247-296.

Amado-Filho, G.M., Maneveldt, G.W., Manso, R.C.C., et al. 2007. Structure of rhodolith beds from 4 to 55 meters deep along the southern coast of Espírito Santo State, Brazil. *Ciencias Marinas* 33(4): 399-410.

_____, Maneveldt, G.W., Pereira-Filho, G.H. et al. 2010. Seaweed diversity associated with a Brazilian tropical rhodolith bed. *Ciencias Marinas* 36(4): 371-391.

_____, Moura, R.L., Bastos, A.C., et al. 2012a. Rhodolith beds are major $CaCO_3$ bio-factories in the Tropical South West Atlantic. *Plos One* 7(4): e35171.

_____, Pereira-Filho, G.H., Bahia, R.G. et al. 2012b. Occurrence and distribution of rhodolith beds on the Fernando de Noronha Archipelago of Brazil. *Aquatic Botany* 101: 41-45.

_____, Pereira-Filho, G.H. 2012c. Rhodolith beds in Brazil: a new potential habitat for marine bioprospection. *Revista Brasileira de Farmacognosia* 22(4): 782-788.

_____, Moura, R.L., Bastos, A.C., et al. 2016. Mesophotic ecosystems of the unique South Atlantic atoll are composed by rhodolith beds and scattered consolidated reefs. *Marine Biodiversity* 46(4).

_____, Pereira-Filho, G.H., Bahia, et al. 2017. South Atlantic Rhodolith Beds: Latitudinal distribution, species composition, structure and ecosystem functions, threats and conservation status. *In* Riosmena-Rodrigues, R., Nelson, W., Aguirre, J. (eds). *Rhodolith/Maërl Beds: A Global Perspective*. Coastal Research Library, Springer 15: 299-318.

Araújo, L.S., Magdalena, U.R., Louzada, et al. 2021. Growing industrialization and poor conservation planning challenge natural resources' management in the Amazon shelf off Brazil. *Mar. Policy* 128: 104465.

Armstrong, R.A., Singh, H., Torres, J., et al. 2006. Characterizing the deep insular shelf coral reef habitat of the Hind Bank marine conservation district (U.S. Virgin Islands) using the SeaBED autonomous underwater vehicle. *Cont Shelf Res* 26: 194–205.

_____, Pizarro, O., Roman, C. 2019. Underwater robotic technology for imaging mesophotic coral ecosystems. *In* Loya, Y., Puglise, K.A., Bridge, T.C.L. (eds). *Mesophotic coral ecosystems*. Springer, New York: 973–988

Bahia, R.G., 2014. *Algas calcárias formadoras de rodolitos da Plataforma Continental Tropical e ilhas oceânicas do Brasil: levantamento florístico e taxonomia.* Tese de doutorado. Escola Nacional de Botânica Tropical. Rio de Janeiro, Brasil. 231p.

_____, Amado-Filho, G.M., Azevedo, J., Maneveldt, G.W. 2014a. *Hydrolithon improcerum* (Foslie & M.A. Howe) Foslie and *Mesophyllum macroblastum* (Foslie) Adey: New records of crustose coralline red algae for the Atlantic Ocean. *Phytotaxa* 190(1): 038–044.

_____, Amado-Filho, G.M., Maneveldt, G.W. 2014b. *Sporolithon molle* (Heydrich) Heydrich (Sporolithales, Corallinophycidae, Rhodophyta): An addition to the Atlantic flora found on a remote oceanic island. *Cryptogamie Algologie* 35(1): 07-14.

_____, Amado-Filho, G.M., Maneveldt, G.W., et al. 2014c. *Sporolithon tenue* sp. nov. (Sporolithales, Corallinophycidae, Rhodophyta): A new rhodolith-forming species from the tropical southwestern Atlantic. *Phycological Research* (62): 44–54.

_____, Maneveldt, G.W.; Amado-Filho, G.M.; Yoneshigue-Valentin, Y. 2015. New diagnostic characters for the order Sporolithales (Corallinophycideae, Rhodophyta). *Journal of Phycology* 51: 1137–1146.

Bassi, D., Iryu, Y., Nebelsick, J.H. 2012. To be or not to be a fossil rhodolith? Analytical methods for studying fossil rhodolith deposits. *Journal of Coastal Research* 28 (1): 288–295.

_____, Iryu, Y., Humblet, M., et al. 2012. Recent macroids on the Kikai-jima shelf, Central Ryukyu Islands, Japan. *Sedimentology* 59: 2024–2041.

Basso, D. 1998. Deep rhodolith distribution in the Pontian Islands, Italy: a model for the paleoecology of a temperate sea. *Paleogeography, Paleoclimatology, Paleoecology* 137: 173–187.

_____, Nalin, R., Nelson, C.S. 2009. Shallow-water *Sporolithon* rhodoliths from North Island (New Zealand). *Palaios 24*: 92–103.

_____, Granier, B. 2018. Johnson & Kaska 1965 Fossil Coralline Algae from Guatemala (Revision of the Jesse Harlan Johnson collection, Part 4). *Rivista Italiana di Paleontologia e Stratigrafia* 124(1): 91-104.

Bastos, A.C., Moura, R.L., Amado-Filho, G.M., et al. 2016. Origin and sedimentary evolution of sinkholes (buracas) in the Abrolhos continental shelf, Brazil. *Paleogeography, Paleoclimatology, Paleoecology* 462: 101-111.

Beijbom, O., Edmunds, P.J., Roelfsema, C., et al. 2015. Towards automated annotation of benthic survey images: Variability of human experts and operational modes of automation. *Plos One* 10: e0130312.

Bezerra, F.H.R., Barreto, A.M.F., Suguio, K. 2003. Holocene sea level history on the Rio Grande do Norte State Coastal, Brazil. *Mar. Geol.* 196: 73–89

Blanchon P., Jones, B., Ford, D.C. 2002. Discovery of a submerged relic reef and shoreline off Grand Cayman: further support for an early Holocene jump in sea level. *Sedimentary Geology* 147: 253-270.

Brasileiro, P.S., Pereira-Filho, G.H., Bahia, R.G. 2015. Macroalgal composition and community structure of the largest rhodolith beds in the world. *Marine Biodiversity* 46(2): 407–420.

Bridge, T., Guinotte, J. 2013. Mesophotic coral reef ecosystems in the Great Barrier Reef World Heritage Area: their potential distribution and possible role as refugia from disturbance. Research Publication no 109. Great Barrier Reef Marine Park Authority, Townsville.

_____, Beaman, R.J., Bongaerts, P., et al. 2019. The Great Barrier Reef and Coral Sea. *In* Loya, Y., Puglise, K.A., Bridge, T.C.L. (eds). *Mesophotic coral ecosystems*. Springer, New York: 351–367.

Caldas, L.H.O., Stattegger, K., Vital, H. 2006. Holocene sea-level history and coastal evolution: Evidences from coastal sediments of the northern Rio Grande do Norte coast, NE Brazil. *Mar. Geol*. 228: 39–53.

Camoin, G.F., Seard, C., Deschamps, P., et al. 2012. Reef response to sea-level and environmental changes during the last deglaciation: Integrated Ocean Drilling Program Expedition 310, Tahiti Sea Level. *Geology 40*(7): 643-646.

Carvalho, V.F., Assis, J., Serrão, E.A., et al. 2020. Environmental drivers of rhodolith beds and epiphytes community along the South Western Atlantic coast. *Marine Environmental Research* 154: 104827.

Cavalcanti, V.M.M. 2011. Recursos minerais marinhos. *In* Cavalcanti, V.M.M. (ed). *Plataforma continental: a última fronteira da mineração brasileira.* Departamento Nacional de Produção Mineral *(DNPM)*, Brasília: 19-50.

Cavalcanti, G.S., Gregoracci, G.B., Longo, L.L., et al. 2013. Sinkhole-like structures as bioproductivity hotspots in the Abrolhos Bank. *Continental Shelf Research* 70: 126-134.

Coles, V.J., Brooks, M.T., Hopkins, J., et al. 2013. The pathways and properties of the Amazon River Plume in the tropical North Atlantic Ocean. *Journal of Geophysical Research: Oceans* 118: 6894–6913.

Collette, B.B., Rützler, K. 1977. Reef fishes over sponge bottoms of the mouth of Amazon River. *Proceedings, Third International Coral Reef Symposium*. Miami, Florida, EUA: 305-310.

Coutinho, P.N. 2000. Oceanografia Geológica. *In* Coutinho P.N. (ed). *Levantamento do Estado da Arte da Pesquisa dos Recursos Vivos Marinhos do Brasil (Programa REVIZEE).* Ministério do Meio

Ambiente dos Recursos Hídricos e da Amazônia Legal, Secretaria de Coordenação dos Assuntos do Meio Ambiente, Brasília: 0-75.

Coutinho, L.M., Penelas Gomes, F., Nasri Sissini, M. 2021. Cryptic diversity in non-geniculate coralline algae: a new genus Roseolithon (Hapalidiales, Rhodophyta) and seven new species from the Western Atlantic. *European Journal of Phycology*: 1-24.

Costa, I.O., Jesus, P.B., Jesus, T.S., et al. 2019. Reef-building coralline algae from the Southwest Atlantic: Filling gaps with the recognition of *Harveylithon* (Corallinaceae, Rhodophyta) on the Brazilian Coast. *J. Phycol.* 55: 1370–1385

Dias, G.T.M. 2000. Granulados Bioclásticos – Algas Calcárias. *Brazilian Journal of Geophysics* 18(3): 307-318.

Dunham, R.J. 1962. Classification of carbonate rocks according to depositional texture. *In* Ham, W.E. (eds.). *Classification of Carbonate Rocks*. American Association of Petroleum Geologists Memoir 1: 108–121.

Embry, A.F., Klovan, J.E. 1972. Absolute water depth limits of late Devonian paleoecological zones. *Geol. Rundsch*. 61 (2): 672–686.

Englebert, N., Bongaerts, P., Muir, P.R., et al. 2017. Lower mesophotic coral communities (60-125 m depth) of the northern Great Barrier Reef and Coral Sea. *Plos One 12*(2): e0170336.

Fairbanks, R.G. 1989. A 17,000-year glacio-eustatic sea level record: influence of glacial melting rates on the Younger Dryas event and deep-ocean circulation. *Nature 342*(6250): 637-642.

Fontes, L.C.S., Santos, J.R., Santos, L.A., Oliveira Junior, E.A. 2017. Geologia da Margem Continental da Bacia de Sergipe -Alagoas, NE do Brasil. *In* Carneiro M.E.R. (ed). *Geologia e geomorfologia da bacia de Sergipe-Alagoas*. Editora UFS, Coleção Projeto MARSEAL, São Cristóvão 1, 9-23.

_____, Santos, J.R., Santos, L.A., Mendonça, J.B.S., Santos, M.S. 2017. Sedimentos superficiais da plataforma continental de Sergipe-Alagoas. *In* Carneiro M.E.R. (ed). *Geologia e Geomorfologia da Bacia de Sergipe-Alagoas*. Editora UFS, Coleção Projeto MARSEAL, São Cristóvão 1, 64–96.

Foster, M.S. 2001. Rhodoliths: between rocks and soft places - Minireview. *Journal of Phycology* 37: 659-667.

_____, Amado-Filho, G.M., Kamenos, N.A., et al. 2013. Rhodoliths and Rhodoliths Beds. *In* Lang, M.A., Marinelli, R.L., Roberts, S.J, Taylor, P.R. (eds). *Research and Discoveries: The Revolution of Science Through SCUBA*. Smithsonian Institution Scholarly Press, Washington DC: 143-155.

Francini-Filho, R.B., Asp, N.E., Siegle, E., et al. 2018. Perspectives on the Great Amazon Reef: Extension, Biodiversity, and Threats. *Front. Marine Science* 5: 142.

Gherardi, D.F.M. 2004. Community structure and carbonate production of a temperate rhodolith bank from Arvoredo Island, southern Brazil. *Brazilian Journal Oceanographic* 52: 207- 224.

Guimarães, S.M.P.B., Amado-Filho, G.M. 2008. Deep-water gelatinous rhodophytes from southern Espírito Santo State, Brazil. *Botanica Marina* 51: 378–387.

Guimarães, C.R.P. 2010. *Composição e distribuição dos sedimentos superficiais e da fauna bêntica na plataforma continental de Sergipe*. Tese de doutorado. Instituto de Geociências, Universidade Federal da Bahia. Salvador, Brasil. 159p.

Heaton, T.J., Köhler, P., Butzin, M., et al. 2020. Marine20-the marine radiocarbon age calibration curve (0-55,000 cal BP). *Radiocarbon* 62(4): 779-820.

Hinderstein, L.M., Marr, J.C.A., Martinez, F.A., et al. 2010. Theme section on Mesophotic Coral Ecosystems: Characterization, Ecology and Management. *Coral Reefs* 29: 247–251.

Holz, V.L., Bahia, R.G., Karez, C.S., et al. 2016. Structure of Rhodolith Beds and Surrounding Habitats at the Doce River Shelf (Brazil). *Diversity* 12: 75.

Horta, P.A., Riul, P., Amado-Filho, G.M., et al. 2016. Rhodoliths in Brazil: Current knowledge and potential impacts of climate change. *Brazilian Journal of Oceanography* 64(2): 117-136.

Jesionek, M.B., Bahia, R.G., Hernández-Kantún, J., et al..2016. A taxonomic account of non-geniculate coralline algae (Corallinophycidae, Rhodophyta) from shallow reefs of the Abrolhos Bank, Brazil. *Algae* 31: 317–340.

Jesus, P.B., Dias, F.F., Muniz, R.A., et al. 2017. Holocene paleo-sea level in southeastern Brazil: an approach based on Vermetids shells. *Journal of Sedimentary Environments* 2(1): 35-48.

Kahng, S.E., Kelley, C. 2007. Vertical zonation of habitat forming benthic species on a deep photosynthetic reef (50–140 m) in the Au'au Channel, Hawaii. *Coral Reefs* 26: 679–687.

Keith S.A., Kerswell A.P., Connolly S.R. 2014. Global diversity of marine macroalgae: environmental conditions explain less variation in the tropics. *Glob Ecol Biogeogr* 23: 517–529.

Kempf, M. 1970. Notes on the benthic bionomy of the N-NE Brazilian shelf. *Marine Biology* 5(3): 213-224.

Konar, B., Riosmena-Rodriguez, R., Iken, K. 2006. Rhodolith bed: A newly discovered habitat in the North Pacific Ocean. *Botanica Marina* 49: 355–359.

Lavagnino, A.C., Bastos, A.C., Amado-Filho, G.M., Moraes, et al. 2020. Geomorphometric Seabed Classification and Potential Megahabitat Distribution in the Amazon Continental Margin. *Frontiers Marine Science* 7: 190.

Leão, L.A.S., Bahia, R.G., Jesionek, M.B., et al. 2020. *Sporolithon franciscanum* sp. nov. (Sporolithales, Rhodophyta): a New Rhodolith-Forming Species from Northeast Brazil. *Diversity* 12: 199.

Lesser, M.P., Slattery, M., Leichter, J.J. 2009. Ecology of mesophotic coral reefs. *Journal of Experimental Marine Biology and Ecology* 375: 1-8.

Le Gall, L., Paytri, C., Bittner, L., Aunders, G.W. 2010. Multigene phylogenetic analyses support recognition of the Sporolithales ord. nov. *Molecular Phylogenetics and Evolution* 54: 302–305.

Loya, Y., Puglise, K.A., Bridge, T.C. 2019. *Mesophotic coral ecosystems* (Vol. 12). Springer.

Mabessone, J.M., Kempf, M., Coutinho, P.N. 1972. Characterization of surface sediments on the northern and eastern Brazilian shelf. *Trabalhos Instituto Oceanográfico Universidade Federal Pernambuco* 13: 41-48.

Machado, A.L.S., Pacheco, J.B. 2010. Serviços ecossistêmicos e o ciclo hidrológico da bacia hidrográfica amazônica - The biotic pump. *Revista GeoNorte* 1(01): 71-89.

Mahiques, M.M., Siegle, E., Francini-Filho, R.B., et al., 2019. Insights on the evolution of the living Great Amazon Reef System, equatorial West Atlantic. *Science Reports* 9: 13699.

Marins, B.V., Amado-Filho, G.M., Barreto, et al. 2012. Taxonomy of the southwestern Atlantic endemic kelp: *Laminaria abyssalis* and *Laminaria brasiliensis* (Phaeophyceae, Laminariales) are not different species. *Phycological Research* 60: 51– 60.

Metri, R. 2006. *Ecologia de um banco de algas calcárias da Reserva Biológica Marinha do Arvoredo, SC, Brasil*. Dissertação de Mestrado. Universidade Federal do Paraná, Curitiba, Brasil. 125p.

Medeiros, P.R.P. 2003. *Aporte fluvial, transformação e dispersão da matéria em suspensão e nutrientes no estuário do rio São Francisco, após a construção da usina hidroelétrica do Xingó (AL/SE)*. Tese de Doutorado. Universidade Federal Fluminense, Rio de Janeiro, Brasil. 184p.

_____, Knoppers, B.A., Júnior, R.C.S., et al. 2007. Aporte fluvial e dispersão na zona costeira do rio São Francisco (SE/AL). *Geochimica Brasiliensis* 21(2): 212-231.

Meirelles, P.M., Gadelha-Jr, L.M.R., Francini-Filho, R.B., et al. 2015. BaMBa: Towards the integrated management of Brazilian marine environmental data. *Database The Journal of Biological Databases and Curation* (1): 01-10.

Milliman, J.D., 1977. Role of calcareous algae in Atlantic continental margin sedimentation. *In* Flügel E. (ed). *Fossil Algae*. Springer, Berlin, Heidelberg: 232-247.

_____, Amaral, C.A.B. 1974. Economic potential of Brazilian continental margin sediments. *Anais do XXVIII Congresso Brasileiro Geologia* 28: 335-344.

Moura, R.L., Francini-Filho, R.B., Sazima, I. 1999. Unexpected richness of reef corals near the southern Amazon River mouth. *Coral Reefs* 18: 170.

_____, Secchin, N.A., Amado-Filho, G.M., et al. 2013. Spatial patterns of benthic megahabitats and conservation planning in the Abrolhos Bank. *Continental Shelf Research* 70: 109-117.

_____, Amado-Filho, G.M., Moraes, F.C., et al. 2016. An extensive reef system at the Amazon River mouth. *Science Advanced* 2: e1501252.

Mutti, M., Hallock, P. 2003. Carbonate systems along nutrient and temperature gradients: some sedimentological and geochemical constrains. *International Journal of Earth Sciences* 92: 465-475.

Nascimento, A.A. 2011. *Sedimentação holocênica na plataforma continental de Sergipe, nordeste do Brasil*. Dissertação de Mestrado. Instituto de Geociências, Universidade Federal da Bahia. Salvador, Brasil. 105p.

Nittrouer, C.A., DeMaster, D.J., 1996. The Amazon shelf setting: tropical, energetic, and influenced by a large river. *Continental Shelf Research* 16(5): 553–573

_____, DeMaster, D.J., Kuehl, S.A., et al. 2021. Amazon sediment transport and accumulation along the continuum of mixed fluvial and marine processes. *Annu. Rev. Mar. Sci.* 13: 501-536.

Omachi C.Y., Asp, N.E., Siegle, E., et al. 2019. Light availability for reef-building organisms in a plume-influenced shelf. *Continental Shelf Research* 181: 25-33.

Palma, J.J.J. 1979. Geomorfologia da Plataforma Continental Norte Brasileira. *Série Projeto REMAC* (7): 25-51.

Pascelli, C., Riul, P., Riosmena-Rodríguez, R.S. 2013. Seasonal and depth-driven changes in rhodolith bed structure and associated macroalgae off Arvoredo Island (Southeastern Brazil). *Aquat. Bot*. 111: 62–65.

Pereira-Filho, G.H., Amado-Filho, G.M., Guimarães, S.M.P.B., et al. 2011. Reef Fish and Benthic assemblages of the Trindade and Martin Vaz Island group, Southwestern Atlantic. *Brazilian Journal of Oceanography* 59(3): 201-212.

_____, Amado-Filho, G.M., Moura, R.L., et al. 2012. Extensive Rhodolith Beds Cover the Summits of Southwestern Atlantic Ocean Seamounts. *Journal of Coastal Research* 28(1): 261-269.

_____, Francini-Filho, R.B., Pierozzi-Jr, I., et al. 2015. Sponges and fish facilitate succession from rhodolith beds to reefs. *Bulletin of Marine Science* (91): 45-46.

_____, Shintate, G.S., Kitahara, M.V., et al. 2019. The southernmost Atlantic coral reef is off the subtropical island of Queimada Grande (24° S), Brazil. *Bull. Mar. Sci.* 95: 277–287.

Pinheiro, H.T., Mazzei, E., Moura, R.L., et al. 2015. Fish Biodiversity of the Vitória-Trindade Seamount Chain, Southwestern Atlantic: An Updated Database. *Plos One* 10(3): e0118180.

Pyle, R.L., Copus, J.M. 2019. Mesophotic Coral Ecosystems: Introduction and Overview. *In* Loya, Y., Puglise, K.A., Bridge, T.C.L. (eds). *Mesophotic coral ecosystems*. Springer, New York: 3–27.

Richards, J.L., Bahia, R.G., Jesionek, M.B., Fredericq, S. 2019. *Sporolithon amadoi* sp. nov. (Sporolithales, Rhodophyta), a new rhodolith-forming non-geniculate coralline algae from offshore the northwestern Gulf of Mexico and Brazil. *Phytotaxa* 423: 49–67.

Riul, P., Lacouth, P., Pagliosa, P.R., et al. 2009. Rhodolith beds at the easternmost extreme of South America: Community structure of an endangered environment. *Aquatic Botany* 90: 315-320.

Santos, J.R. 2019. *Feições morfológicas e biofacies como indicadores evolutivos da Plataforma Continental de Sergipe e sul de Alagoas.* Tese de Doutorado. Centro de Tecnologia, Universidade Federal de Sergipe, Recife, Brazil. 221p.

_____, Souza, R.M., Andrade, E., Fontes, L.C.S. 2019. Biogenic components as environmental indicators of the Continental Platform of the state Sergipe and south of Alagoas. *Geociências* 38 (2): 409 – 425.

Sinniger F., Harii S., Humblet M., et al. 2019. Ryukyu Islands, Japan. *In* Loya, Y., Puglise, K.A., Bridge, T.C.L. (eds). *Mesophotic coral ecosystems*. Springer, New York: 231–247.

Sissini, M.N., Koerich, G., de Barros-Barreto, M.B., Coutinho, L.M., et al. 2021. Diversity, distribution, and environmental drivers of coralline red algae: the major reef builders in the Southwestern Atlantic. *Coral Reefs*.

Spalding, M.D., Fox, H.E., Allen, G.R., et al. 2007. Marine ecoregions of the world: a bioregionalization of coastal and shelf areas. *Bioscience* 57: 573–583

Steneck, R.S. 1986. The ecology of coralline algal crusts: convergent patterns and adaptive strategies. *Annual Review of Ecological Systematics* 17: 273-303.

Stuiver, M., Reimer, P.J., Reimer, R.W. 2020. CALIB 8.2. Disponível online: http://calib.org. (Acessado em: maio-junho-2020).

Testa, V. 1997. Calcareous algae and corals in the inner shelf of Rio Grande do Norte, NE Brazil. *Proceedings 8th International Coral Reef Symposium* 1: 737-742.

_____, Bosence, D.W.J. 1999. Physical and biological controls on the formation of carbonate and siliciclastic bed forms on the northeast Brazilian shelf. *Sedimentology* 46: 279-301.

Vale, N.F.L., Amado-Filho, G.M., Braga, J.C., et al. 2018. Structure and composition of rhodoliths from the Amazon River mouth. *Journal of South American Earth Science* 84: 149-159.

Vicalvi, M.A., Milliman, J.D. 1977. Calcium carbonate sedimentation on continental shelf off southern Brazil with special reference to benthic foraminifera. *In* Frost S.H., Weiss M.P., Saunders J.B. (eds). *Reefs and Related Carbonates–Ecology and Sedimentology.* American Association of Petroleum Geologists, Studies in Geology. Boulder, Tulsa 4: 313-328.

Villas-Boas, A.B., Riosmena-Rodriguez, R. Amado-Filho, G.M., et al. 2009. Taxonomy of rhodolith-forming species of *Lithophyllum* (Corallinales; Rhodophyta) from Espírito Santo State, Brazil, including the description of *L. depressum* sp. nov. *Phycology* 48(4): 237-248.

Weil-Accardo, J., Feuillet, N., Jacques, E., et al. 2016. Relative sea-level changes during the last century recorded by coral microatolls in Belloc, Haiti. *Global and Planetary Change* 139: 1-14.

Weinstein, D. K., Tamir, R., Kramer, N., et al. 2021. Mesophotic reef geomorphology categorization, habitat identification, and relationships with surface cover and terrace formation in the Gulf of Aqaba. *Geomorphology 379*: 107548.

Webster, J.M., Clague, D.A., Riker-Coleman, K., et al. 2004. Drowning of the –150 m reef off Hawaii: A casualty of global meltwater pulse 1A ? *Geology* 32: 249–252.

_____, Braga, J. C., Humblet, M., et al. 2018. Response of the Great Barrier Reef to sea-level and environmental changes over the past 30,000 years. *Nature Geoscience* 11(6): 426-432.

Woodroffe, C.D., Brooke, B.P., Linklater, M., et al. 2010. Response of coral reefs to climate change: Expansion and demise of the southernmost Pacific coral. *Geophysical Research Letters* 37: L15602.

Woelkerling, W.J., Irvine, L.M., Harvey, A.S. 1993. Growth-forms in non-geniculate coralline red algae (Corallinales, Rhodophyta). *Aust. Syst. Bot. 6*: 297–293.

Yokoyama, Y., Esat, T.M., Thompson, W.G., et al. 2018. Rapid glaciation and a two-step sea level plunge into the Last Glacial Maximum. *Nature* 559: 603–607.

Apêndices

Apêndice 1

Published in *Marine Geology* **2022**, v. 447, 106779.
DOI: 10.1016/j.margeo.2022.106779
Impact factor 3.548; SJR: 1.236

Contents lists available at ScienceDirect

Marine Geology

journal homepage: www.elsevier.com/locate/margo

Research Article

Distribution, morphology and composition of mesophotic 'reefs' on the Amazon Continental Margin

Nicholas F. Vale [a,b], Juan C. Braga [b], Rodrigo L. de Moura [c], Leonardo T. Salgado [a], Fernando C. de Moraes [a,d], Claudia S. Karez [a], Rodrigo T. de Carvalho [a], Paulo S. Salomon [c], Pedro S. Menandro [e], Gilberto M. Amado-Filho [a,1], Alex C. Bastos [e,*]

[a] Instituto de Pesquisas Jardim Botânico do Rio de Janeiro, Rio de Janeiro 22460-030, Brazil
[b] Departamento de Estratigrafía y Paleontología, Universidad de Granada, Granada 18071, Spain
[c] Instituto de Biologia and SAGE-COPPE, Universidade Federal do Rio de Janeiro, Rio de Janeiro 21941-599, Brazil
[d] Museu Nacional, Universidade Federal do Rio de Janeiro, Rio de Janeiro 20940-040, Brazil
[e] Departamento de Oceanografia e Ecologia, Universidade Federal do Espírito Santo, Vitória 29075-910, Brazil

ARTICLE INFO

Editor: Edward Anthony

Keywords:
'Amazon reefs'
Carbonate and siliciclastic deposits
Sea-level changes
Last Glacial Maximum
Reef morphology

ABSTRACT

The geomorphology of the Amazon Continental Margin (ACM) is highly heterogeneous and includes a variety of reef-like formations found in deep-water along the shelf-slope transition. The ACM has been divided into three Sectors (Northern, Central and Southern) according to the distribution of the carbonate producers and the 'reefs', influenced by the Amazon River plume. Here, we characterize these structures that were sampled with a manned submersible and multibeam surveys to depths of up to 230 m, exploring their relationship with the Amazon river plume and changing sea level following the Last Glacial Maximum (LGM). The shelf-slope transition and a deeper shelf break in the Northern Sector of the Brazilian portion of the ACM carry a series of prominent high-relief structures (HRS) that experience a strong fluvial influence. The tops of these features are between 110 and 165 m depths and seem to have originated during lowstands, through erosion of Pleistocene sandstones. Siliciclastic and carbonate deposits accumulated on the tops of these features in shallow waters during the LGM and early deglaciation and were gradually submerged by rising sea level and subsidence. A thin layer of encrusting organisms, coralline algae, sponges, bryozoans and serpulids presently colonizes most of these surfaces at the sites sampled and contributes to the aggregation of thin fine-grained siliciclastic deposits. The Central Sector, off the river mouth, is associated with long-term sediment accumulation and lacks a shelf break. Nevertheless, living benthic communities occur on rock outcrops. The Southern Sector is less influenced by the river plume and includes a shallower shelf-break and a prominent canyon. The surveyed outcrops of Pleistocene carbonate and siliciclastic rocks at 180 m carry thin covers of a benthic community dominated by sponges and coralline algae, which is responsible for the accumulation of a thin (up to a few centimeters) deposit of carbonate bioclasts, quartz sand and mud on the rocky substrate. Thus, the 'reefs' of the outer shelf and mesophotic Amazon margin are typically eroded older rocks, colonized by encrusting organisms during the LGM and deglaciation forming a carbonate veneer, which now support a mesophotic community.

1. Introduction

The Amazon Continental Margin (ACM), extending in the northwestern part of the Brazilian Equatorial Margin (BEM), resulted from the opening of the Equatorial Atlantic Ocean in the Early to Late Cretaceous (Doré, 1991; Tetteh, 2016; Pérez-Díaz and Eagles, 2017). It represents one of the world's largest mixed carbonate-siliciclastic platforms, developed during the Neogene in a period of transition from carbonate to siliciclastic-dominated environments in the region (Gorini et al., 2013; Cruz et al., 2019). During the late Miocene, between 8 and 5.5 Myr ago, carbonate sedimentation was dominant, but progressively increasing terrigenous sediment input from the Amazon buried the

* Corresponding author
E-mail address: alex.bastos@ufes.br (A.C. Bastos).
[1] Deceased, March 2019.

https://doi.org/10.1016/j.margeo.2022.106779
Received 22 October 2021; Received in revised form 17 March 2022; Accepted 21 March 2022
Available online 24 March 2022

Apêndice 2

Published in the Journal *Diversity* **2022**, v. 14(4), 282.
DOI: 10.3390/d14040282
Impact factor 2.465; SJR: 0.697

diversity

MDPI

Article

Structure and Composition of Rhodolith Beds from the Sergipe-Alagoas Basin (NE Brazil, Southwestern Atlantic)

Nicholas F. L. Vale [1,2], Juan C. Braga [2], Alex C. Bastos [3], Fernando C. Moraes [1,4], Claudia S. Karez [1], Ricardo G. Bahia [1], Luis A. Leão [1], Renato C. Pereira [1,5], Gilberto M. Amado-Filho [1,†] and Leonardo T. Salgado [1,*]

1 Diretoria de Pesquisas, Instituto de Pesquisas Jardim Botânico do Rio de Janeiro, Rio de Janeiro 22460-030, RJ, Brazil; nicholasdovale@gmail.com (N.F.L.V.); fmoraes@mn.ufrj.br (F.C.M.); claudia.karez@gmail.com (C.S.K.); ricardo.bahia@gmail.com (R.G.B.); luisrleao@gmail.com (L.A.L.); rcrespo@idd.uff.br (R.C.P.); gfilho@jbrj.gov.br (G.M.A.-F.)
2 Departamento de Estratigrafía y Paleontología, Universidad de Granada, 18071 Granada, Andalucía, Spain; jbraga@ugr.es
3 Departamento de Oceanografia, Universidade Federal do Espírito Santo, Vitoria 29075-910, ES, Brazil; alexcardosobastos@gmail.com
4 Museu Nacional, Universidade Federal do Rio de Janeiro, Rio de Janeiro 20940-040, RJ, Brazil
5 Departamento de Biologia Marinha, Universidade Federal Fluminense, Niteroi 24001-970, RJ, Brazil
* Correspondence: lsalgado.jbrj@gmail.com
† Deceased, March 2019.

Abstract: Rhodolith beds are biogenic benthic habitats mainly formed by unattached, non-geniculate coralline algae, which can be inhabited by many associated species. The Brazilian continental shelf encompasses the largest continuous rhodolith bed in the world. This study was based on samples obtained from seven sites and videos taken by a Remotely Operated Vehicle (ROV) at four transects off the Sergipe-Alagoas Coast on the northeast Brazilian shelf. ROV operations and bottom trawl sampling revealed the occurrence of rhodolith beds between 25 and 54 m depths. At the shallower depths, fruticose (branching) rhodoliths (maërl) appear in troughs of ripples, and other non-branching rhodoliths occur associated with corals and sponge patches surrounded by bioclastic sand. Rhodoliths also occur in patches from 30 to 39 m depth; some are fused, forming larger, complex tridimensional structures. At deeper depths, from 40 to 54 m, the abundance of rhodoliths increases and occur associated with fleshy macroalgae on a smooth seafloor; some rhodoliths are fused into complex structures, locally some are fruticose (maërl), and others are partially buried by fine-grained sediment. The collected rhodoliths vary from fruticose in two sites to encrusting to lumpy, concentric and boxwork nodules in the rest; their size ranges from small (<1.5 cm) to large (~6 cm) and are mostly sub-spheroidal to spheroidal. A total of 16 red algal morpho-taxa were identified in the study sites. Two phases of growth can be distinguished in some rhodoliths by changes in color. The brownish inner cores yielded ages of 1600–1850 cal years before the present, whereas outer layers were much younger (180–50 years BP old). Growth layers appeared to have been separated by a long period of burial in the seafloor sediment. Other rhodoliths have ages of hundreds of years.

Keywords: non-geniculate coralline read algae; rhodolith beds; maërl; morpho-anatomy; ROV; Brazilian Northeast continental shelf

check for updates

Citation: Vale, N.F.L.; Braga, J.C.; Bastos, A.C.; Moraes, F.C.; Karez, C.S.; Bahia, R.G.; Leão, L.A.; Pereira, R.C.; Amado-Filho, G.M.; Salgado, L.T. Structure and Composition of Rhodolith Beds from the Sergipe-Alagoas Basin (NE Brazil, Southwestern Atlantic). *Diversity* **2022**, *14*, 282. https://doi.org/10.3390/d14040282

Academic Editors: Fernando Tuya and Michael Wink

Received: 4 March 2022
Accepted: 2 April 2022
Published: 10 April 2022

Publisher's Note: MDPI stays neutral with regard to jurisdictional claims in published maps and institutional affiliations.

1. Introduction

Throughout their evolutionary history, non-geniculate coralline algae have been present in carbonate platforms as well as siliciclastic and mixed carbonate-siliciclastic systems [1]. Living and fossil non-geniculate coralline algae occur as crusts of varying thickness on both hard and soft substrates and free-living (unattached) nodules, also called rhodoliths and maërl, which can occur in large concentrations on the seafloor, known